Title
Repair of the Cerebral Vasculature After Traumatic Brain Injury and the Influence of Beta-Catenin in New Vessel Formation and Injury Outcome

Permalink
https://escholarship.org/uc/item/9282k75m

Author
Salehi, Arjang

Publication Date
2019

Peer reviewed|Thesis/dissertation

UNIVERSITY OF CALIFORNIA
RIVERSIDE

Repair of the Cerebral Vasculature After Traumatic Brain Injury and the Influence
of Beta-Catenin in New Vessel Formation and Injury Outcome

A Dissertation submitted in partial satisfaction
of the requirements for the degree of

Doctor of Philosophy

in

Cell, Molecular and Developmental Biology

by

Arjang Salehi

June 2019

Dissertation Committee:
      Dr. Andre Obenaus, Co-Chairperson
      Dr. Nicole Zur Nieden, Co-Chairperson
      Dr. Kaustabh Ghosh

The Dissertation of Arjang Salehi is approved:

_____

_____
Committee Co-Chairperson

_____
Committee Co-Chairperson

University of California, Riverside

Acknowledgments

Chapter 1, in part, is a reprint of the material as it appears in "Response of the cerebral vasculature following traumatic brain injury" (Journal of Cerebral Blood Flow and Metabolism, 2017). Chapter 2, in full, is a reprint of the material as it appears in "A Novel Technique for Visualizing and Analyzing the Cerebral Vasculature in Rodents" (Translational Stroke Research, 2018). Chapter 3, in full, is a reprint of the material as it appears in "Up-regulation of Wnt/beta-catenin expression is accompanied with vascular repair after traumatic brain injury" (Journal of Cerebral Blood Flow and Metabolism, 2018). Dr. Andre Obenaus listed in the publications directed and supervised the research which forms the basis for this dissertation.

For the article entitled "Response of the cerebral vasculature following traumatic brain injury," Dr. Andre Obenaus drafted a significant portion of the manuscript and figures; Dr. John H. Zhang and Dr. Andre Obenaus edited the final draft.

For the article entitled "A Novel Technique for Visualizing and Analyzing the Cerebral Vasculature in Rodents", Dr. Amandine Jullienne, Kara M. Wendel, Mary Hamer, Dr. Andre Obenaus contributed to the conception and design of the study; Dr. Amandine Jullienne, Kara M. Wendel, and Mary Hamer acquired and analyzed the data; Dr. Amandine Jullienne and Dr. Andre Obenaus drafted a

ABSTRACT OF THE DISSERTATION

Repair of the Cerebral Vasculature After Traumatic Brain Injury and the Influence
of Beta-Catenin in New Vessel Formation and Injury Outcome

by

Arjang Salehi

Doctor of Philosophy, Cell Molecular and Developmental Biology Program
University of California, Riverside, June 2019
Dr. Andre Obenaus, Co-Chairperson
Dr. Nicole Zur Nieden, Co-Chairperson

Traumatic brain injury (TBI) often results in damage to the cerebral

vasculature which leads to hypoperfusion, edema, and hemorrhage. Repairing

the injured vasculature after TBI is critical for neuroprotection and improving

outcomes. While numerous studies have shown that the cerebral vessels are

damaged after TBI, there are scant studies looking at repair of the vessel

network following brain injury. Furthermore, there is a paucity of studies that have

examined the molecular mechanisms underlying vascular repair after TBI. One

possible signaling factor is β-catenin, which promotes blood vessel formation

during embryonic development. To address this gap in knowledge, we developed

a novel method to stain, visualize, and analyze the cerebral vasculature in the

entire rodent brain. This technique, referred to as Vessel Painting (VP),

effectively stains pial, penetrating, and parenchymal vessels and cerebral

vessels can be imaged by wide-field fluorescent microscopy to acquire whole

brain images. We introduce two complimentary methods to analyze vessel

morphology and complexity in the whole brain. Our novel VP and analysis protocol was used to study the vascular alterations after TBI. Adult male mice received a moderate controlled cortical impact followed by VP at 1 and 7 days post injury (dpi). We assessed β-catenin inside blood vessels around the injury site and utilized a Wnt reporter mouse line (TCF/LEF:H2B-GFP) to monitor Wnt gene expression. We report that TBI results in vascular loss at 1 dpi followed by an increase in new vessels at 7 dpi. We observed an acute increase in β-catenin expression and increased Wnt reporter activity in cerebral vessels after TBI. To assess the role of β-catenin in vascular repair, we utilized Lithium to increase β-catenin expression and JW74 to reduce β-catenin expression. Lithium treatment after TBI enhanced vascular repair and lead to elongated vessel segments at 7 dpi while JW74 treatment after TBI reduced vascular repair and lead to fragmented vessels. Overall, these findings suggest that β-catenin becomes activated after TBI to initiate vascular repair. Treatment strategies to enhance β-catenin appear to contribute to vascular repair after TBI and represents a potential target for future therapeutics.

Table of Contents

List of Figures

List of Tables

Chapter 1

Introduction

<u>Preface</u>

This chapter has been adapted from… Salehi, A., J. H. Zhang and A. Obenaus (2017). "Response of the cerebral vasculature following traumatic brain injury." Journal of Cerebral Blood Flow and Metabolism 37(7): 2320-2339 *with permission from SAGE Publishing*

This chapter describes vascular complications that occur after traumatic brain injury, the temporal response of the cerebral vasculature to injury, and putative signaling factors involved in vascular repair. This chapter gives an overview of beta-catenin and discusses beta-catenin's role in blood vessel formation during embryonic development and its involvement in repair processes after traumatic brain injury.

Reproduced from manuscript: Figure 1.1 – 1.3, 1.6, Table 1.1 – 1.2

Over the last decade, traumatic brain injury (TBI) research has focused almost exclusively on neuroprotective strategies that reduce neuronal cell loss[1]. Unforutantely, this approach has failed to develop any meaningful therapeutics for clinical treatment. One less explored potential target has been the brain vasculature and its impact on TBI outcomes[2-4]. A major consequence of TBI is direct damage to the cerebral vasculature. Hemorrhage, edema, blood flow abnormalities, and blood brain barrier disruption are immediate and early events that are commonly observed in patients and in animal models of TBI. These early events are then later followed by hypoperfusion, altered delivery of metabolic substrates, and hypoxic and ischemic tissue damage. The vasculature is comprised of several key cellular elements termed the expanded neurovascular unit (eNVU) and includes neurons, astrocytes, endothelial cells, pericytes, and smooth muscle cells. The eNVU elements work together to regulate cellular metabolism and activity through local blood flow[5]. After TBI, secondary injury mechanisms result in the dysregulation of the eNVU leading to subsequent cellular degeneration in severe injuries to altered function in more mild injuries[4, 6].

Emerging research now suggests that the injured vasculature attempts to undergo repair[7-9]. Angiogenesis and vasculogenesis are the two primary processes initiated after TBI. The multiple components of the eNVU are actively involved in this response and are regulated by a myriad of cellular and molecular injury-induced signaling factors and processes. A greater understanding of how these signaling pathways coordinate vascular repair will provide insight into new

potential drug targets and open up unexplored avenues for therapeutic

intervention. Elucidating these pathways will also have broad implications for a

host of other brain injuries that impact the vasculature.

Traumatic Brain Injury

TBI is the most common acquired brain injury worldwide with millions of

individuals affected across a broad age spectrum[10]. In the United States, the

incidence of TBI is 1.7 million, resulting in 52,000 deaths annually[11]. The number

of trauma-related deaths is higher in European countries[12]. Along with causing

significant mortality, the short and long-term consequences associated with TBI

have become more apparent and include cognitive deficits (loss of memory, loss

of reasoning) and behavioral abnormalities (anxiety, depression, poor social

interactions)[13]. Indeed, it is estimated that 43% of TBI survivors develop

subsequent chronic disabilities for which there are no clinically effective

treatments to assist in functional recovery after TBI[14].

TBI is a heterogeneous condition with regards to etiology. In general, TBI

has been defined as damage to the brain caused by an external impact, such as

penetration by an object or blast wave[15]. The primary causes of TBI are sports-

related injuries, blast exposures, automobile accidents, and falls. In sports,

concussions (or repeated TBIs) have gained increased public awareness and are

known to increase the risk of dementia and can lead to chronic traumatic

encephalopathy and other cognitive disorders in retired athletes[16]. Blast TBIs are

the result of blast pressure waves from explosive devices and are frequently observed in soldiers from Iraq and Afghanistan[17]. Clinical studies usually classify brain injuries based on severity (mild to severe). However, in studies using animal models the resulting injury can be sub-classified based on the form of injury (open or closed head injury), type of impact (impact or blast), location within the brain (focal or diffuse), and symptoms (sub-concussive or post-concussive).

The severity of the injury is initially scored on the Glasgow Coma Scale, a tool used to evaluate a patient's motor, verbal, and eye opening response. Advances in medical imaging, such as computed tomography (CT) and magnetic resonance imaging (MRI), are used extensively to confirm the existence and severity of injury. TBI is grouped into three severities: mild, moderate, or severe. Mild TBI (mTBI) is the most common and results in no overt changes within the brain. Skull fractures, hemorrhage, and altered brain structure(s) are rarely observed by CT scan and standard MRI following mTBI[18]. mTBI often leaves the patient with temporary symptoms; however, clinical studies along with research in animal models show progressive long-term neuropsychological disruptions[19, 20]. In contrast, moderate and severe TBIs result in visible neuroimaging changes within the brain, including hemorrhage and edema[21]. Most survivors are left with permanent cognitive and physical impairments[21]. Severe TBIs require immediate medical attention and often exhibit involvement in multiple brain regions. The

long term pathological consequences in these mild to severe TBI cases appears to be a disruption of the white matter tracts and systemic inflammation[22].

Neuropathology of TBI from the initial primary injury is followed by a secondary injury cascade. Primary injury is the mechanical damage that occurs at the time of injury and results in shearing of neurons, glia, and blood vessels. Primary injury is untreatable and only preventable by limiting exposure to the inciting event and taking safety precautions. Secondary injury, on the other hand, occurs over time and initiates a variety of signaling cascades that alter cell function and/or cause cell death. Some common events include oxidative stress, excitotoxicity, mitochondrial dysfunction, and inflammation[23]. These secondary events can last hours to years after the injury and can contribute to functional deficits and long-lasting disabilities[24]. Thus, preventing or mitigating the effects of secondary injury is potentially critical to improving the lives of TBI victims.

Vascular Consequences of TBI

Extensive research has been conducted to identify potential therapeutic targets for TBI, but none have successfully been translated to the clinic. One major consequence of TBI that has not been extensively investigated is damage to the cerebral vasculature. The disrupted vasculature participates in the pathogenesis of TBI and can lead to secondary injury in the form of hemorrhage, edema, changes in blood flow, and blood brain barrier disruption. A better understanding of how these vascular effects after TBI result in chronic disabilities

could lead to the development of improved therapeutics. Here, we will review

different types of cerebrovascular complications that occur after TBI and their

impact on brain pathology.

Hemorrhage

Hemorrhage occurs in 46% of all TBIs and is increasingly prevalent in

moderate and severe injuries[25]. An insult to the brain results in bleeding that can

gradually progress over the first 24-48 hours. In some cases, the leaking blood

collects outside the vessel forming a hematoma. Three distinct types of

hemorrhage are reported after TBI and are based on their location in the brain:

epidural hematomas (between the dura mater and skull), subdural hematomas

(between dura and arachnoid mater), and subarachnoid hemorrhage (between

the arachnoid and pia mater). Of the three types, post-traumatic subarachnoid

hemorrhage is the most severe and is associated with increased mortality and

poor outcomes[26]. The effects of hemorrhage results in increased intracranial

hypertension, vasospasms, and compression of structures in the brain[27].

However, this depends on the amount and degree of bleeding into the

parenchyma. While most hemorrhage resolves on its own, microbleeds can still

be present causing deposition of hemosiderin that is detectable by MRI[28].

Accumulation of ferritin/hemosiderin is known to be toxic to brain cells and can

elicit an inflammatory response[29]. Interestingly, preclinical studies demonstrated

that delayed microbleeds following TBI are associated with white matter damage[30, 31].

<u>Edema</u>

Cerebral edema, the excess accumulation of fluid within the brain, accounts for 50% of deaths in severe head injuries[32]. Pediatric patients are at greater risk of developing edema than adults[33]. After TBI, cerebral edema forms at the lesion and incorporates into the surrounding tissue. Two distinct types have been observed, cytotoxic and vasogenic edema. Cytotoxic edema results in water accumulation in cells and is caused by dysregulation of the sodium and potassium pumps on the cell surface[34]. The retention of water and ions can adversely affect cell function and even lead to apoptosis. The blood brain barrier remains intact in cytotoxic edema[34]. Vasogenic edema results in water accumulation in the extracellular space and is caused by the disruption of the blood brain barrier[34]. Vasogenic edema is associated with elevated intracranial pressure, tissue swelling, changes in blood flow, and compression of brain structures[35]. Although it has been accepted that cytotoxic edema occurs immediately after injury and leads to vasogenic edema, recent studies have expanded on this concept and proposed two transitional forms of edema that occur after stroke[6, 34]. In this model, anoxic and ionic edema result in dysregulation of the components of eNVU which leads to increased vascular permeability and development of vasogenic edema[34].

Changes in Cerebral Blood Flow (CBF)

Altered CBF is one of the most common outcomes of TBI. Both regional and global changes in blood flow are observed but depends on the size, location, and type of tissue injury (i.e. contusion, hematoma, or diffuse edema)[36]. A majority of TBI patients have significant reductions in CBF within the first 12 hours after injury[36, 37], but this is dependent on the severity of the injury. It has been reported that CBF values can reach ischemic levels falling to 18-20 ml/100 ml/min after severe TBI (normal values in humans are ~45–50 ml/100 ml/min)[36, 38]. After this initial period, many patients experience hyperemia (increase in CBF values compared to normal tissue) while others have shown low or normal CBF values[39, 40]. Interestingly, at later times after injury there is an apparent uncoupling between blood flow and tissue metabolism, with long-term outcomes being vasospasms and hypoperfusion[39]. These decrements in CBF can result in ischemic brain injury, which is the leading cause of death after severe TBI[39]. Although CBF typically normalizes within several weeks, therapeutic procedures to enhance blood flow acutely are needed and could have significant clinical benefits for TBI patients[41].

Vasospasms

Vasospasms, or the abnormal constriction of blood vessels, can adversely affect functional recovery after TBI. The reported incidence of vasospasms after

head injury ranges from 19-68%[42]. While most vasospasms are short-lived, severe episodes can last longer but typically resolve by 14 days in closed head injuries[43]. Blast TBI victims have been reported to have a higher frequency of developing vasospasms than other forms of head injuries and can last up to 30 days after injury[44]. The cause of vasospasms after TBI remains undetermined, but others have suggested that it triggered by hypertension and subarachnoid hemorrhage[45]. A study by Dore-Duffy indicated that pericytes release endothelin-1, a potent vasoconstrictor molecule, near the blood vessels after TBI[46]. Vasospasms can reduce cerebral perfusion to regions of the brain, which could lead to ischemic injury and infarction if untreated[45]. Clinicians undertake extensive efforts to manage vasospasms early in order to avoid long-term injuries.

Blood brain barrier (BBB) Disruption

BBB disruption following TBI has been well-established. The most common technique to assess BBB disruption in humans is by cerebral spinal fluid/serum albumin quotient, which measures albumin in cerebral spinal fluid in reference to blood serum. Ho et al. in a retrospective cohort study of patients with severe non-penetrating TBI found that 44% of patients experience BBB disruption which was associated with poor long-term outcome[47]. Although BBB disruption typically returns to normal by several weeks, some patients have reported it to last months and years after mild injuries[48]. The BBB regulates the

9

movement of substrates between the blood and central nervous system (CNS)

and is critical in maintaining cellular homeostasis. This selective barrier is

composed of tightly connected endothelial cells together with astrocytes,

neurons, and pericytes (forming the eNVU). The endothelial tight junction

proteins that seal the BBB become disrupted after TBI, either by the contusion

and/or increased intracranial pressure[49]. Neutrophils also exacerbate BBB

disruption by secretion of proteases and cytokines[50]. The disruption of BBB leads

to the release of harmful molecules into the local injury microenvironment such

as iron, reactive oxygen species, and blood toxins.[51]. Such molecules can

augment inflammation and increase the risk of edema and hypertension[47].

Coagulopathy

Altered coagulation profiles after TBI have been reported in numerous

studies[52-54]. Harhangi et al.[52] in a systematic review of 82 studies confirmed that

coagulopathies were present in TBI patients with a prevalence of 33% and that

there was a significant correlation between mortality and poor outcomes. One

key finding of most studies is that the severity of the TBI is related to the degree

of coagulopathy which is in turn related to outcomes and mortality. Further, the

time course of the coagulation abnormalities is also dependent upon the severity

of injury[55]. The coagulation cascade appears to be dramatically altered after

moderate and severe TBIs, initiated in large part by the release of tissue factor

(TF) into the circulation leading to depletion of coagulation factors (extrinsic

pathway), decreased platelets, altered BBB and leading to increases in circulating microparticles[56-58]. Hyperfibrinolysis, with increases in d-Dimer, have also been proposed to be a marker of outcomes via a potential cascade wherein TF can increase activation of the extrinsic pathway[59]. Alternatively, low platelet levels may also contribute to increased hemorrhagic evolution particularly early after hospitalization[60].The hemostasis mechanisms that can be impacted by TBI are clearly varied but ultimately lead to inflammation, hyperfibrinolysis, endothelial dysfunction, and platelet abnormalities. Thus, it is clear that early coagulation mechanisms play a significant role in TBI outcomes but more research is warranted on improved biomarkers and therapeutic interventions[61, 62].

Chronic Inflammation

While the inflammatory response is initiated minutes after injury and protects against pathogens, eliminates necrotic cells, and promotes tissue repair, it has become apparent that chronic inflammation is associated with CNS damage[63, 64]. Microglia cells, the resident macrophages in the brain, have drawn much attention. Microglia are rapidly activated in response to injury and work to limit the extent of tissue damage[63]. However, persistent microglial activation is a key contributor to secondary brain injury. Several studies have shown that microglia can become activated for weeks to years after brain injury[65-67]. Assessment of postmortem tissue of TBI patients who died months after the injury revealed increased activation of microglia in the white matter tracts[67].

Microglia can become over-active in response to danger-associated molecular pattern factors that are released by damaged cells[68]. As a result, over-active microglia produce high levels of inflammatory cytokines and cytotoxic factors that cause further neurodegeneration[69]. Additionally, the sustained release of these factors disrupts the BBB, resulting in the transit of inflammatory factors and peripheral immune cells into the brain thereby further increasing the inflammatory response[51].

Cerebral Vascular Injury: Repair or Pathology?

At present, there are scant reports looking at repair of the vessel network following brain injury. Several studies suggested that the injured cerebral vasculature is repaired by 14-28 days, but repair results in morphologically abnormal vessels [9, 70-73]. To address this gap in knowledge, we developed a novel method to stain, visualize, and analyze the cerebral vasculature in the whole mouse brain and applied this method to study the vascular alterations following TBI [74]. We reported that TBI results in vascular loss followed by an increase in new vessels at 7 days post injury (dpi) [75]. The newly formed vessels appeared irregular and showed increased branching and smaller vessel structures in compared to the uninjured vessels. Additionally, we used our novel vessel staining and analysis technique to document the acute changes to the cerebral blood vessels after TBI and observed dramatic alterations in vascular parameters not only at the injury site but also in the contralateral brain in a rat

model of TBI [76]. Extending these early studies we observed that moderate TBI which results in gross vascular injury is subsequently followed by repair over the course of 2 weeks (unpublished results, Fig. 1.1). The degree of vascular repair is dependent on the severity of the injury [9] and age [77]. Our own recent findings showed that at 7 dpi male mice have increased vessel number and complexity in the injured cortex compared to female mice suggesting that vascular repair mechanisms may be dependent on sex [78]. Similarly, blood flow resumes to the perilesional tissue by 14-21 days [70, 79, 80]. However, some studies reported hypoperfusion in the restored vessel network indicating that vascular repair does not implicitly result in improved vascular function [70, 81]. Steinman et al.[71] indicated that abnormal patterning of the repaired vasculature is associated with hypoperfusion 4 weeks after controlled cortical impact. Collectively, research indicates that there is delayed repair of the blood vessels after TBI and that when repair occurs it can lead to morphological and functional vascular abnormalities.

It is clear that the vascular repair process is influenced by the severity of the injury. Park et al. [9] explored vascular loss and recovery using a fluid percussion injury model. Their study utilized two injury severities, a moderate (2 atm) and a severe (3 atm) injury and evaluated the vasculature at 1 and 14 days post injury. Both severities resulted in significant vascular injury at 1 day post injury compared with sham animals. The moderately injured animals showed improvements by 14 days after injury, where microvascular density in the injured cortex recovered to near-sham levels. Conversely, the severely injured animals

showed a significant reduction in microvascular density in the injured cortex by 14 days post injury. The repaired vasculature of moderately and severely injured animals was abnormal, with an increase number of irregular and torturous vessels. This study highlights that vessel repair can be abnormal and may contribute to the pathological outcomes after brain injuries.

Other studies have noted significant alterations to the newly formed blood vessels. While morphological changes to the cerebral vessels are apparent early after TBI[82, 83], it appears that these deficits do not fully recover and can persist for weeks and months after the initial injury. Electron microscopy showed aberrations to the vessel walls, ridged elastic lamina, swelled and apoptotic endothelial cells, and degraded extracellular matrix[84-86]. Both large and small vessels appear to be affected. In a fluid percussion injury model, injured rats had fragmented capillaries and reduced capillary diameter at 30 days post injury [73]. Gama Sosa et al. [72] utilized a blast model of mTBI and observed a unique vascular pathology that led to chronic changes in the vessels 6 months after injury. These malformed vessels likely increase the risk of delayed hemorrhage, hypoperfusion, and other secondary effects[31, 87]. Also an outcome of poor vascular repair when coupled with cerebrovascular dysfunction can lead to further exacerbation of tissue injury. Thus, damaged and abnormal repair of the vasculature may be an important contributing factor to poor outcomes often observed after TBI in humans and in rodent models.

New Vessel Formation Following Injury

The formation of new blood vessels (or vascular repair) after acquired brain injury has increasingly gained interest. It has been well-documented that after TBI two primary mechanisms, angiogenesis and vasculogenesis occur (Fig. 1.2). While both angiogenesis and vasculogenesis are active during embryonic development and lead to the formation of a primitive vascular network, they also play a role in promoting vascular repair in the adult after injury. These complex but distinct processes play an important role in repairing the injured vasculature after TBI.

Angiogenesis

Angiogenesis is the formation of new blood vessels from an existing vasculature. New vessels form by sprouting from the main vessels (sprouting angiogenesis) or splitting in two daughter vessels (intussuscepted angiogenesis). Sprouting angiogenesis is commonly observed after injury and is mediated by resident endothelial cells (ECs), which line the luminal surface of the blood vessels forming the endothelium[88]. As previously mentioned, new vessel sprouts are detected at a relatively short time after injury with many studies reporting increased capillary density after TBI[7, 9, 70, 89], where new capillaries appear to migrate from the peri-lesional tissue into the injury site[75].

Tissue hypoxia, or low tissue oxygenation, is one of the primary triggers of angiogenesis. Clinical studies have reported the presence of hypoxia after TBI,

which is typically caused by cerebral hypoperfusion and ensuing ischemia[37, 90].

Experimental TBI animal models revealed an up-regulation of hypoxia-driven

molecules in the injured brain. One key reporter molecule is Hypoxia-inducible

factor-1α (Hif-1α)[9, 91], which has been associated with vascular repair in stroke

and other disease models. Low oxygen inhibits the degradation of Hif-1α where it

accumulates and binds to hypoxia-inducible factor-1β. This transcription factor

promotes expression of a number of angiogenic growth factors[92]. These factors

constitute a class of signaling molecules that are involved in vascular repair. For

example, VEGF exhibits robust expression in the latter stages of experimental

and clinical TBI[93, 94]. Other factors are also up-regulated and contribute to

vascular repair (a more thorough discussion of angiogenic factors will be

described later in this review).

Sprouting angiogenesis is an important repair process that requires the

coordinated interactions of ECs. The endothelium is activated in response to

brain trauma[95]. The hypoxic tissue causes release of angiogenic growth factors

into the nearby tissue[92]. These factors signal to the nearby vessels to detach the

pericytes and degrade the local extracellular matrix[92]. ECs form vessel sprouts

and then migrate and proliferate in the direction of the hypoxic tissue[96]. To

facilitate this process, ECs specialize into distinct phenotypes known as

endothelial tip and stalk cells: tip cells migrate and lead the vessel sprout while

neighboring stalk cells proliferate and form the vessel lumen[88]. Initially, an

immature and unstable vascular structure is formed. Following recruitment of the

pericytes, this immature vessel is remodeled to form a stable, functioning vessel[92].

Vasculogenesis

Vasculogenesis is the de novo formation of new blood vessels. The term vasculogenesis has been used in various injury models and refers to a subset of bone marrow-derived cells with vasculogenic potential. Increasing evidence suggests that endothelial progenitor cells (EPCs) play an important role in postnatal vasculogenesis[97]. These CD34+ cells originate from the bone marrow and circulate through the vasculature in response to injury. Many TBI studies have detected increased numbers of EPCs in the blood as well as blood vessels at the injury site[98-100].

The initiator(s) of vasculogenesis has been a subject of debate, but many speculate that it is triggered in a hypoxic-dependent fashion. A prime example where this is known to occur is in tumor biology, in which many tumors create a hypoxic environment that leads to vascularization. In hypoxic tumors, Hif-1 mobilizes EPCs to induce vascular growth[101]. Stromal-derived factor-1α (SDF-1α), a chemo-attractant factor that is regulated by Hif-1, helps recruit EPCs to the tumor site[102]. Similar to tumors, tissue hypoxia is evident at the TBI lesion site and leads to the expression of angiogenic growth factors including SDF-1α[92]. These factors enter the blood circulation and signal to the bone marrow to mobilize EPCs. Serum VEGF and angiopoietin-1 levels show a significant

correlation with circulating EPCs in patients with severe TBIs suggesting that these growth factors may mediate recruitment of EPCs into the blood stream[98]. Thus, hypoxia is likely the driving force for vasculogenesis after moderate and severe TBI.

Unlike angiogenesis, vasculogenesis is initiated in the bone marrow. EPCs remain adhered to the marrow stromal cells under physiological conditions. After injury, EPCs become activated where they are released from the stromal cells and enter the blood stream[101]. In TBI patients, EPC levels decrease at 1-2 days post injury and rapidly increase and peak by 5-7 days after injury[98, 99, 103]. Within the blood, EPCs mature and acquire similar phenotypes as ECs[104]. EPCs are known to home to sites of vascular injury[101]. Gou et al.[100] detected CD34+ EPCs around the lesion at 1 day after TBI which peaked at 7 days post injury. The levels of EPCs correlated with angiogenesis after TBI. The function of EPCs has been much debated, but many studies suggest that EPCs play a dual structural and instructive role in vasculogenesis. EPCs can incorporate into the injured vessels and differentiate into new ECs[7, 100]. Additionally, others have shown that EPCs act as supporting cells that release trophic factors to the injured vessels[105, 106]. These secreted factors induce angiogenesis by promoting proliferation and migration of ECs[106].

Supportive role of the eNVU

Various cells types participate in angiogenesis and vasculogenesis after injury. Although EPCs and ECs are considered the two primary players in these repair processes, the other components of the eNVU, such as astrocytes, pericytes, and neurons, also possess angiogenic functions and have been largely overlooked in TBI repair. Additionally, macrophages and perivascular macrophages are thought to play a significant role in the vascular response to injury (Table 1.1).

Astrocytes

Astrocyte activation after injury has been well described and are known to accumulate around a lesion, in a process known as astrogliosis. These cells perform numerous functions, some of which are related to vascular repair. Reactive astrocytes are known to secrete trophic factors that promote angiogenesis and BBB repair. Astrocytes are an important source of angiogenic growth factors after TBI, including VEGF and SDF-1α[89, 107]. High mobility group box 1 (HMGB-1), a danger-associated molecular pattern molecule, has been suggested to have beneficial effects in the chronic stages after brain injury. HMGB-1 mediates crosstalk between astrocytes and ECs and EPCs after injury and can lead to neurovascular remodeling[108-110]. Additionally, astrocytes can produce tenascin, thrombospondin, and other proteins found in the extracellular matrix[111].

Astrocytes also participate in glial scarring. Although much of the focus has been placed on its inhibition related to axonal regeneration after injury[112], glial scarring may play a beneficial role in vascular repair. During scarring, reactive astrocytes have close interactions with peri-lesional vessels[113]. These intimate interactions with blood vessels are evident at 7-60 days post injury, which coincides with the formation of the new vasculature. Astrocytes are integral components of the BBB and are essential for normal BBB function[114]. Thus, these astrocyte-vessel interactions may function in stabilizing the blood vessels and restoring blood flow to the injured tissue.

Pericytes

Accumulating evidence suggests that pericytes are important players in vascular repair. Pericytes, or mural cells, cover the surface of the micro-vessels where they reside within the basement membrane in direct contact with the endothelium[115]. The pericyte population declines in the first few days after controlled cortical impact (CCI)[116]. Additionally, a majority of the pericytes are observed leaving the blood vessels after weight drop impact. Their detachment from the vessels facilitates a critical step for angiogenesis[46], as pericytes are required to destabilize and detach from the vessel wall which allows ECs to form vessel sprouts. A number of angiogenic factors are responsible for their detachment from the vessels[117].

At later stages of injury, pericytes become reactive and dramatically increase around the lesion, in a process known as pericytosis. When active, pericytes secrete angiogenic growth factors that mediates EC activity and vascular integrity[115]. Angiopoietin-1 is one such factor and has been shown to induce expression of the tight junction protein occludin[118]. Along with providing trophic support, active pericytes make close interactions with newly formed vessels[119]. Pericyte recruitment is critical for the latter stages of angiogenesis and contributes to stabilizing the new vessel[119].

Neurons

While neurons are essential for functional recovery after injury, there is some evidence that they may also participate in vascular repair. Following brain injury increased neurogenesis is observed in the sub-ventricular zone[120], in which new neurons are localized to the peri-lesional vessels[121]. Administration of neural progenitor cells after TBI results in a transient increase in angiogenesis adjacent to the lesion border[122]. Neural stem and progenitor cells are known to secrete trophic factors into the injury microenvironment, including a number of angiogenic growth factors[123]. Interestingly however, one study showed that neurons limit angiogenesis by binding and sequestering angiogenic factors in the retina[124]. Although this work was specific to retinal neurons, it is plausible that cortical neurons act in a similar manner and may guide angiogenic branching toward the

injury site. Thus, this raises the possibility that neuronal cells may be important in regulating post-injury angiogenesis.

Macrophages

Macrophages, a monocyte-derived cell that is part of the inflammatory response, have been implicated in vascular repair. Activated macrophages are grouped into two forms: classically activated, anti-angiogenic macrophages (M1) or alternatively activated, pro-angiogenic macrophages (M2 including the M2a and M2c subsets)[125]. However, primary human M1 macrophages have been shown to secrete pro-angiogenic molecules in vitro[126]. After CCI macrophages are broadly activated adopting both an M1 and M2 phenotype[125, 127], but appear to be a shift to M1 phenotype at later time points[128]. Macrophages can express angiogenic growth factors and matrix remodeling proteases after TBI, including VEGF, FGF, and MMP-9[89, 129]. In fact, they contribute significantly to late increases in VEGF levels[89]. Additionally, macrophages may mediate vascular pruning through secretion of pro-apoptotic factors[130]. Along with providing trophic support, these cells physically interact with the sprouting vessels. Liu et al.[131] demonstrated that macrophages promote repair of cerebrovascular ruptures in a zebrafish model. Macrophages were seen adhering to the ends of the ECs and ligating the ruptured vessels. Also, during development macrophages mediate fusion between endothelial tip cells leading to vessel growth and anastomoses[132].

Perivascular macrophages

Unlike peripheral macrophages that infiltrate the brain parenchyma, perivascular macrophages reside in the perivascular space and are closely associated with vessel walls[133]. After weight drop injury, there was a significant increase in the number of CD163+ perivascular macrophages between 2-4 days post injury, which was mainly localized to the lesion site[134]. The extent to which perivascular macrophages mediate vascular repair after TBI is presently unknown, but are likely to have similar functions as peripheral macrophages. Perivascular M2 macrophages have been implicated in tumor angiogenesis and depletion of these cells attenuates vascularization and tumor growth[135]. Additionally, perivascular macrophages are critical in maintaining vascular integrity under physiological conditions[133]. M2 macrophages, but not M1 macrophages, have a significant impact on barrier integrity which is likely due to strong interactions with the endothelium [133]. Thus, perivascular macrophages may function in stabilizing the new vessels after trauma.

Injury-Induced Signaling Factors Involved in Vascular Repair

The growth of new blood vessels after injury involves an intricate timing of various angiogenic factors and downstream signaling cascades. There is growing body of work that suggests TBI increases levels of angiogenic factors into the injured brain parenchyma to mediate vascular repair. Several growth factors,

chemokines, protease enzymes, and certain cytokines have been identified and possess angiogenic functions after TBI. Here we review several important extracellular factors that are known to directly affect the vasculature and discuss their respective roles in the vascular repair process (Table 1.2). We propose a molecular mechanism in which these signaling factors interact and lead to vascular repair (Fig. 1.3). Other factors, such as pro-inflammatory cytokines, may indirectly affect vascular repair and will not be described here but have been reviewed extensively previously[136].

Vascular endothelial growth factor (VEGF)

VEGF is a key regulator of angiogenesis and modulating its levels has a significant effect on vessel formation[93]. Krum et al.[94] utilized a specific neutralizing antibody to inhibit endogenous VEGF and tested its effect on tissue repair after brain infusion injury. Neutralizing VEGF levels resulted in a significant reduction in vessel proliferation and an increase in vessel degeneration. Administration of VEGF has emerged as a potential treatment for vascular injuries. Several studies have shown that VEGF treatment enhances angiogenesis in TBI[137, 138], ischemia[139, 140], and stroke[141]. VEGF signaling is mediated through Flt-1 (VEGF-R1) and Flk-1 (VEGF-R2) that are expressed on ECs[142]. Flk-1 is the predominate receptor and is associated with angiogenesis[142]. Binding of VEGF to Flk-1 (and neurophilin-1 co-receptor) induces down-stream signaling pathways such as Mitogen activated protein kinase (MAPK) and

Phosphoinositide 3′ kinase (PI3K)[143]. Together these pathways promote EC proliferation, migration, and survival, which are indispensable for angiogenesis[143]. These effects are prevalent in the chronic stages of TBI, where VEGF levels are increased around the injury site[89].

VEGF has been shown to increase EPC expression and induce vessel formation after hind limb and myocardial ischemia as well as physiological conditions, confirming its role in postnatal vasculogenesis[97]. As we have stated earlier in this review, much of the work on VEGF-mediated vasculogenesis was performed in tumors and its role in TBI is limited to correlative studies in patients[98, 144]. VEGF regulates EPC activity in a similar manner as ECs. In EPCs, VEGF binds to Flk-1 and leads to their mobilization and release from the bone marrow and induces differentiation[101]. The effects are mediated by the PI3K pathway which leads to expression of nitric oxide (NO; a potent vasodilator) and MMP-9[145].

Fibroblast growth factor 2 (FGF2)

Similar to VEGF, FGF2 is a potent mitogen and stimulator of angiogenesis. Given its angiogenic effects, FGF2 administration has been utilized in several brain injury models. FGF2 treatment after closed head injury has been shown to increase vessel density compared with non-treated animals[138]. However, animals treated with VEGF alone showed higher vessel growth than FGF2. ECs express both FGF receptors (FGFR-1 and FGFR-2) and

are sensitive to the FGF family. Binding of FGF2 to its receptors leads to

activation of proliferative, migratory, and survival processes[146]. MAPK, PI3K, and

Phospholipase C gamma (PLCγ) pathways have been linked with these

important angiogenic processes[146]. Alternatively, Kano et al. have proposed a

mechanism involving FGF2 induction of VEGF with FGF2 signaling acting in

conjunction with VEGF signaling to promote angiogenesis[147].

FGF2 is critical in maintaining vascular integrity. Wang et al.[148] showed

that FGF2 treatment after CCI preserved BBB integrity and improved

neurological function. The authors found that FGF2 activates the PI3K pathway

and leads to up-regulation of tight junction proteins (claudin-5 and occludin) and

inhibits RhoA, an antagonist of BBB formation. Rac-1, a down-stream effector of

the PI3K, is responsible for FGF-2 protective effects of the BBB[148]. Similar

findings were observed in a model of intracerebral hemorrhage, wherein FGF2

treatment reduced BBB damage, cerebral edema, and improved outcomes[149].

Stromal cell-derived factor 1 alpha (SDF-1α)

SDF-1α is an important chemokine for various cell types. Recent studies

found that SDF-1α attracts CD34-expressing cells from the bone marrow, which

include EPCs and ECs. Inhibition of endogenous SDF-1α after TBI reduces the

number of CD34+ cells, which coincides with decreased vessel density around

the injury site[150]. Further evidence suggests that exogenous SDF-1α has

angiogenic benefits. Administration of SDF-1α after fluid percussion and weight

drop impact acceleration injury enhances vessel formation, reduces BBB

damage, and improves neurological outcomes[150, 151]. The most extensively

studied SDF-1α receptor is CXCR4, which is expressed on EPCs, ECs, and

smooth muscle cells[152]. Following injury, neural stem/progenitor cells and other

damaged cells release SDF-1α into the injury microenvironment. ECs are known

to up-regulate SDF-1α expression when exposed to hypoxia[152]. SDF-1α binding

to CXCR4 activates PLCγ and Rho pathways to promote a chemotactic

response[153]. As a result, CD34-expressing cells are activated and migrate toward

the SDF-1α gradient[154]. Along with recruiting cells, SDF-1α has been shown to

directly regulate EC and EPC function via the PI3K and MAPK pathway[153].

Matrix metalloproteinase-9 (MMP-9)

MMP-9 is a protease enzyme that is necessary for initiating

angiogenesis[155]. This enzyme is expressed by ECs and functions by degrading

the extracellular matrix, which provides for sufficient space for EC migration and

the formation of new vessel lumens[156]. Some matrix proteins that are degraded

by MMP-9 include collagen, laminin, thrombospondin, and fibronectin[157].

Additionally, it is critical in the processing and activation of growth factors thereby

affecting the levels of pro- and anti-angiogenic factors in the tissue[157]. For

example, MMP-9 can cleave and release activated VEGF in tumors cells[157].

MMP-9 also mediates vasculogenesis by affecting EPC activity. In animal

models of TBI, MMP-9 levels increase and localize to EPCs and cortical vessels

around the lesion[158]. Serum MMP-9 levels correlate with increases in EPC levels in clinical TBI[144]. Huang et al. [159] showed that MMP-9-deficient mice have reduced vascularization after ischemic injury resulting from reduced EPC expression and stem cell activating cytokines such as Kit ligand. These cytokines promote activation of stem cells into the bone marrow and have been implicated in hematopoiesis. EPCs are normally quiescent and remain attached to the stromal cells of bone marrow mediated by membrane bound Kit ligand (inactive form) [160]. After injury, bone marrow cells activate the PI3K pathway to increase production of NO which in turn up-regulates MMP-9[161]. MMP-9 converts the inactive Kit ligand to its active soluble form, sKit[160]. Consequently, sKitL disrupts EPC adhesion to the bone marrow allowing for their mobilization and release into the blood circulation.

Angiopoietin-1 (Ang-1)

Ang-1 promotes vessel stabilization in the latter stages of vascular repair. Because of its angiogenic effects, delivery of exogenous Ang-1 may have significant benefits if administered early. Pharmaceutical compounds, such as simvastatin, can increase Ang-1 expression and are known to improve vascular function in stroke models[162]. Under physiological conditions, cerebral vessels express high levels of Ang-1. After cryogenic injury, there is a marked decrease in Ang-1 in the acute stages[163]. This is accompanied by increases in Ang-2, which is an Ang-1 antagonist and is associated with BBB breakdown. At 2-6 days

post injury, Ang-1 levels slowly increase which correlates with angiogenesis[163]. Ang-1 is primarily produced by pericytes and directly interacts with ECs[164]. Both Ang-1 and Ang-2 signal through the Tie-2 receptor, with Ang-1 acting as an agonist and Ang-2 as an antagonist[164]. The balance between Ang-1 and Ang-2 determines its signaling. Ang-1/Tie-2 signaling promotes EC proliferation, migration, and survival, in part through activation of the VEGF pathway[164].

Ang-1 has also been linked to vasculogenesis. Serum Ang-1 and EPCs showed similar expression profiles in patients with severe TBIs, suggesting a possible role in mobilizing EPCs from the bone marrow[98]. The mechanism is not completely understood, but many suggest that Ang-1 stimulates vasculogenesis through the VEGF pathway. Activation of the PI3K pathway is critical and leads to the up-regulation of NO, MMP-9, and sKit[160].

Erythropoietin (EPO)

EPO, a well-recognized hematopoietic cytokine, can act as a growth factor in different tissues[165]. Although EPO controls erythropoiesis (production of red blood cells), emerging evidence suggests that EPO contributes to angiogenesis. EPO treatment has shown promising results in animal models of TBI. Delayed EPO treatment after CCI increases vascularization around the injury site and improves vascular function in a dose-dependent manner[166]. EPO treatment after CCI resulted in enhanced CBF induced by L-arginase administration, likely by stimulating production of NO[167]. Although EPO is mostly produced in the kidney,

increased expression of EPO and its receptor (EPO-R) are evident in ECs, neurons, and astrocytes after injury[168]. EPO expression is regulated by HIF-1[143]. In ECs, EPO/EPO-R signaling stimulates VEGF expression which in turn activates VEGF signaling[169].Neural progenitor cells are also affected and may interact with ECs to promote angiogenesis[170]. In addition, EPO can activate the PI3K pathway independent of VEGF[169].

The angiogenic effects of EPO are partly the result of vasculogenesis. Wang et al. [171] studied the effects of recombinant human EPO treatment in a rat fluid percussion injury model. Human EPO treated animals showed significantly higher EPC levels after TBI, with increased numbers of CD31+ and CD34+ cells found around the lesion. Treated animals also showed improved spatial learning and memory. Similarly, EPO has been shown to increase EPC expression and enhance angiogenesis after myocardial infarction and stroke[172, 173]. EPO is thought to stimulate vasculogenesis through VEGF signaling and the down-stream PI3K pathway, increasing the expression of NO and MMP-9[169].

von Willebrand factor

von Willebrand factor (vWF) is a glycoprotein that is increased in response to TBI, with elevated serum levels are an indicator of poor outcomes[174]. vWF is well-recognized for its role in blood coagulation by promoting platelet adhesion to sites of damaged vessels and aggregation to form the hemostatic plug[175-177]. It is also known to complex with coagulation Factor VIII. This protein is normally

present in its inactive form when bound to vWF, but is activated and released following blood vessel damage[176]. Upon release, Factor VIII interacts with other coagulation factors to promote blood clotting. After vascular injury, the endothelium rapidly secretes vWF into the plasma and basement membrane[175]. vWF binds to collagen near sites of vessel damage and acts as a bridging molecule that interacts with circulating platelets. vWF interaction with the platelet receptor (GPIb-IX) leads to platelet activation and firm integrin-dependent adhesion to the vessel wall[175].

Unlike most growth factors, vWF has been shown to inhibit angiogenesis. Loss of vWF results in increased vessel formation in vitro and in vivo[178]. vWF modulates VEGF-R2 dependent angiogenesis by either interacting with integrin αvβ3 on the cell surface and/or affecting storage of Ang-2 within Weibel-Palade bodies[179]. Thus, vWF likely controls premature vessel formation by countering angiogenic factors. Additionally, staining for vWF is routinely used to detect for activated vessels that are subjected to high levels of pro-angiogenic factors[180].

Wnt/β-catenin in Vascular Repair

Given the need to develop new therapies, it is important to identify other signaling mechanisms that may be activated after TBI. One novel unexplored factor is β-catenin, which regulates the canonical Wingless and INT-1 (Wnt) signaling pathway and cell-cell adhesion.

Functions of β-catenin and small molecules to modulate β-catenin

Wnts are secreted, lipid modified glycoproteins that are essential for many biological processes including cell proliferation, migration, polarity, and differentiation. Wnt ligands activate two types of signaling pathways: canonical Wnt pathway (or Wnt/β-catenin pathway) which acts through β-catenin and noncanonical Wnt pathway which acts independently of β-catenin [181]. The noncanonical Wnt pathway encompasses the Wnt/planar cell polarity and Wnt/Ca^{2+} pathways. Of the three pathways, the canonical Wnt pathway is the best characterized. Many studies support a role of deficient and aberrant canonical Wnt pathway in birth defects, cancers, neurodegenerative diseases, and central nervous system injuries [182, 183].

β-catenin is transcriptional coactivator of the canonical Wnt signaling pathway (Fig. 1.4). In the absence of Wnts, the levels of β-catenin levels are kept low by the actions of the destruction complex consisting of Axin, Adenomatous polyposis coli (APC), Glycogen Synthase Kinase 3 (GSK3), and Casein Kinase 1 (CK1). CK1 and GSK3 phosphorylate β-catenin which targets it for ubiquitination and degradation by the proteasome. In presence of Wnts, Wnts bind to the Frizzled receptor and Low density lipid receptor-related protein 6 (LRP5/6) co-receptor which leads to dissociation of the destruction complex. This results in accumulation of β-catenin in the cytoplasm where it can enter the nucleus and bind to Lymphoid enhancer factor/T-cell factor (LEF/TCF) transcription factors to activate transcription of Wnt target genes. Among the many Wnt target genes is

32

CCND1, which encodes the cell cycle regulator Cyclin D1 [184]. Wnt components such as Frizzled, LRP5/6, Axin, and TCF/LEFs, are often positively and negatively regulated by TCF/β-catenin [181].

In addition to its role in the canonical Wnt signaling pathway, β-catenin is also an adaptor protein of the adheren junctions involved in cell-cell adhesion. β-catenin binds to the cytoplasmic domain of cadherins and in association with α-catenin links cadherin proteins to the actin cytoskeleton. The cadherin-catenin complex is regulated by phosphorylation: phosphorylation of β-catenin leads to dissociation of the cadherin-catenin complex and loss of cell-cell adhesion while dephosphorylation of β-catenin has the opposite effect [185]. Furthermore, cadherins act as negative regulators of the canonical Wnt signaling by binding β-catenin to the cell surface and sequestering it from the nucleus [186, 187]. Thus, the function of β-catenin is based on its location in the cell (membrane bound vs. nuclear).

A number of small molecules have been reported to modulate the canonical Wnt signaling by targeting various components of the pathway. One commonly used compound is Lithium Chloride (LiCl), which was shown to increase expression of β-catenin and Wnt genes in multiple studies[188-190]. There are a few studies that have used LiCl in animal models of TBI[191-194]. LiCl inhibits GSK3 of the destruction complex and increases β-catenin levels [188] (Fig. 1.5). However, GSK3 also regulates multiple other pathways in addition Wnt signaling including AKT-dependent signaling [195]. JW74 is a small molecule which

increases degradation of β-catenin leading to reduced cellular concentrations[196, 197]. JW74 has been utilized in in vivo studies and shown to inhibit growth of colorectal cancer cells in mouse xenograft models [196]. JW74 is an inhibitor of Tankyrase 1 and 2, which marks Axin for degradation and its inhibition enhances Axin stability in the destruction complex and leads to β-catenin degradation [197] (Fig. 1.5).

Wnt/β-catenin in Vascular Development and TBI

The canonical Wnt signaling pathway has been demonstrated to promote blood vessel formation during vascular development. Several studies using Wnt reporter lines observed increased TCF/LEF activity in endothelial cells of the central nervous system (CNS) starting at embryonic day (E) 9.5 [198, 199] followed by a gradual downregulation as the vessels mature [200]. Several canonical Wnts, such as Wnt7a and Wnt7b, are expressed in the neural tube that coincides with CNS angiogenesis [198]. Loss of Wnt7a/b or endothelial specific deletion of β-catenin impairs formation of the embryonic vasculature leading to malformed vessels, diffuse hemorrhage, and ultimately early lethality in utero [198, 199, 201]. Endothelial specific increase of β-catenin alters vascular development leading to reduced length and branching of vessels and loss of venous structures [202]. Developmentally, the timing and access to β-catenin is critical to the formation of the nascent vasculature.

The canonical Wnt pathway in conjunction with Notch signaling plays an important role in the formation of nascent blood vessels [202]. The canonical Wnt signaling regulates Sox17 and this transcription factor induces Notch signaling leading to formation of arteries and veins [203, 204]. Furthermore, canonical Wnt signaling regulates formation of the blood brain barrier by stabilizing adheren junctions and increasing expression of the glucose transporter Glut-1 [198, 200, 201, 205].

There are several reports that conclude that the canonical Wnt signaling pathway is reactivated after brain injury and participates in repair processes. White et al. [206] using a Wnt reporter line observed increased TCF/LEF activity in glial progenitor cells and astrocytes after TBI, suggesting that Wnt/β-catenin signaling may be involved in gliogenesis. Several studies found upregulation of Survivin and Serum- and glucocorticoid-regulated kinase in neuronal cells after TBI which were implicated in neurogenesis and neuronal survival [191, 207, 208]. Survivin and Serum- and glucocorticoid-regulated kinase are anti-apoptotic factors and inhibitors of GSK3-β. Furthermore, post injury LiCl treatment reduces neuronal cell death and results in improved cognitive performance [191-194]. We recently reported increased β-catenin expression in cerebral vessels after TBI which coincides with vascular repair [75]. Taken together, the published record would strongly suggest that Wnt/β-catenin signaling is a key regulator for neuronal, glial and vascular repair after TBI. However, there have been no

studies explicitly examining the role of Wnt/β-catenin signaling in TBI and its

temporal evolution (Fig. 1.6).
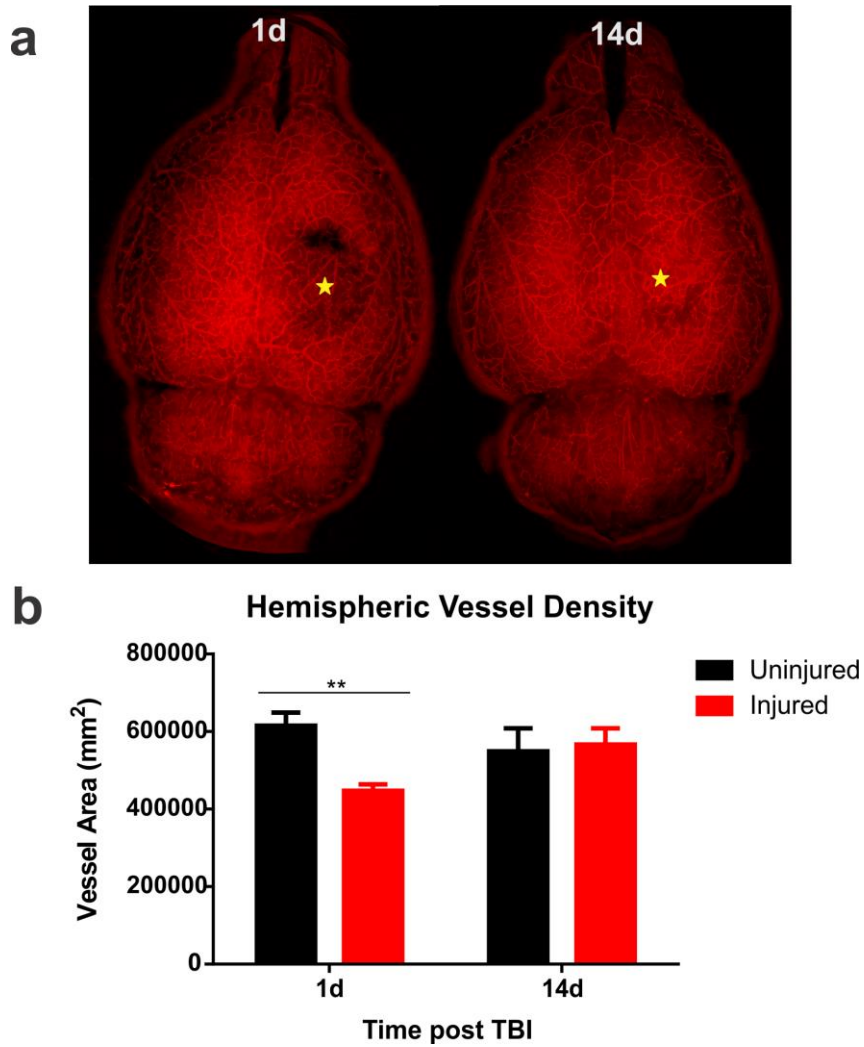
Figure 1.1. TBI results in vascular injury with subsequent repair. A) We induced a moderate controlled cortical impact (CCI) in the right hemisphere of adult rats (n=5-6/group). Animals underwent vessel painting to stain the cerebral vasculature at 1 and 14 days after injury. Our vessel painting technique is performed by injecting DiI (lipophilic 1,1′-dioctadecyl-3,3,3′,3′-tetramethylindocarbocyanine Perchlorate) solution into the left ventricle followed

by cardiac perfusion and fixation. Whole brain axial images were obtained using wide-field fluorescent microscopy (representative images are shown). Moderate CCI elicits a loss of vasculature that extends beyond the injury site. Over the ensuing 14 days, there is increased vascular density at the injury site. Injury site (star). B) We performed a classical vascular analysis to quantify the features of labeled vessels in the injured and uninjured hemisphere. Vascular analysis of the injured hemisphere revealed a reduction in vessel density at 1 day in compared to the uninjured hemisphere (t-test, **$p<0.01$). Vessel density was restored and returned to baseline levels by 14 days (t-test, $p=0.82$). All error bars are presented as standard error of mean.
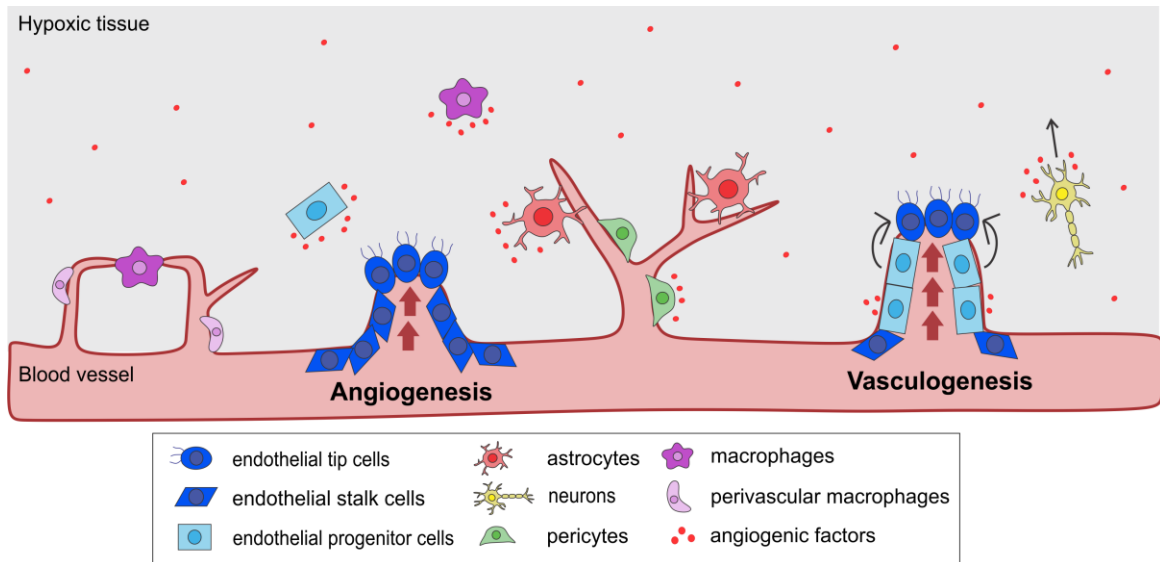
Figure 1.2. New vessel formation after TBI. Brain trauma leads to damage to the cerebral vasculature with subsequent repair via angiogenic and vasculogenic processes. Mature endothelial cells, in particular endothelial tip and stalk cells, are involved in various steps of angiogenesis. Tip cells (blue oval shape) are found at the end of the vessel sprout and they use their filipodia to guide the sprout toward the angiogenic growth factor source, while stalk cells (blue trapezoid shape) are found inside the vessel lumen and they proliferate to extend the sprout. Circulating endothelial progenitor cells (light blue rectangular shape) play a key role in postnatal vasculogenesis but also contribute to angiogenesis. Endothelial progenitor cells are recruited from the bone marrow that then incorporate into the damaged vessels and differentiate into endothelial cells. Endothelial progenitor cells also are important for the release of angiogenic factors, which regulate angiogenesis. Other cell types support or augment angiogenesis and vasculogenesis. Astrocytes (red), pericytes (green), and

perivascular macrophages (light purple globular shape) cooperate with the newly formed vessel and promote vessel stabilization. Neuronal cells (yellow) are associated with the blood vessels and release angiogenic factors that may guide the vessel sprout toward the injury site. Macrophages (dark purple star shape) have been shown to adhere and ligate ruptured vessels in the brain. Additionally, a majority of these cells release angiogenic growth factors into the hypoxic tissue.
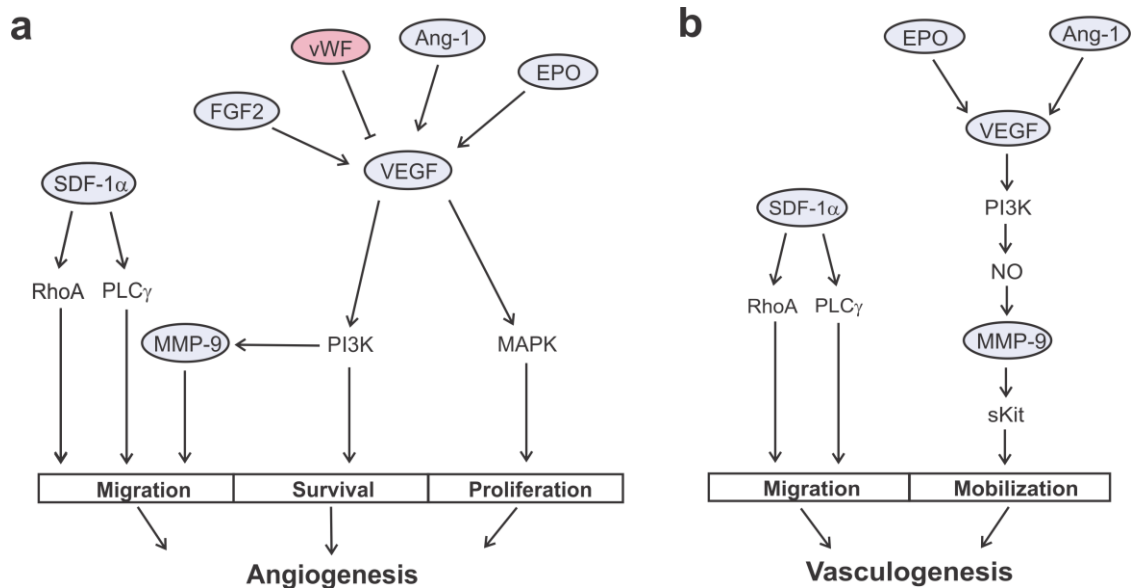
Figure 1.3. Possible interactions between signaling molecules. A) The interplay between these angiogenic factors is critical in understanding the molecular mechanism(s) of vascular repair. After trauma, active cells release angiogenic factors into the injured tissue. VEGF is the key inducer of angiogenesis, which activates PI3K and MAPK pathway leading to EC survival and proliferation. FGF2, Ang-1, and EPO are also up-regulated at distinct times after TBI and these factors signal through VEGF signaling, either by increasing expression of VEGF and/or initiating down-stream PI3K and MAPK pathways. Along with pro-angiogenic factors, anti-angiogenic factors, including vWF, have been shown to inhibit angiogenesis. Migratory processes are controlled by SDF-1α, which activates down-stream PLCγ and RhoA pathway. MMP-9, a target of the PI3K pathway, is pivotal for EC migration. B) Angiogenic factors are released into the blood stream which can activate cells from bone marrow. Serum VEGF, EPO, and Ang-1 are elevated after TBI and have been associated with postnatal

vasculogenesis. Similar to angiogenesis, vasculogenesis is mediated by the

VEGF signaling pathway. VEGF causes activation of the PI3K pathway and

leads to the up-regulation of NO and MMP-9. MMP-9 converts the Kit ligand to its

active, soluble form (sKit). sKit is responsible for mobilizing EPCs from the bone

marrow. Activated EPCs then migrate to sites of injury in a process known as

chemotaxis. SDF-1α activates down-stream PLCγ and RhoA pathway to induce

EPC migration.
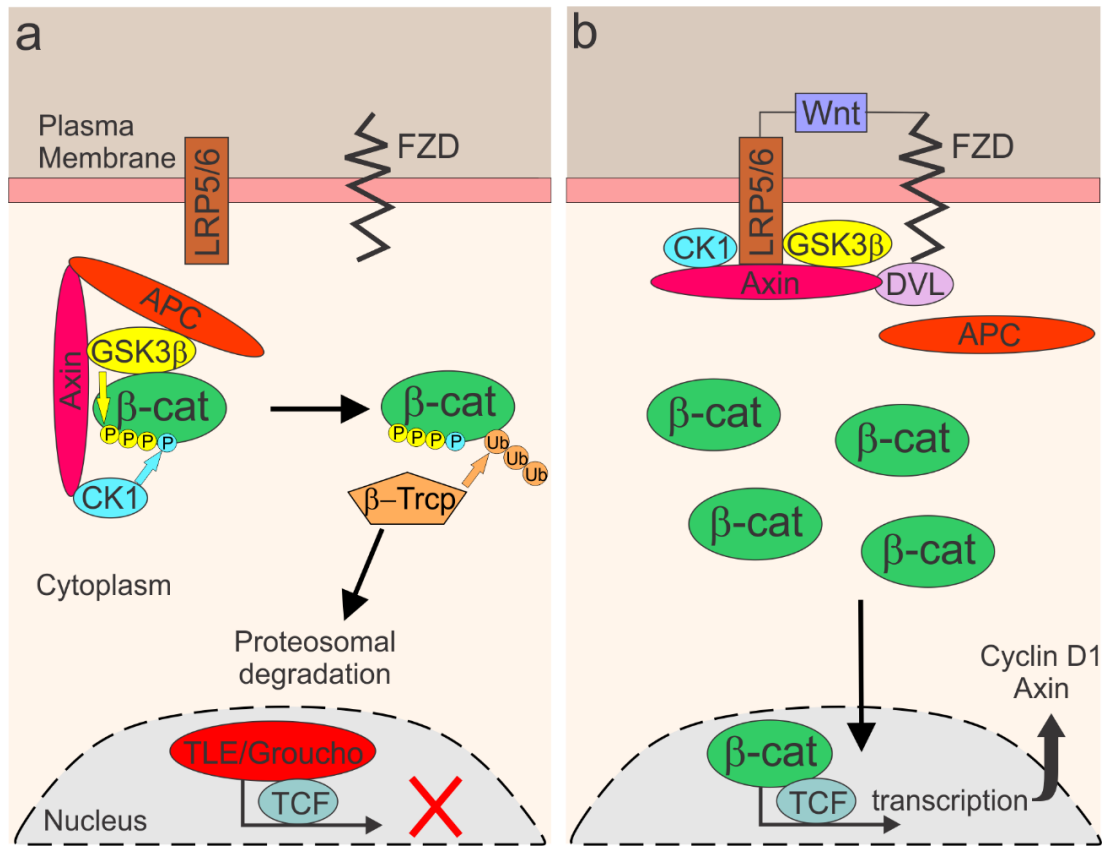
Figure 1.4. The canonical Wnt signaling pathway. (A) In the absence of Wnt, cytoplasmic β-catenin forms a complex with Axin, APC, GSK3β, and CK1 and β-catenin is phosphorylated by CK1 (blue) and then by GSK3β (yellow). Phosphorylated β-catenin is recognized by β-Trcp and it is ubiquitinated (orange) and targeted for proteosomal degradation. Wnt target genes in the nucleus are repressed by TLE-Groucho. (B) In the presence of Wnt, Wnt binds to FZD and LRP5/6 which recruits DVL. DVL then recruits Axin/CK1/GSK3β to the cell membrane. This disrupts phosphorylation and degradation of β-catenin, allowing β-catenin to accumulate in the cytoplasm and enter the nucleus to serve as a co-activator of TCF to activate Wnt target gene such as Cyclin D1 and Axin.

Abbreviations: APC, adenomatous polyposis coli; CK1, casein kinase 1; β-cat, β-catenin; DVL, Dishevelled; FZD, Frizzled; GSK3β, glycogen synthase kinase 3 β; LRP, low-density lipoprotein receptor-related protein; TCF, T cell factor; TLE, transducing like enhancer of split 1; β-Trcp, β-tranducin repeats containing protein.
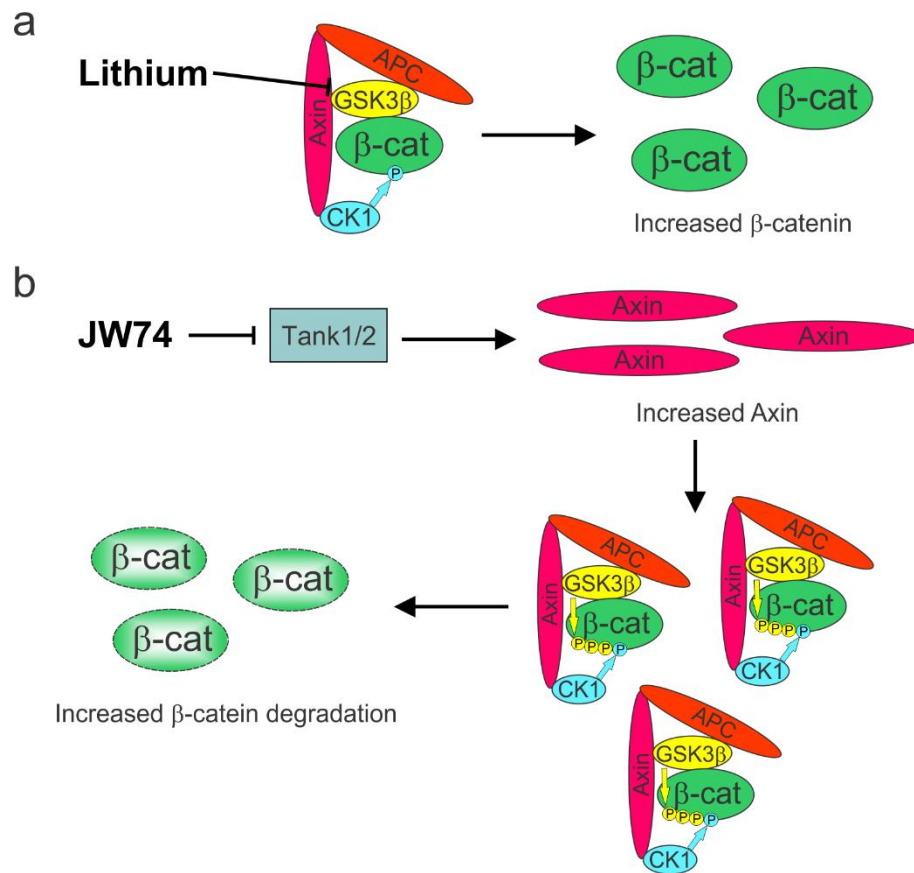
Figure 1.5. Mechanism of action by Lithium Chloride and JW74 on β-catenin. (A) Lithium Chloride inhibits GSK3β which prevents phosphorylation of β-catenin and leads to an increase in β-catenin levels. (B) JW74 inhibits Tank1/2 leading to stabilization of Axin and leads to accumulation of Axin, APC, GSK3β, and CK1 complexes that then controls enhanced β-catenin degradation.

Abbreviations: Tank1/2, Tankyrase1/2
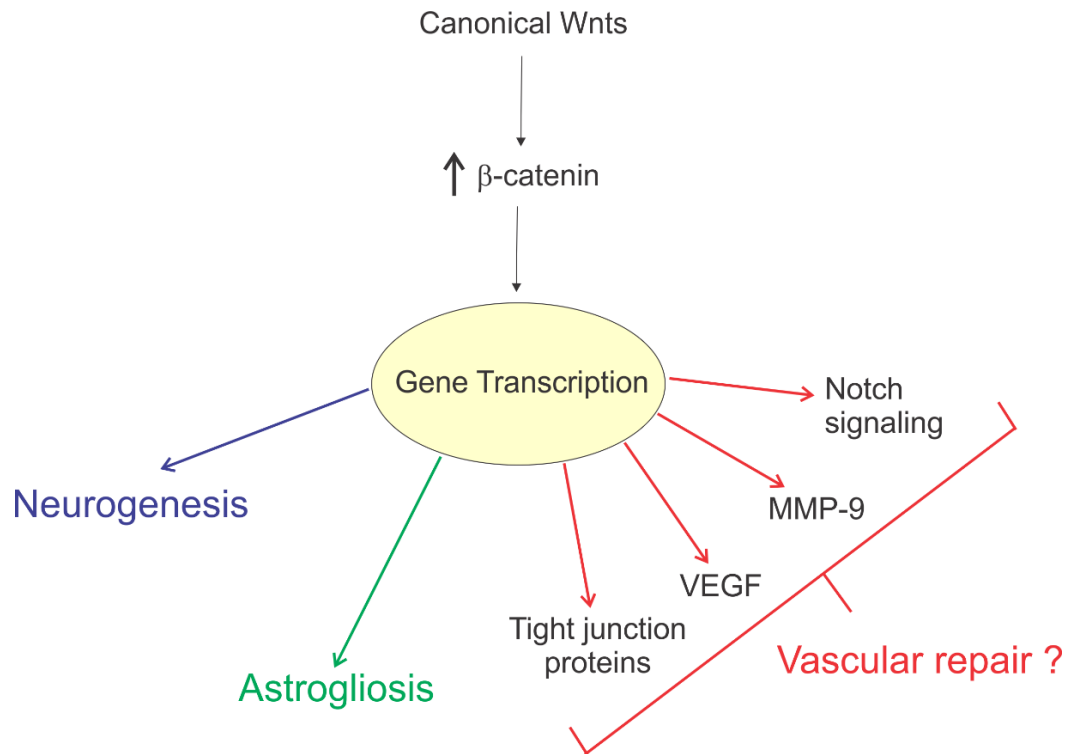
Figure 1.6. Wnt/Beta-catenin signaling in TBI. The Wnt/β-catenin pathway is tightly regulated by soluble Wnt factors. In the presence of these factors, β-catenin escapes degradation where it accumulates and promotes transcription of Wnt target genes. The role of Wnt/β-catenin signaling after TBI is not completely understood, but many suggest that it is involved in regenerative processes such as astrogliosis and neurogenesis. It is unclear at the present times what role Wnt/β-catenin signaling plays in vascular repair, but there is compelling data in support for it. During vascular development, Wnt/β-catenin signaling is required for the development of CNS blood vessels and works in conjunction with Notch signaling in arterial-venous specification. Additionally, many angiogenic growth factors (VEGF), metalloproteases (MMP-9), and tight junction proteins (Claudin 3

and ZO-1) are both directly and indirectly modulated by the Wnt signaling cascade. Thus, Wnt/β-catenin pathway and its associated molecules may be involved in repairing the injured vasculature after TBI.

Table 1.1. Active cell types in vascular repair.

Cells	Functions	References
Endothelial cells	Proliferation and migration to form new vessels	88*
Endothelial progenitor cells	Mobilization from the bone marrow, homing to sites of vascular injury, and in situ differentiation/trophic support	98-100, 103
Astrocytes	Trophic support, vessel stabilization	111, 113, 136
Pericytes	Triggering angiogenesis, trophic support, vessel stabilization	116, 119*
Neurons	Trophic support, possible role in vessel guidance	122, 123*
Macrophages	Trophic support, vessel adhesion and ligation	89, 131
Perivascular macrophages	Vessel stabilization	133

* Papers covers general aspects of vascular repair

Table 1.2 Role of extracellular factors in modulating vascular response.

Factors	Functions	References
VEGF	Promotes angiogenesis and vasculogenesis	94, 98, 137, 138, 209, 210
FGF2	Promotes angiogenesis and maintains BBB integrity	138, 148, 211
SDF-1α	Attractant for ECs, EPCs, and other vascular cells	150, 151, 212, 213
MMP-9	Extracellular matrix degradation and expression of cell activating cytokines	158, 159
Ang-1	Maintains and stabilizes blood vessels; associated with vasculogenesis	98, 163
EPO	Contributes to angiogenesis and vasculogenesis	166, 171, 214
vWF	Controls hemostasis and inhibits angiogenesis	177, 178

Chapter 2

Novel Protocol to Visualize and Analyze the Cerebral Vasculature

<u>Preface</u>

This chapter has been reproduced from … Salehi, A., A. Jullienne, K. M. Wendel, M. Hamer, J. Tang, J. H. Zhang, W. J. Pearce, R. A. DeFazio, Z. S. Vexler and A. Obenaus (2018). "A Novel Technique for Visualizing and Analyzing the Cerebral Vasculature in Rodents." Translational Stroke Research *with permission from Springer Nature*

This chapter discusses a novel protocol to stain, visualize, and analyze the cerebral vasculature in the rat and mouse brain.

Reproduced from manuscript: Figure 2.1 – 2.9, Table 2.1

Abstract

We introduce a novel protocol to stain, visualize, and analyze blood vessels from the rat and mouse cerebrum. This technique utilizes the fluorescent dye, DiI, to label the lumen of the vasculature followed by perfusion fixation. Following brain extraction, the labeled vasculature is then imaged using wide-field fluorescence microscopy for axial and coronal images and can be followed by regional confocal microscopy. Axial and coronal images can be analyzed using classical angiographic methods for vessel density, length and other features. We also have developed a novel fractal analysis to assess vascular complexity. Our protocol has been optimized for adult rat, adult mouse, and neonatal mouse studies. The protocol is efficient, can be rapidly completed, stains cerebral vessels with a bright fluorescence, and provides valuable quantitative data. This method has a broad range of applications and we demonstrate its use to study the vasculature in assorted models of acquired brain injury.

Introduction

The brain is one of the most metabolically active organs in the body. In order to satisfy its high metabolic needs, the brain requires an intricate network of blood vessels that constitutes the cerebral vasculature. Cerebral vessels are responsible for maintaining constant blood flow throughout the brain[215]. Perturbations or cessation in blood flow, for example during ischemic stroke, can

lead to irreparable neuronal injury in a matter of minutes[216, 217]. At the cellular level, the cerebral vessels engage with neuronal and non-neuronal cells to regulate blood flow in accordance to neuronal activity (neurovascular coupling)[215, 218, 219]. The vascular endothelium forms a restricted barrier called the blood brain barrier, which controls the entry of molecules into the brain and is essential for creating a protective environment for neurons[215]. Thus, maintaining an intact blood brain barrier with blood flow regulated in response to metabolic need is crucial for cerebral health.

An important challenge facing preclinical research are methods to rapidly visualize the cerebral vasculature at the whole brain level. The ability to image cerebral vessels would be invaluable in understanding the vascular anatomy in healthy developing and mature brains. Neuroscientists need a reliable method to study cellular and morphological aspects of vascular pathology following a variety of brain injuries and diseases. In addition, the effects of promising therapeutics targeting the cerebrovasculature require methods for assessment. Thus, there is an urgent need to develop sensitive and more efficient techniques to visualize the cerebral vessels in the entire brain.

Several techniques have been developed that permit for visualization of cerebral vasculature of the rodent brain. One such technique is called Vessel Painting (VP), which was originally developed to visualize the 3D blood vessel network in the retina and was recently modified to stain the cerebral vasculature[220-222]. The VP technique utilizes a lipophilic carbocyanine dye, 1,1′-

dioctadecyl-3,3,3′,3′-tetramethylindocarbocyanine perchlorate (DiI) to label endothelial cell membranes. VP is achieved through measured intracardiac injection of an aqueous DiI solution followed by perfusion brain fixation. When the DiI molecules come in contact with the vessel lumen, it is incorporated within the lipid membranes thereby staining the entire vessel lumen[220]. Originally, a major drawback of this technique was that it had low success rate and labeled vessels typically exhibited heterogeneous staining, precluding repeatable quantitative whole or regional analysis. Furthermore, the original retinal studies were not adapted to stain the cerebral vasculature in rats.

Vascular analysis has been accomplished using manual analytical programs (ImageJ plugins) and semi- and full-automated software programs[223, 224]. A recently developed tool is AngioTool, a fully automated program that performs a comprehensive quantitative analysis focusing particularly on vessel network features and computes various morphometric and spatial parameters including number of vessels, vessel length, branching, lacunarity, amongst others. AngioTool has been utilized in simple vascular systems such as murine embryonic hindbrain, retinal and allantois explants[225]. AngioTool features have not been optimized for large scale analysis of the rodent cerebrovasculature. Use of fractals as a measure of complexity has not been routinely employed in neuroscience and few reports exist for its utilization in morphological characterization of cerebral vessels[226, 227]. Fractal analyses have been used to evaluate roughness and patterning of neuron structures and microglial

morphology[228-230]. Fractals have recently been used to study tumor and retinal vessels[231, 232], and we have been one of the first to use it in evaluation of whole brain rodent cerebrovasculature[233].

Here, we present a novel protocol to stain, visualize, and analyze the blood vessels in the rodent brain. Our novel VP technique has been adapted for the adult rat brain and further improved to label vessels in the adult and neonatal mouse brain. Unlike previous techniques, our technique stains cerebral vessels with a bright red fluorescence that allows for visualization by wide-field fluorescence and confocal microscopy. Another key advantage of our technique is that it stains the blood vessels in the entire brain (in 3D) across rodent species and ages. We will introduce two complimentary analysis approaches that have been adapted for brain vasculature in rodents: classical analysis to assess vessel characteristics and fractal analysis to measure vascular complexity. We applied our protocol to analyze the cerebral vasculature in adult and neonatal mice and obtained quantitative parameters of vessel density, length, and complexity. Finally, we demonstrate its ability to be used in a variety of acquired brain injury models where vascular alterations are known to occur. Further, the protocol is uncomplicated, involves a minimum number of steps, and requires only a handful of standard laboratory materials.

Materials

<u>Reagents</u>

DiI (1,1'-dioctadecyl-3,3,3'3'-tetramethylindocarbocyanine perchlorate, Life

Technologies, Carlsbad, CA)

Ethanol (Absolute, 200 proof)

Sodium Nitroprusside (SNP, dihydrate, Sigma Aldrich, Saint Louis, MO)

Heparin, sodium injection 1000 USP units/mL (Sagent pharmaceuticals,

Schaumburg, IL)

Phosphate buffered saline (PBS, 1x; MP Biomedicals, Solon, OH; catalog

number 0928103)

- PBS contains 2.68mM Potassium Chloride, 1.47mM Potassium

   Phosphate Monobasic, 136.89mM Sodium Chloride, and 8.10mM Sodium

   Phosphate Dibasic at pH 7.4

Paraformaldehyde (PFA, 32%)

Dextrose (Anhydrous, Fisher Scientific, Fair Lawn, NJ)

<u>Preparation of reagents</u>

DiI stock solution: 100mg DiI, 33.4mL 100% ethanol. Cover with aluminum foil

and store at room temperature for up to 1 year.

Diluent solution: 2g dextrose, 1ml 10x PBS, adjust with ddH$_2$O to 50mL. Filter

through a 0.22µm bottle-top filter. Stable at 4°C for several months. Diluent

solution is warmed to 37°C prior to adding the DiI stock solution.

DiI working solution (see Note 1):

Method 1

i. Adult rat (250g): 200μL DiI stock solution, 900μL 100% ethanol, adjust with Diluent solution to 50mL.

ii. Adult mouse (25g): 40μL DiI stock solution, 180μL 100% ethanol, adjust with Diluent solution to 10mL.

Method 2

i. Adult mouse (25g): 50μL DiI stock solution, 450μL Diluent solution.

ii. Neonatal mouse (12g): 25μL DiI stock into 225μL of Diluent solution.

SNP stock solution: 0.75mg SNP, 1ml sterile 1x PBS. Protect from light and refrigerate at 4°C. Stable for 1 week

SNP-heparin injection solution: 0.75mg/kg SNP stock solution, 2000 units/kg heparin (see Note 2).

Equipment

Method 1

Nitrogen tank

Two 100mL bottles

PE-50 tubing

Tygon lab silicone tubing, 1/32 inch (Cole-Parmer, Vernon Hills, IL)

Three-way stopcock (cat# WU-30600-02, Cole-Parmer)

22 gauge Luer stub adapters (cat# 724439, Harvard Apparatus, Holliston, MA)

Male to male Luer lock connectors (cat# 12090, Qosina, Edgewood, NY)

Pressurized air tank, 2L empty plastic bottle with air tight cap

27 gauge Luer stub

30 gauge needle

1mL syringe with plunger cut

10mL syringe

Syringe pump (Harvard Pump II Plus single syringe, Harvard Apparatus,

Holliston, MA)

Method 2

Two 100mL bottles

FH100 Peristaltic pump (Thermo Fisher Scientific, Waltham, MA)

1mL syringe with 23 gauge needle

1mL syringe with plunger cut

Tygon lab silicone tubing, 1/32 inch (origin)

Methods

Two methods to stain the cerebral vasculature

Method 1 procedure

Method 1 was initially based on a protocol developed for mice by Hughes and

colleagues[220] and modifications to the protocol were made to improve the

efficiency and facilitate its use in rats (Fig. 2.1a). The initial protocol utilized a

pressurized air tank to deliver the perfusion solutions, but air leakage often

resulted in an inability to maintain constant pressure throughout the system.

Thus, to overcome these limitations we switched to nitrogen compressed gas

tank that provided continuous delivery of perfusion solutions under careful and

constant pressure (1.7 PSI). PBS and PFA solutions were then delivered under

constant pressure while the DiI solution was delivered under constant flow rate

using a syringe pump. The three-way stopcock assembly controlled which

solutions were flowing from the outflow port (Fig. 2.7).

1. Assemble the perfusion apparatus. A detailed description of how to
   construct the perfusion apparatus can be found in Hughes' article[220] (Fig.
   2.7). As stated above, the pressurized air tank was replaced with a
   compressed gas nitrogen tank.

2. Before starting the procedure, it is imperative that the entire system is
   airtight and devoid of all air bubbles.

3. Anesthetize mouse or rat by intraperitoneal injection of ketamine
   (90mg/kg) and xylazine (10mg/kg) or by other institutionally approved
   method.

4. In a perfusion tray, secure the animal on its back. Make an incision along
   the thoracic midline to open the abdominal cavity. Cut the diaphragm.
   Carefully cut the chest wall on both sides. Take a small hemostat to hold
   the sternum and turn it toward the head to expose the chest cavity.

5. Inject the SNP-heparin solution (0.75mg/kg SNP stock solution and 2000 units/kg heparin) into the left ventricle

6. Insert the butterfly needle from the perfusion device into the left ventricle and then make a large incision in the right atrium.

7. Rotate the stopcock knob for the PBS to the "on" position. Perfuse with 1x PBS (rats: 150mL, mice: 10mL) to remove the blood. A sign of a good perfusion is uninterrupted flow of blood exiting the right atrium.

8. Rotate the stopcock knob for the DiI solution to the "on" position and then activate the syringe pump. Perfuse with DiI solution (rats: 50mL, mice: 10mL) at a constant flow rate (rats: 10mL/min, mice: 1mL/min). During perfusion with DiI solution, the nose and palms of the animal will turn slightly pink.

9. Rotate the stopcock knob for the PFA to the "on" position. Perfuse with 4% PFA (rats: 200mL, mice: 20mL) to fix the brain tissue.

10. Remove brain from the skull and post-fix in 4% PFA for 24 hours. Brains can be left in 1x PBS in the dark for several weeks at 4°C.

Method 2 procedure

While Method 1 works in adult mice, visual examination found that a majority of mice (75%) showed heterogeneous staining of the cerebral vessels. Imaging of vessel painted brains revealed lack or reduced staining of capillary structures indicating that the DiI solution was not successfully penetrating into the

capillaries using nitrogen tank as the pressure source. To improve circulation of the DiI solution into these fine vessels in the mouse brain, we modified the Method 1 protocol by direct manual injection of the DiI solution into the left ventricle of the heart (Fig. 2.1b). By performing an intracardiac injection of DiI solution into a beating heart prior to the PBS perfusion step, this allows for the DiI to circulate through the entire cerebral vasculature, thereby labeling all the blood vessels, including fine capillaries. The PBS and PFA solutions were then delivered at a pulsating flow rate using a peristaltic pump (9mL/min for adult mice and 5mL/min for neonatal mice). The labeling efficiency rate for the adult and neonatal mice was higher with the peristaltic pump than the compressed gas nitrogen tank because it is likely that the pulsating flow rate perfusion better mimics the physiological conditions in the mouse than the constant pressure perfusion. The syringe pump, stopcock assembly, and its associated components are not needed for Method 2 (see Note 3 for methodological differences between Method 1 and 2).

1. Before starting the procedure, make sure that the perfusion line is devoid of air bubbles.

2. Anesthetize mouse or rat by intraperitoneal injection of ketamine (90mg/kg) and xylazine (10mg/kg) or by other institutionally approved method.

3. Secure the animal on its back and open the abdominal cavity. See Step 4 in Method 1 for more detail.

4. Inject the SNP-heparin solution (0.75mg/kg SNP stock solution and 2000 units/kg heparin) into the left ventricle

5. Manually inject the DiI solution (adult mice: 500μL, neonatal mice: 250μL) into the left ventricle slowly over the course of 10-12 seconds (see Note 4). In a few cases, the heart in neonatal mice stopped beating as the DiI solution was being injected and the heart was manually pumped using forceps to assist in circulating the solution (see Note 5). During incubation with the DiI solution, the nose and palms of the animal will turn slightly pink.

6. Insert the butterfly needle from the perfusion device into the left ventricle and then make a small incision in the right atrium

7. Perfuse with 1x PBS (adult mice: 10mL, neonatal mice: 8mL) to remove the blood. A sign of a good perfusion is uninterrupted flow of blood exiting the right atrium.

8. Perfuse with 4% PFA (adult mice: 20mL, neonatal mice: 15mL) to fix the brain tissue.

9. Remove brain from the skull and post-fix in 4% PFA for 24 hours. Brains can be left in 1x PBS in the dark for several weeks at 4°C.

Different variations of our VP protocol have utilized in other studies and are described in Note 6.

Removal of brain and assessment of vessel painting success

To assess the success of our VP, brains were carefully removed from the cranium without damaging the vasculature or the underlying tissues. The dura mater was gently removed from the surface of the brain which left the pial vessels intact within the pial and arachnoid layers. Extracted brains were then post-fixed in 4% PFA for 24 hours before being placed in 1x PBS. Success of VP was confirmed by visual inspection of the brain parenchyma. Excellent VP was determined if brains had uniform pink staining of the surface and deep structures of the brain (Fig. 2.1c) and excellent labeling of pial, penetrating, and parenchymal vessels assessed by wide-field fluorescence microscopy (Fig. 2.2). Animals that did not meet these two criteria were excluded from subsequent analysis. Method 1 showed excellent vessel staining from 67% (6/9) of adult rats and 25% (6/24) of adult mice; Method 2 showed excellent vessel staining from 71% (5/7) of adult mice and 37.5% (6/16) of neonatal mice (Table 2.1). Failed vessel painted brains exhibited heterogeneous staining and pale spots within the pink tissue (Fig. 2.1c, asterisks). Vessel painted brains with lack of pink staining were classified as "No staining". Method 1 and 2 have also been utilized in other applications and their success rates are reported in Note 7.

Wide-field fluorescence imaging of vessel painted brains

Vessel painted brains were imaged by wide-field fluorescence microscopy (BZ-X700, Keyence Corp, Osaka, Japan). The BZ-X700 fluorescent microscope

can image to a depth of 41.7 μm which allows for imaging of the surface cortical

vessels and parenchymal vessels of the brain. Acquisition of whole brain axial

images of the dorsal view was executed through careful positioning of the brain

between two glass slides. Gentle pressure was applied to minimally flatten the

dorsal surface of the brain to facilitate imaging of the entirety of the surface

cortical vascular network of the cerebrum without causing damage (Fig. 2.8). The

brains were gently pressed onto the glass slides until the compression ring is

formed in the outer perimeter of the brain resulting in clear view of the middle

cerebral artery trunk and its branching vessels. Z-stacks of the surface cortical

vessels were obtained at 2x magnification at 1mm depth of field to collect VP

data as the cortical surface curves laterally. Following acquisition, axial Z-stacks

were merged into full focus images using BZ-II Analyzer software (Keyence

Corp, Osaka, Japan). After axial images were collected, coronal images were

obtained by placing brains into an Acrylic Brain Matrix (Ted Pella, Inc., Redding,

CA) and slicing 5mm posteriorly from the olfactory bulbs to create an anterior and

posterior half-brain. The posterior half brain was placed on a glass slide (Fig. 2.8)

and imaged at 2x magnification at 1mm depth of field. The coronal Z-stacks were

merged into a full focus images.

Axial view images revealed uniform staining of the cortical vessels on the

surface of the brain (Fig. 2.2, top row). The pial vessel network, including

branching arteries from the middle, anterior, and posterior cerebral arteries and

leptomeningeal anastomosis, are clearly visible in our axial images. However,

there was limited staining of the superior sagittal sinus, transverse sinuses, and other venous structures (see Note 8 for limitations of our VP protocol). Coronal images of the anterior half brains confirmed well-defined staining of deep vessel structures within the brain (Fig. 2.2, bottom row). We observed distinct labeling of the penetrating vessels on the cortical surface and parenchymal micro-vessels in subcortical brain regions. Furthermore, there was no apparent leakage of the DiI working solution from the vessels into the cerebral tissue.

High resolution confocal microscopy

The DiI molecule has an intense fluorescence and fades slowly when exposed to excitation light during image acquisition[234]. Given its strong fluorescence intensity and slow fading properties, we tested whether DiI-labeled vessels are amendable to laser scanning confocal microscopy. Laser scanning confocal microscopy (Zeiss LSM 710 NLO, Jena, Germany) was used to acquire axial images from the dorsal surface of the cortex (wavelength Absorbance: 549nm, Emission: 565nm). Axial views of the brain were obtained between the middle and anterior cerebral arteries using a 5x magnification with 300μm depth of field. Images were subsequently processed to create maximum intensity projections using Zeiss software (Zeiss Zen 2010, Jena, Germany).

Axial confocal images revealed uniform staining of the pial, penetrating, and micro-vessels on the surface of the brain (Fig. 2.2, middle row). Adult mice stained with Method 1 typically showed heterogeneous staining of large vessels

and reduced or absent staining of micro-vessels, while adult mice stained with Method 2 had more uniform staining of large vessels and improved micro-vessel staining (compare confocal images of adult mice from Method 1 and Method 2). We detected small red aggregates attached to the vessel lumen using Method 1, which have been reported in other VP protocols[235, 236]. These dye aggregates were absent from adult mice stained with Method 2.

Classical vascular analysis

Wide-field fluorescence and/or confocal images can be utilized in a broad range of analysis methods. Quantitative analysis of vessel characteristics has previously been reported for simple vascular systems such as retinal explants (AngioTool)[225]. For the first time, we demonstrate that AngioTool can be utilized for large scale vascular analysis of the rodent brain (Fig. 2.3b, c). Analysis of the cerebrovasculature can be undertaken from the entire cortical surface or in regional sections based on the scientific question being studied. Herein we describe our analysis of the blood vessels from the left and right hemispheres. Using BZ-X Analyzer software, the raw fluorescent images were first processed for black balance and haze reduction (Blur/Brightness/Reduction: 10/10/1) to enhance the appearance of the vessels from wide-field fluorescent images (Fig. 2.3a). The processed fluorescent images displayed high resolution of the labeled vessels with reduced background signal (Fig. 2.9). The processed images were then imported into Fiji software (https://fiji.sc/) and region of interests (ROIs) were

drawn around the left and right hemispheres. The compression ring was

excluded from the analysis by drawing a ROI that encompassed the brain

surface along the curvature of the brain. The ROIs were saved and imported to

AngioTool software. The software then selects vessels based on their diameter

and fluorescence intensity and the values can be individually adjusted. For whole

brain analysis, the vessel diameter was set to 2 which selects vessels with

diameters greater than 2µm. The vessel intensity was set from 0 (minimum) to

255 (maximum) which indicates that vessels with a large range of fluorescence

intensity (faint to bright) were included in the analysis. The classical vascular

analysis generates an AngioTool image related to the number of vessels and

their branch points (Fig. 2.3b). The size and color of the features can be adjusted

according to the user, where the AngioTool image displays vessels in red, branch

points in blue, and vessel area outlines in yellow. Additionally, the software

provides vessel morphometric and spatial features, including vessel area, total

number of junctions, number of endpoints, and total vessel length (Fig. 2.3c, see

Note 9 for limitations of classical analysis). A detailed description of these

parameters can be found in the article from Zudaire and colleagues[225].

Fractal geometry analysis

The complex vasculature of the rodent brain can also be quantified by

fractal geometric analysis[226]. The use of fractals to analyze vascular structures is

rare and in the few reported studies it is used to assess retinal or tumor

vessels[231, 232]. We have developed a novel fractal analysis protocol that has been

adapted for analyzing the rodent cerebrovasculature (Fig. 2.3d-f). Our fractal

analysis provides unique and complimentary data on vascular complexity of the

whole brain, which cannot be derived using the classical vascular analysis

method (see Note 10 for differences between classical and fractal analysis).

Processed axial images were imported to Fiji software and converted into a

binary image. The polygon tool was used to outline the ROIs on the whole brain

hemispheres. Fractal analysis was performed using the ImageJ plugin that was

developed for microglia analyses, FracLac[237]. A local fractal dimensions (LFD)

analysis was performed from the binary images at each pixel using the box

counting method. The method applies the following formula D_{Bmass} =

$\lim_{\varepsilon \to 0} [\ln(\mu_\varepsilon)/\ln(\varepsilon)]$, where ε is the side length of the box and μ_ε is the mean pixels

per box of side ε. A $\ln(\mu_\varepsilon)$ vs. $\ln(\varepsilon)$ graph was generated and LFD was calculated

by taking the slope of the log regression line[228]. All output data and graphs were

saved. Following analysis, the software generated a colorized image visually

encoding the degree of complexity (Fig. 2.3d) where the color scale used can be

adjusted by the user (lookup table LUT4 used in this study) (Fig. 2.3e). The brain

vasculature is colorized with a gradient of low LFD (low complexity) in blue,

medium LFD (medium complexity) in yellow, and high LFD (high complexity) in

pink. The different colors correlate with the complexity of vessels, with large pial

vessels appearing more complex than micro-vessels. The distribution of LFD

displays a histogram with local fractal dimensions (complexity) in the x-axis and

frequency (vessel number) in the y-axis (Fig. 2.3f). Kurtosis, skewness, and peak

fractal frequency values are extracted from the fractal histograms. Kurtosis

describes the peakness (tailness) of the fractal distribution, skewness describes

the uniformity of the fractal distribution, and peak fractal frequency is the peak

fractal value.

<u>Notes</u>

1. Direct labeling of the cerebral vessels was achieved through the lipophilic

   carbocyanine dye DiI ($DiIC_{18}$ (3)), a lipid-soluble molecule that becomes

   incorporated into endothelial cell membranes upon contact. To facilitate

   efficient circulation of the DiI in the rodent circulatory system, an aqueous DiI

   working solution was prepared as previously described[220, 221]. This aqueous

   DiI working solution contains high concentrations of PBS along with dextrose

   in order to maintain osmolarity. In our preliminary work, we found that DiI had

   a tendency to precipitate out of solution at room temperature and this issue

   was resolved by heating the solution at 37°C prior to injection.

2. The doses for SNP (vasodilator) and heparin (anticoagulant) were based on

   previously published work[220]. The SNP-heparin injection prevents blood clot

   formation, improves homogeneity of the staining, and enhances DiI solution

   penetration into micro-vessels, facilitating improved vessel resolution.

3. There are several differences in methodology that must be noted. First,

   Method 2 is reliant on intrinsic blood flow to circulate the DiI solution

throughout the brain. As a result, this procedure only labels blood vessels with active perfusion. In cases when cerebral blood flow is reduced or absent, such as in acquired and non-acquired brain injuries, this could potentially affect the quality of the vessel staining and lead to poorly labeled vessels. Conversely, Method 1 is reliant on the PBS solution (under constant pressure) to remove the blood throughout the cerebrovasculature and subsequent delivery of DiI solution to label the vessels. Method 1 does not rely on the heart to circulate the DiI solution. Second, each method used different concentrations of the DiI working solution (12.8μM for Method 1 vs. 321μM for Method 2). The total volumes were also adjusted according to the rodent strain and age. We found that these DiI concentrations effectively labeled all the blood vessels in the entire mouse and rat brain, while also preventing the formation of dye aggregates. Third, the order in which the perfusion solutions were delivered differ between methods. Methods 1 delivered the DiI solution following the PBS solution, while Method 2 delivered the DiI solution prior to the PBS solution.

4. It is imperative that DiI working solution is injected at a steady rate. Following injection, quickly start the perfusion with PBS and PFA solutions. A long delay at this step can lead to incomplete vessel painting.

5. Surgeries in neonates were challenging because of their small size and difficulty in performing injections and insertion of the butterfly needle into the heart. Some neonates underwent cardiac arrest during the intracardiac

injection inhibiting the circulatory system from naturally distributing the DiI

solution throughout the brain. If cardiac arrest did occur, the heart was

manually pumped to create perfusion but at a limited capacity. A possible

solution could be to inject a smaller volume of DiI solution and administer it at

a slower pace. Additionally, the SNP-heparin injection could be administered

several minutes prior to euthanasia.

6. A very recent modified VP protocol has been shown to label blood vessels in

   adult and neonatal mice[236, 238]. This modified technique resembles our

   Method 1 procedure but with a few minor modifications: SNP-heparin was

   injected subcutaneously five minutes prior to euthanizing, and infusion of PBS

   and PFA solution was performed with a peristaltic perfusion pump. The

   authors reported strong labeling of pial vessel network on axial images, but it

   was unclear whether this modified protocol stained parenchymal vessels as

   efficiently as our technique. A recent study by Konno and colleagues[235]

   utilized neutral liposomes and $DiIC_{12}$ to achieve brighter and uniform labeling

   of the blood vessels in the mouse brain. The addition of liposomes to the DiI

   solution prevented the formation of DiI aggregates which improved the

   homogeneity of the vessel painting. This technique is similar to our Method 1

   procedure, except that the PBS flush was omitted and DiI/liposome solution

   was manually injected.

7. Method 2 has been utilized in healthy female mice with a success rate of 67%

   (unpublished data). We previously utilized Method 1 in adult rats that received

moderate TBI and found that 70% of rat brains showed excellent vessel staining[233]. Similarly, we used Method 2 in adult male mice that received a moderate TBI and found that 65% of mouse brains showed excellent vessel staining including labeling of new, immature micro-vessels[75].

8. The VP protocol described here has several limitations. First, DiI may label cerebral arteries and veins differently, a feature that is difficult to elucidate. Other protocols that use DiI reported high staining of arteries and arterioles and limited staining of veins and venules[220, 236]. Based on these studies, we do not recommend this VP protocol if one has an interest in studying the cerebral venous system. Second, this protocol provides only a snapshot of the cerebral vasculature at a single time point in an individual animal. Thus, large numbers of animals are needed to study temporal alterations of the cerebral vessels over time. Techniques for real-time imaging of the *in vivo* brain vasculature are available and these could be combined with our protocol[239, 240]. Third, while this protocol enables visualization of the blood vessels in the entire brain, it does not provide meaningful data on blood flow. Non-invasive techniques such as magnetic resonance perfusion weighted imaging (PWI MRI) or two-photon approaches could be utilized prior to VP to provide dynamic information on blood flow[241, 242]. This is of particular importance in brain pathologies where blood flow is reduced or heterogeneous[39]. Since effective labeling is predicated on perfusion of DiI through the vessels, labeled vessels must possess some degree of blood flow

or the capacity to perfuse blood (and likely a mature vessel lumen). Thus, this protocol offers only indirect data regarding perfusion status of the vessels.

9. One limitation of our analysis approaches is that it does not report on average vessel diameter which would be useful in determining the type of blood vessels. An alternative approach would be to measure vessel diameter with ImageJ plugins such as Vessel Diameter or Vessel Analysis.

10. The classical and fractal analyses apply different parameters and algorithms for quantification and measure distinct features of the vessel network. For the classical analysis, AngioTool identifies vessel segments using a multiscale Hessian enhancement filter[243]. A vessel segment is defined as any segment between two branch points, two end points, or a branch point and an end point. Vessel segments are skeletonized and then analyzed by counting and morphometric algorithms which computes various morphological features of the vessels. For the fractal analysis, FracLac assigns fractal properties to the blood vessels in the image[228]. Fractals are defined as geometric patterns that are repeated across different scales. An LFD analysis is performed at each pixel using the box counting method to measure fractal dimensions (quantitative index of complexity) and frequency (number of occurrences in each box). The resulting fractal data measures morphological complexity in the entire vessel network.

Application of the vessel painting procedure

       We have synthesized the process of VP and analysis into a schematic that provides an overview (Fig. 2.4). Additional details are described in the text. We now discuss the applications of our VP technique and analyses.

Classical and fractal analysis of cerebral vessels in adult and neonatal mice

       To validate our vessel painting technique and vascular analysis approaches for particularly detection of a range of blood vessels sizes in the brain, we analyzed the cortical vasculature in healthy adult (8 week-old, 25-28g, Jackson Laboratories, n=4) and neonatal (P14, 10-12g, Jackson Laboratories, n=4-5) male C57BL/6 mice. The vasculature of adult and neonatal mice were labeled with Method 2 and whole brain axial images were obtained and analyzed by classical vascular analysis, as described above. Comparison of classical vascular analysis images revealed reduced vessel features in neonatal brain compared to the brain of adult mice (Fig. 2.5a). Vascular analysis of the entire hemispheric cortex demonstrated reductions in vessel percentage area ($16.3 \pm 2.1\%$ versus $21.3 \pm 1.1\%$, unpaired student T-test, $p<0.05$), total number of junctions ($7.3 \times 10^{-4} \pm 9.6 \times 10^{-5}$ versus $1.5 \times 10^{-3} \pm 1.3 \times 10^{-4}$, unpaired student T-test, $p<0.05$) and total vessel length ($1.4 \times 10^{-4} \pm 9.1 \times 10^{-6}$mm versus $2.1 \times 10^{-4} \pm 1.1 \times 10^{-5}$mm, unpaired student T-test, $p<0.05$) in neonatal mice in compared to adult mice (Fig. 2.5b). There was an increase in lacunarity (space between vessels) (unpaired student T-test, $p=0.08$) in neonatal mice brains in compared to adult

brains but this did not reach significance (Fig. 2.5b). Collectively, this data suggests that vessel characteristics in the cortex increases from adolescence to adulthood.

We next analyzed vascular complexity between the adult and neonatal mice vasculature using fractals. Comparison of fractal colorized images revealed a reduction in vessel complexity in neonatal brain in compared to the brain of adult mice (Fig. 2.5c). When we analyzed the entire hemispheric cortex, we observed a leftward shift (reduced vascular complexity) and a decrease in peak frequency values (reduced vessel numbers) in the histogram from the neonatal mice brains compared to the adult brains (Fig. 2.5d). Quantitative analysis of the distribution of the LFD revealed a 3.9% reduction (unpaired student T-test, p=0.30) in skewness and 22.6% reduction (unpaired student T-test, p=0.11) in kurtosis values, but did not reach significance. The peak frequency value, a measure of the number of vessels, revealed a 5% reduction in neonatal mice (unpaired student T-test, p=0.08) compared to the adult mice, but this did not reach significance. While the complexity values were not significantly different between neonatal and adult brain, there was a clear increase in vascular complexity as the mice progressed to adulthood. These changes in the cerebral vasculature are consistent with other published studies[239, 244, 245]

Assessment of vascular architecture in various animal models of brain injury

A critical question for our vessel painted technique is whether it could also be used to study the vasculature following acquired brain injuries where the vasculature is known to be compromised. To test this, we induced brain injuries in adult male Sprague Dawley rats (2-3 months old, 250-275g, Harlan Laboratories) using a moderate controlled cortical impact (CCI) model of traumatic brain injury (TBI)[233], collagenase-induced intracerebral hemorrhage (ICH)[246], endovascular perforation-induced subarachnoid hemorrhage (SAH)[247], and permanent middle cerebral artery occlusion model (MCAO) model of ischemic stroke[248]. Injured rats underwent Method 1 vessel painting at 24 hours following injury. Rats with a moderate CCI showed a loss of the cortical and subcortical vessels in the right somatosensory cortex (Fig. 2.6a). The injury extended to a depth of about 0.5mm confirming the moderate nature of the brain injury. ICH resulted in loss of vessels in the right striatum at the site of hemorrhage (Fig. 2.6b). The SAH model induced bleeding in the subarachnoid space at the base of the brain (Fig. 2.6c). In this model, the injury site is external to the brain parenchyma, however, there was a clear deformation of the brain tissue indicative of brain swelling. One intriguing finding in the SAH model was that there was loss of micro-vessels which accentuated resolution of the pial and penetrating vessels (see axial view). This is likely due to the edematous compression of the brain. Rats with a permanent MCAO showed a clear loss of

vascular components in the right hemisphere which is evident on the coronal and axial views (Fig. 2.6d). There was also expansion of the ipsilateral hemisphere due to ongoing edema and brain swelling. Thus, our VP technique has broad utility in normal brain vascular morphology as well assessment in an extensive range of brain injury models.

We previously performed classical and fractal analysis to assess acute changes in the cortical vessels of adult rats after a moderate CCI and found a brain-wide reduction in vessel length, junctions, and complexity 24 hours after injury[233]. Furthermore, we performed classical analysis to assess sub-acute changes in the cortical vessels in adult mice after a moderate CCI and found an increase in vessel density in the brain along with an increase in vessel density, length, and junctions in the peri-lesional tissue at 7 days after injury[75]. Thus, the classical and fractal analyses provide a comprehensive assessment of the cerebrovasculature in the injured brain.

Potential applications of vessel painting procedure

Further applications of the VP procedure could involve studies with magnetic resonance imaging, which would provide a unique opportunity to correlate the vascular features with neuroimaging findings. We recently demonstrated proof of principle[233], where we performed correlations between individual fractal properties (skewness, kurtosis, local fractal dimensions, and peak value frequency) with total hemorrhage and edema volume from *ex vivo* T2

weighted imaging following moderate TBI. Combining perfusion weighted imaging and VP could provide valuable insight into hemodynamic and cerebrovascular changes in the ischemic penumbra following MCAO. Another potential application could be combining VP with tissue-clearing solutions which would allow for imaging at depths of several millimeters along with large scale reconstruction of the vessel structures at high resolution. The success of this method is dependent on utilizing a clearing solution devoid of organic solvents and detergents as these reagents will cause removal of the DiI from the lipid membranes of the vessels. Sca*l*eSQ, a detergent free formulation of Sca*l*eS, could potentially be used for this purpose[249]. FocusClear has also been successfully used to clear thick brain sections following vessel painting[222]. Lastly, although we focus our investigation on the brain, the entire rodent circulatory system is exposed to DiI solution. Thus, other organs such as retinal vasculature may be stained and could be examined using our technique. It should also be noted that lipophilic tracers in the carbocyanine family are available in other colors, for example DiO is a green fluorescent marker and are thus potentially compatible with transgenic and other types of reporter mice[234].

The VP technique we describe here produces detailed images of the cerebral vessels, but these images are restricted to depths of approximately 50 micrometers[250]. Several methods are available to transform the intact brain into transparent form. While these show promise in studying the cerebral vasculature, no single method provides a comprehensive view of how cerebral vessels

respond to injury. One such method utilizes Tie-2/red fluorescent protein (RFP) mice and CLARITY, which allowed for imaging of cerebral vessels up to 3.2mm into the brain[251]. However, RFP expression is controlled by an endothelial-specific promoter and RFP expression may change under different conditions, especially in cases of brain injury and disease. The authors of this same study demonstrated that lectin and anti-claudin-5 antibody can penetrate into the CLARITY-treated brain slices of wild type C57BL/6 mice resulting in labeling of cerebral vessels up to 900 μm[251]. However, fluorescent antibodies can lead to heterogeneous staining of vessels and nonspecific staining of non-vascular cells. Additionally, this method has been shown to cause expansion of the brain tissue which may affect the accuracy of the quantitative analysis. Another method involves transcardial perfusion with Texas Red-labeled lectin followed by ScaleA2, which lead to visualization of cerebral vessels in the hippocampus[252]. ScaleA2-treated samples are often soft and brittle and the clearing method can potentially compromise tissue structures. This method also results brain tissue expansion. Unlike these techniques, our VP technique uniformly stains blood vessels in different rodent strains, ages, and pathological conditions. The DiI molecules are able to laterally diffuse within the lipid membranes of the endothelial cells providing uniform staining of the vessel lumen and no staining of non-vascular cells. Thus, vessel painted brains can be routinely used for various applications with minimal effects on the labeled vessels. Additionally, there was no overt change in the size of brain tissue using our technique.

In summary, we have developed a newly developed protocol to stain, visualize, and analyze the cerebral vasculature in the rodent brain. Among the many approaches for vessel labeling of the brain vasculature, our VP technique provides a simple, more efficient alternative that gives bright red fluorescence and exquisite resolution of the pial, penetrating, and parenchymal vessels including micro-vessels. Thus, the VP technique we describe will be valuable for the high-resolution imaging of the cerebral vessels in intact or injured brain. We also introduced two simple analysis approaches to assess vessel features. The classical and fractal analyses offer extensive quantitative data on vessel morphology and complexity, which has been lacking in the scientific community. Thus, these analysis techniques are critical for assessing the structural and quantitative features in the cerebral vasculature.
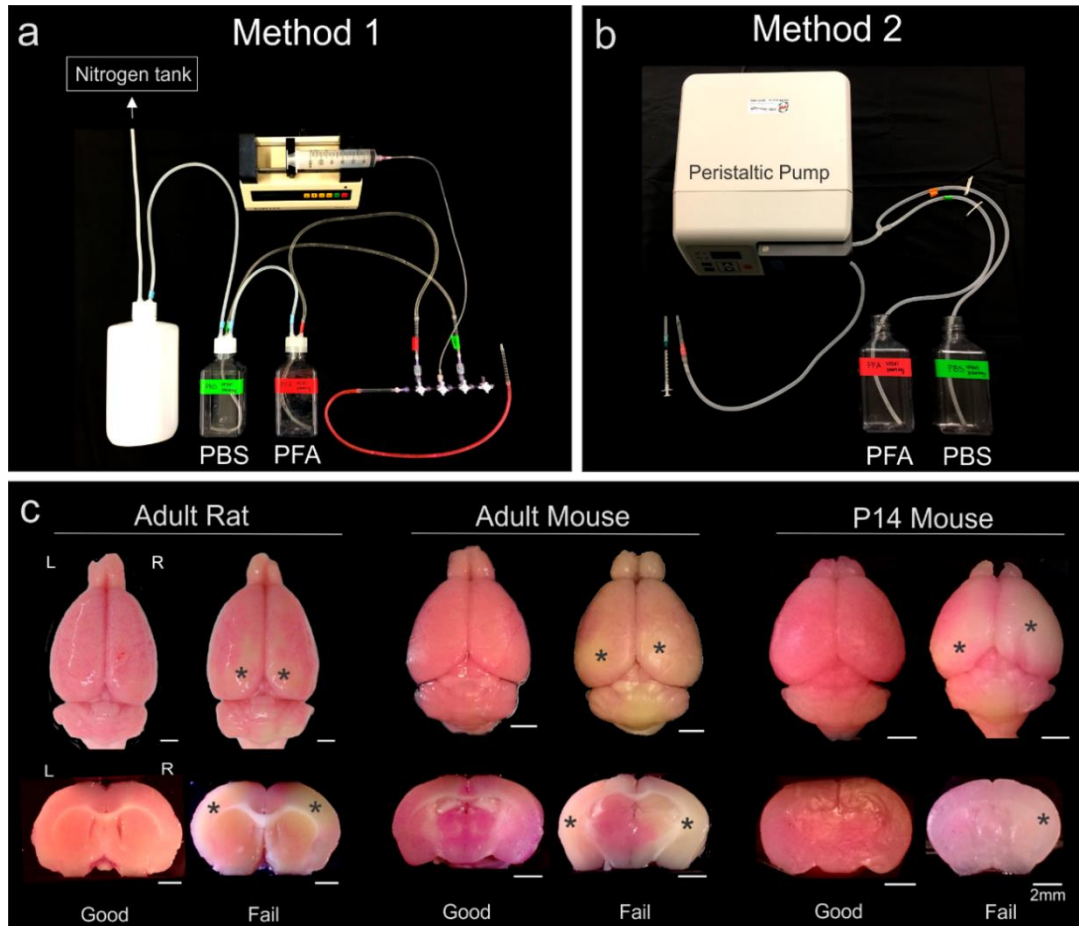
Figure 2.1. Vessel painting perfusion apparatus for rodents. A) Photograph of vessel painting (VP) apparatus for adult mice and rats (Method 1) used in our studies. The apparatus consists of a nitrogen tank, tubes connecting to the stopcock assembly, and an outflow port. The nitrogen tank provides pressure to deliver the phosphate buffered saline (PBS) and paraformaldehyde (PFA) fixative solutions. B) Photograph of VP apparatus for adult and neonatal mice (Method 2). This setup consists of peristaltic pump and syringe containing the DiI solution. The pump is used to deliver the PBS and PFA but the DiI solution is delivered

manually. C) Representative examples of VP adult mice and rat brains as well as a postnatal day 14 (P14) mouse brain. The brains labeled "Good" demonstrate successful VP with uniform pink staining of the tissue spots. The brains labeled "Fail" demonstrate failed VP perfusion with patches of pale tissue (asterisks) within the diffusively pink tissue. Right hemisphere (R) and left hemisphere (L). Scale bar = 2mm
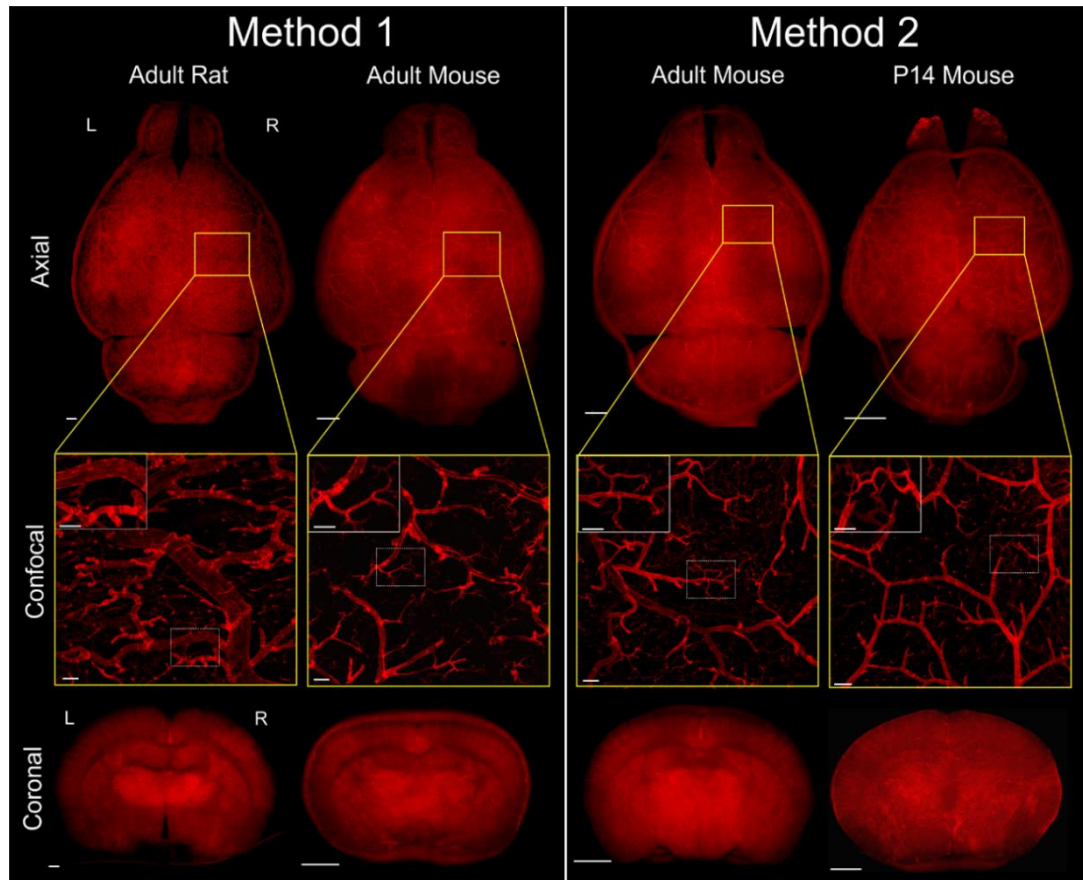
Figure 2.2. Visualization of vessel painted mouse and rat brains. The top row displays examples of axial view images of adult rat and mouse brains as well as P14 mouse neonate brain. The middle row set of images are high magnification confocal images from axial cortical tissues, and the bottom row shows coronal images. The representative brains from either Method 1 or 2 illustrate excellent staining of all the blood vessels within whole brain tissues. The confocal images confirm crisp staining of pial, penetrating, and parenchymal micro-vessels. Adult mouse brain stained with Method 2 revealed more uniform staining of large pial vessels and intense staining of micro-vessels than Method 1 (see confocal images). The boxed areas in the confocal images are magnified in the inserts.

Right hemisphere (R) and left hemisphere (L). Scale bar = 1mm (axial and coronal images), 200μm (confocal), and 100μm (inserts).
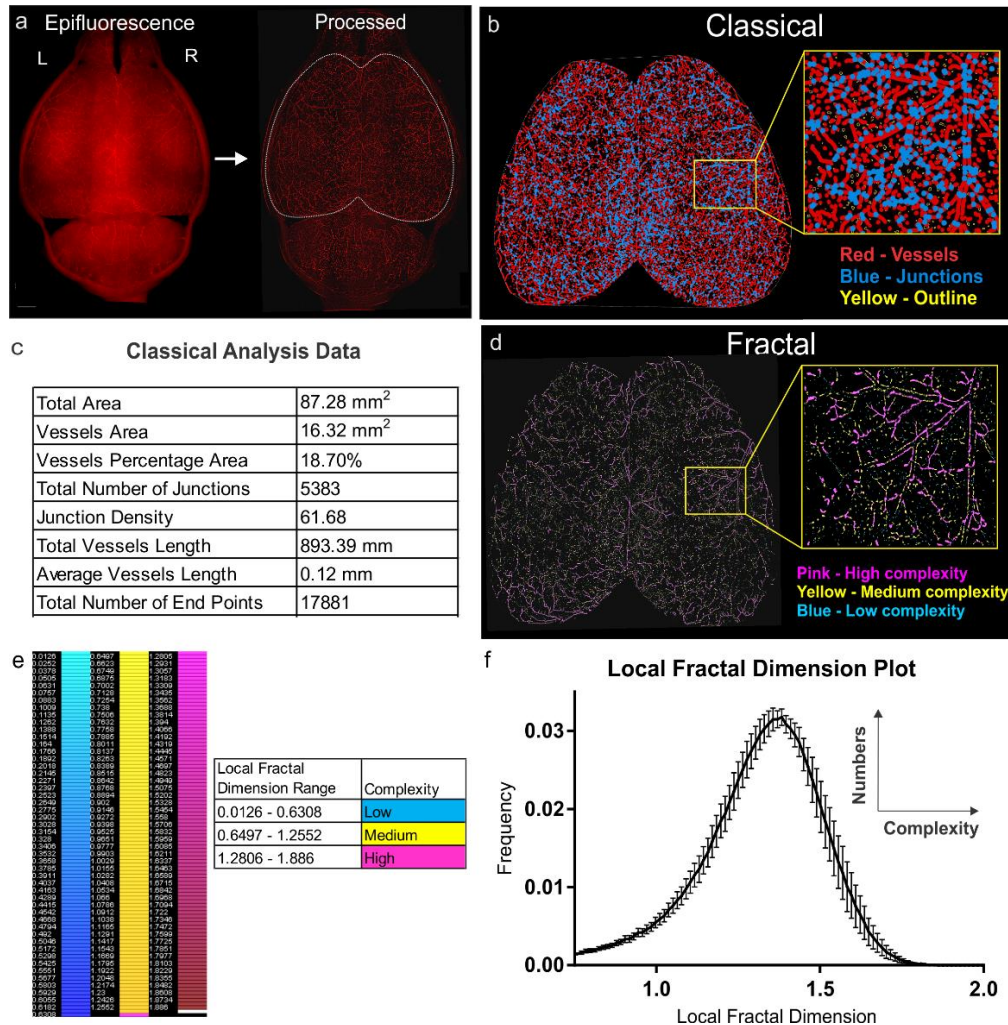
Figure 2.3. Classical and fractal vascular analysis of vessel painted images. A)
The raw epifluorescent image is processed using black balance and haze
reduction algorithms to create an enhanced fluorescent image with reduced
background. A region of interest is drawn around the whole cortex (white outline).
Right hemisphere (R) and left hemisphere (L). B) The enhanced image can be
processed for vascular features (AngioTool software) which results in images
that display vessels in red, junctions in blue, and vessel outline in yellow. C)
Quantitative analysis of vessel characteristics can be derived including vessel

percentage area, number of junctions, vessel length, and lacunarity. D) The enhanced image can be processed for vascular complexity using fractal analysis (FracLac, ImageJ plugin). The fractal analysis extracts the local fractal dimension (LFD) and then color-codes according to the degree of vessel connectivity. The vasculature in the brain is colorized based on corresponding fractal dimension with a gradient from lower LFD in blue (less complex) to higher LFD in pink (more complex). E) The color scale displays LFD values with a gradient from blue (less complex) to pink (more complex). The LFD value ranges and vessel complexity are shown in the chart. F) The resultant LFD histogram displays vessel complexity in the x-axis (LFD) and vessel numbers in the y-axis (frequency). The histograms can be quantitatively analyzed by measuring skewness, kurtosis, and peak frequency. The histogram is a mean of 4 animals with all error bars are presented as standard error of mean.

Vessel Painting Method Schematic

Vessel Painting

Method 1
1. Vasodilator injection
2. PBS flush to remove blood
3. Fluorescent dye solution to label vessels
4. PFA fixation

Method 2
1. Vasodilator injection
2. Fluorescent dye solution to label vessels
3. PBS flush to remove blood
4. PFA fixation

Mouse

1. Brain removal from cranial vault
2. Post-fixation overnight
3. Brain stored in PBS
(Optional step: MRI)

Successful vessel painting is confirmed based on uniform pink stain throughout the brain

Data Acquisition

Wide-field epifluorescence of axial or coronal views

High resolution confocal acquisition

Axial

Confocal

Image Optimization

Processed

Analysis

Classical

Vessel length, junctions etc

Fractal

Fractal dimension, frequency etc

Results

Vascular Features

Vessel area	16.32 mm^2
Total junctions	5383
Total vessel length	893.39 mm
Avg vessel length	0.12 mm

Frequency / Numbers / Complexity / Local Fractal Dimension

Figure 2.4. Workflow of vessel painting and analysis. The workflow is comprised of four components, the actual vessel painting technique (two methods), data acquisition, analysis methods and extraction of the final results. The vessel painting technique consists of two methods: one optimized for the adult rat and mouse (Method 1) and a 2nd modification for adult and neonatal mouse (Method 2). Following the procedure, vessel painted brains are removed from the cranium, visually inspected to ensure adequate staining, and imaged by wide-field and/or high resolution fluorescence microscopy. The raw fluorescent images are processed and subsequently analyzed by classical and fractal analysis. Classical vascular analysis provides quantitative analysis of vessels characteristics and creates an image that displays vessels and branch points. Fractal geometric analysis measures biological vessel complexity and creates a colorized image according to the degree of complexity.
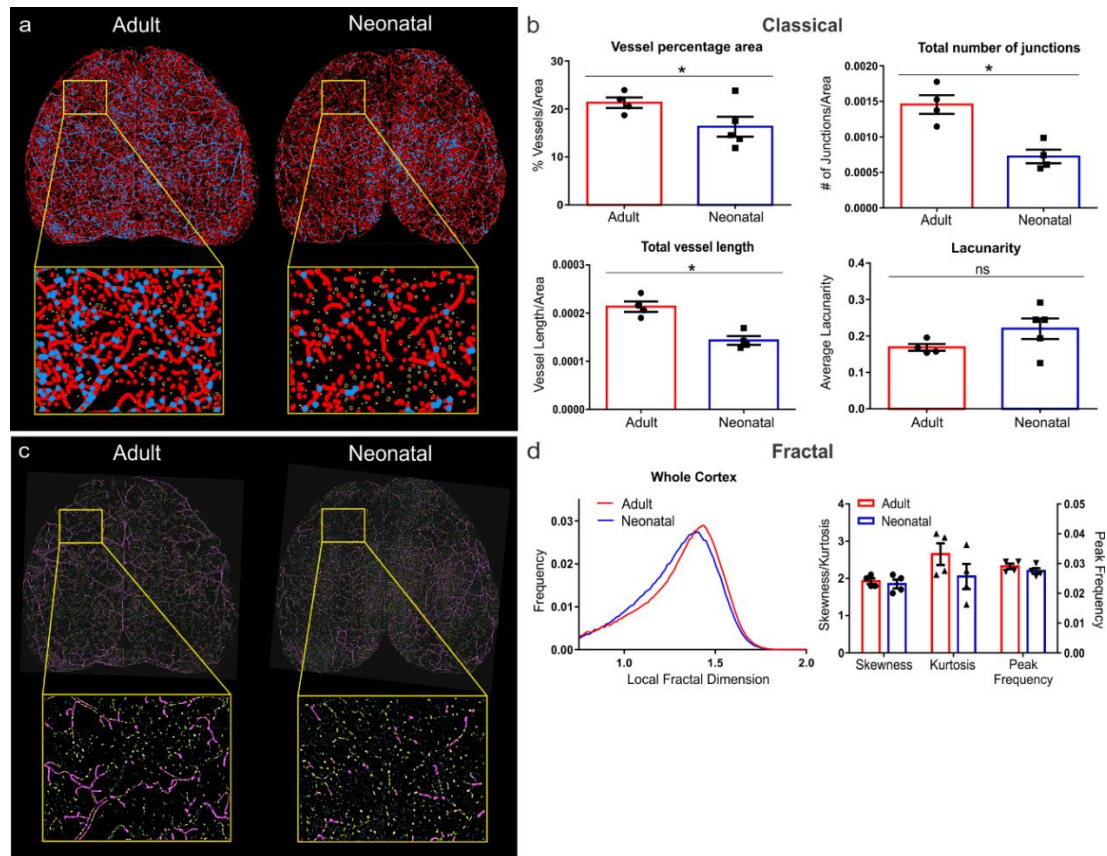
Figure 2.5. Classical and fractal analysis of vessel painted adult and neonatal mouse brains. A) Axial images from classical vascular analysis reveal a reduction in cortical vascular features in neonatal (P14) in compared to adult (8-week-old) mice. The expanded view clearly illustrates decreased vessel density in cortex that increases with age. Vessels (red), junctions (blue), vessel outline (yellow). B) Whole cortex analysis demonstrates a reduction in vessel percentage area (unpaired student t-test, p<0.05), total number of junctions (unpaired student t-test, p<0.05), and total vessel length (unpaired student t-test, p<0.05) in neonatal mice in compared to adults. There was an increase in lacunarity (unpaired student t-test, p=0.14) in neonatal mice in compared to

adults, but did not reach significance. C) Axial images from fractal geometric

analysis reveal a reduction in vessel complexity in neonatal brain (P14) in

compared to adult (8-week-old) brain. The expanded view illustrates decreased

complexity within the cortex. Low complexity (blue), medium complexity (yellow),

and high complexity (pink). D) Local fractal dimension (LFD) distribution in the

whole cortex is representative of a decrease in vessel complexity (leftward LFD

shift) and decrease in vessel numbers (decreased peak frequency). Quantitative

analysis of the distribution of the LFD histogram revealed no significant

alterations in the skewness (unpaired student t-test, p=0.30), kurtosis (unpaired

student t-test, p=0.11), and peak frequency values (unpaired student t-test,

p=0.08) between the two age groups.
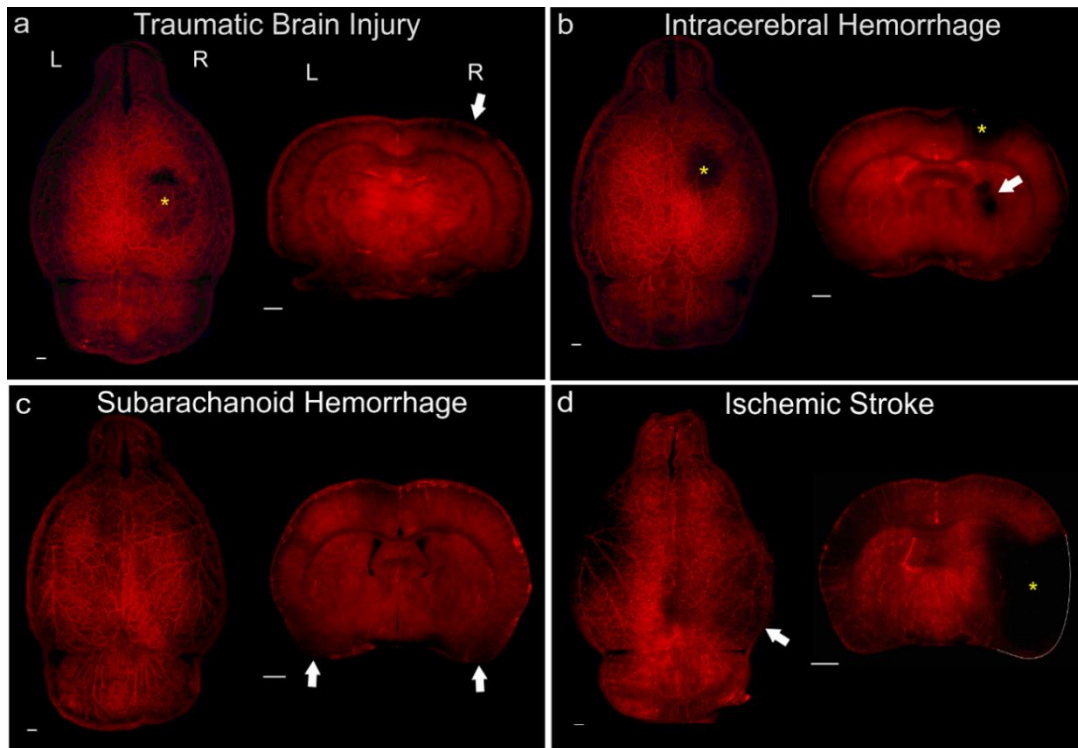
Figure 2.6. Vessel painting applied to different acquired injury models. All injury

models were vessel painted 24hrs after injury induction. A) Traumatic brain injury

reveals a loss of cerebral vessels in the axial views on the right hemisphere

(asterisk) following a controlled cortical impact model (CCI). The CCI-induced

injury extends about 0.5mm from the cortical surface (arrows) as observed in the

coronal view. Right hemisphere (R) and left hemisphere (L). B) Intracerebral

hemorrhage induced by collagenase injection into the striatum reveals an injury

site on the axial view (asterisk). In the coronal sections there is a clear loss of

vessels in the right striatal region (arrow). The needle track also results in a

secondary loss of vessels in the cortex (yellow asterisk). C) Subarachnoid

hemorrhage model based on puncture of the middle cerebral artery (MCA)

illustrates the loss of vascular complexity in the axial images, likely due to

edematous brain swelling. There is loss of vascular structures at the base of the brain as can be seen in the coronal images (arrows). There is no overt injury site as the MCA puncture is at the base of the brain. D) MCA occlusion model of stroke demonstrates a clear loss of perfusion in the right hemisphere on the axial image (solid arrows) with expansion of the right hemisphere due to edema formation. The coronal image clearly illustrates the loss of the vascular network in the region supplied by the MCA (asterisk). Scale bar = 1mm
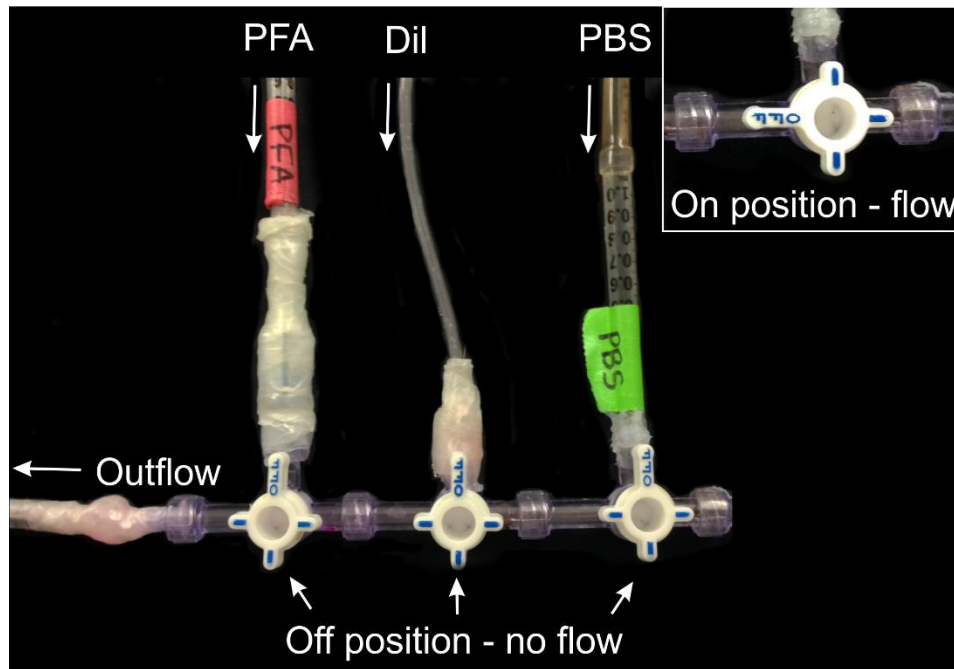
Figure 2.7. Stopcock assembly for method 1. The stopcock assembly allows for the delivery of solutions in sequential order. The three-way stopcocks are connected to perfusion lines for PBS, DiI solution, and fixative. The solution does not flow from the system if the stopcock knob is perpendicular to the outflow port (off position). To permit flow of the solution, the stopcock knob is rotated left by 90 degree (insert, on position). The solution exits the system and is delivered to a butterfly needle. It is important to avoid air from the entering the perfusion lines.
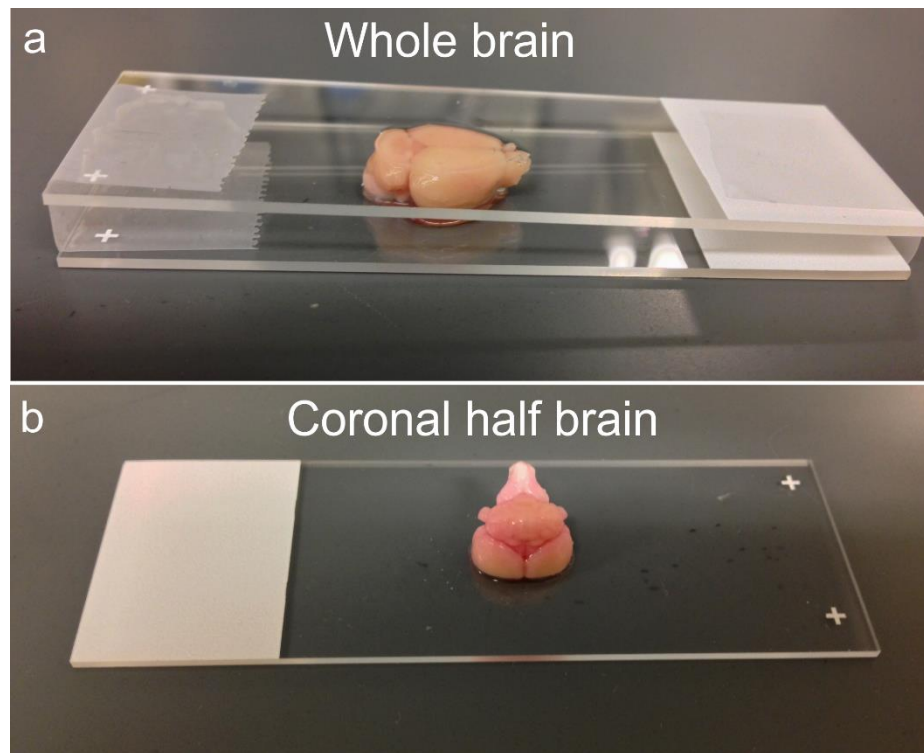
Figure 2.8. Whole and coronal half brain preparation for epi-fluorescent imaging. Adult mouse brains are shown, but identical procedure was used for neonatal mouse and adult rat tissues. a) Whole brains were placed onto a glass slide with the olfactory bulb to the right and cerebellum to the left. A second slide was placed over the brain and gently compressed until the dorsal surface was evenly flattened while minimizing over-compression to prevent tissue damage. The slides were taped on each side. b) Coronal aspects were then imaged by cutting the brain 5mm posteriorly from the olfactory bulb to create an anterior and posterior half brain. The posterior half of the brain was placed on the slide with the cerebellum extending out from the slide, a second slide was not required. The anterior portion of the brain can also be imaged.
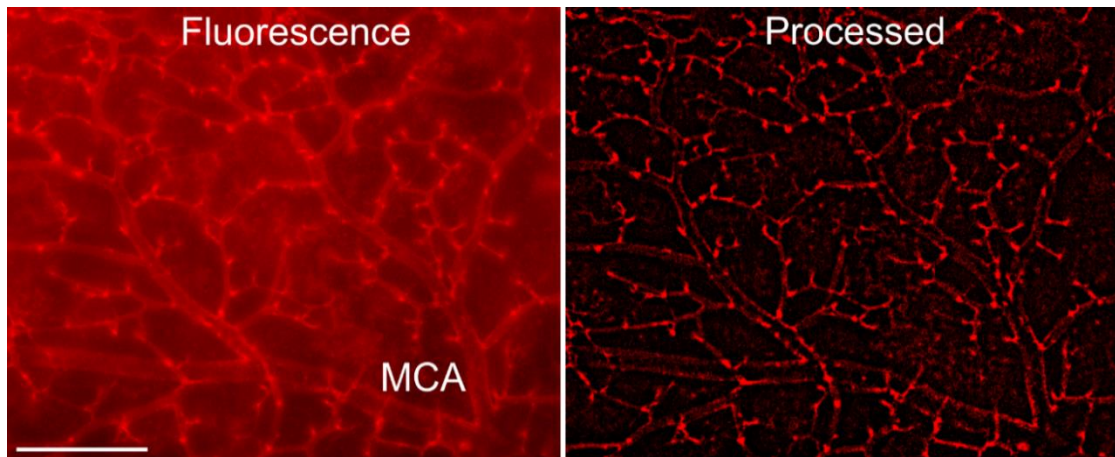
Figure 2.9. Raw and processed vessel painted fluorescent images. Axial image of blood vessels on the dorsal brain surface (2x magnification). The processed fluorescent image reveals high resolution of the middle cerebral artery (MCA) and its branching vessels along with minimal background signal. Scale bar = 1mm

Table 2.1. Evaluation of vessel painted brains following Method 1 and 2.

Method	Excellent[a]	Failed[b]	No staining[c]	Success rate[d]
Method 1 - Adult Rat	6	3	0	67%
Method 1 - Adult Mouse	6	5	13	25%
Method 2 - Adult Mouse	5	2	0	71%
Method 2 - P14 Mouse	6	5	5	37.5%

The table summarizes the number of vessel painted brains with Excellent, Failed, and No staining following Method 1 and 2. [a]Excellent vessel painted brains exhibited homogenous pink staining of the entire brain parenchyma and excellent labeling of vessels on the dorsal surface and deep compartments in the brain. [b]Failed vessel painted brains exhibited heterogeneous pink staining and poor labeling of vessels in the brain. [c]Brains with lack of pink staining were classified as "No staining". [d]The success rate was determined by dividing the number of excellent vessel painted brains by the total number of brains.

Chapter 3

Wnt/Beta-catenin is Upregulated in Cerebral Vessels after Traumatic Brain Injury and it Coincides with Vascular Repair

<u>Preface</u>

This chapter has been reproduced from … Salehi, A., A. Jullienne, M. Baghchechi, M. Hamer, M. Walsworth, V. Donovan, J. Tang, J. H. Zhang, W. J. Pearce and A. Obenaus (2018). "Up-regulation of Wnt/beta-catenin expression is accompanied with vascular repair after traumatic brain injury." Journal of Cerebral Blood Flow and Metabolism 38(2): 274-289 *with permission from SAGE Publishing*

This chapter discusses the temporal and spatial changes in the cerebral vasculature over the course of 7 days following moderate traumatic brain injury. This chapter also examines changes in beta-catenin protein and its association with cerebral vessels following moderate traumatic brain injury

Reproduced from manuscript: Figure 3.1 – 3.9

Abstract

Recent data suggests that repairing the cerebral vasculature after traumatic brain injury (TBI) may help to improve functional recovery. The Wnt/β-catenin signaling pathway promotes blood vessel formation during vascular development, but its role in vascular repair after TBI remains elusive. In this study, we examined how the cerebral vasculature responds to TBI and the role of Wnt/β-catenin signaling in vascular repair. We induced a moderate controlled cortical impact in adult mice and performed vessel painting to visualize the vascular alterations in the brain. Brain tissue around the injury site was assessed for β-catenin and vascular markers. A Wnt transgenic mouse line was utilized to evaluate Wnt gene expression. We report that TBI results in vascular loss followed by increases in vascular structure at 7 days post injury (dpi). Immature, non-perfusing vessels were evident in the tissue around the injury site. β-catenin protein expression was significantly reduced in the injury site at 7 dpi. However, there was an increase in β-catenin expression in perilesional vessels at 1 and 7 dpi. Similarly, we found increased number of Wnt-GFP-positive vessels after TBI. Our findings suggest that Wnt/β-catenin expression contributes to the vascular repair process after TBI.

Introduction

Traumatic brain injury (TBI) is a serious clinical problem that is associated with long-term neurological deficits. Emerging research suggests that the

97

cerebral vasculature is one of the major contributors to TBI-related disabilities[4, 253]. An insult to the brain damages cerebral vessels and often leads to secondary injury. For example, patients with severe TBI experience acute reductions in cerebral blood flow that gradually resolves over the course of several days to weeks[37]. Although improved guidelines for the management of TBI patients have been introduced, they have been largely ineffective in reducing the incidence of post-injury ischemic episodes[254]. Thus, a better understanding of how the cerebral vasculature responds following TBI could provide critical insight into secondary effects and lead to development of new therapies designed to enhance vascular repair.

The time course of vascular repair after TBI has been ill-defined. Injured vessels undergo repair through sprouting angiogenesis (formation of new capillaries from existing vessels). Several studies have suggested that TBI elicits gross vascular injury that is subsequently followed by slow repair over the course of several weeks[9, 73]. The degree of vascular repair is dependent on the severity of the TBI[9]. Interestingly, secondary complications (i.e. hypoperfusion) are observed even once the vascular network has repaired, which may suggest deficits in the repaired vessels[70]. At present, there are no studies that have comprehensively investigated the spatial and morphological changes of the brain vasculature after TBI.

Several putative mechanisms may be responsible for vascular repair after TBI. Vascular endothelial growth factor (VEGF) has been evaluated in several

studies[89, 94]. However, VEGF treatment appears to exhibit adverse side effects making it a poor candidate for future therapeutics[255]. One alternative and unexplored mechanism is the Wnt/β-catenin cascade, which plays a major role in embryonic vascular development. This pathway regulates many aspects of the vascular repair processes, including angiogenesis, vascular sprouting, blood-brain barrier formation, and arterial-venous specification[198, 202, 204, 256, 257]. Additionally, studies in other vascular-related injuries (stroke, hindlimb ischemia and neointimal hyperplasia) demonstrated that the components of Wnt/β−catenin pathway have angiogenic functions[183, 258, 259].

The Wnt/β-catenin pathway has recently been explored in TBI unrelated to the cerebral vasculature. Studies have shown contrasting results, with several reporting up-regulation of β-catenin after TBI[191, 208] while others showing a dramatic reduction[260]. In damaged tissue, Wnt factors are thought to promote proliferation and differentiation of stem and progenitor cells. After TBI, the Wnt/β-catenin pathway has been linked to important repair processes most notably astrogliosis and neurogenesis[191, 206, 207]. It is unclear what role Wnt/β-catenin signaling plays in vascular repair after TBI.

The objective of our study was to evaluate how the cerebral vessels respond in the course of 7 days following a moderate TBI. The second objective was to assess what role the Wnt/β-catenin signaling plays in the vascular repair process. We hypothesized that Wnt/β-catenin signaling is associated with repair of the injured vasculature after TBI. We utilized a controlled cortical impact

mouse model to induce a moderate TBI which lead to gross injury to the cortical vessels. We utilized a novel vessel painting technique to label the cerebral vessels in the whole brain and assessed vascular alterations at specific time points after TBI. We assessed β-catenin inside blood vessels around the lesion and utilized a Wnt transgenic mouse line to monitor Wnt gene expression. In our study, we found that TBI led to a rapid up-regulation of β-catenin expression and activation of Wnt genes in blood vessels that coincided with vascular repair. These results suggest that Wnt/β-catenin expression contributes to vascular repair following TBI and represents a potential target for future therapeutics.

Material and methods

All animal experiments and care complied with federal regulations and were approved by the Institutional Animal Care and Use Committee of Loma Linda University according to Guide For the Care and Use of Laboratory Animals (Eighth edition). Experiments received ethical approval from the LLU IACUC under the protocol numbers 8130051 and 8150023. Animal reporting is according to ARRIVE guidelines.

Animals

Male C57BL/6 mice (6-8 weeks, 25-30g) were purchased from Jackson Laboratory. Male transgenic TCF/Lef:H2B-GFP mice (6-8 weeks, 25-30g) were C57BL/6 background and were purchased from Jackson Laboratory. Animals

were group housed and kept in a temperature controlled animal facility on a 12-hour light/dark cycle with free access to food and water. Home cages contained standard cob bedding. Animals were randomly assigned to three groups: Control, Sham, or TBI. Following brain injury, animals underwent vessel painting, western blot, or immunohistochemistry. All animals were sacrificed at 0.5, 1, 3, or 7 days post injury (dpi). Each experiment was performed by investigators blinded to the treatment/subject.

Traumatic brain injury

A controlled cortical impact (CCI) model of moderate brain injury was utilized as described previously[31]. Briefly, mice were anesthetized with isoflurane (3% induction, 1-2% maintenance) using isoflurane vaporizer (VetEquip Inc., Pleasanton, CA). Anesthetized mice were placed in a stereotaxic frame and body temperature was maintained at 37±1°C with a heating pad during the surgery. A midline incision of the skin was made to expose the skull and a 5 mm craniotomy was carefully performed on the right hemisphere to expose the cortex (between Lambda and Bregma). A moderate CCI (1.5 mm depth, 3 mm diameter, 2.0 m/s speed, 200 ms dwell time) was delivered using an electromagnetically driven piston (Leica Microsystems Company, Richmond, IL). CCI procedure also resulted in visible hemorrhage that gradually resolved in a few minutes. The craniotomy site was not sealed and skin was sutured. After surgery, Buprenorphine (0.01mg/kg, intramuscular) was administered to minimize pain.

Animals were monitored daily following the procedure. Sham animals underwent the exact procedure without cortical impact. In a small cohort of sham animals we noted small degree of hemorrhage which was due to the craniotomy procedure. Control animals underwent anesthesia only for the identical period of time (30 minutes) as well as the Buprenorphine injection. Control and Sham animals were euthanized after 3 days.

<u>Vessel painting procedure</u>

This technique uses a carbocyanine dye (1,1′-dioctadecyl-3,3,3′,3′-tetramethylindocarbocyanine perchlorate, DiI, Life Technologies, Carlsbad, CA) that binds to the lipid membranes, thereby labeling the vasculature of the entire brain[233]. Mice were assigned into 3 groups: Sham, TBI 1 dpi, and TBI 7 dpi (19 total, n=6-7/group). Mice were anesthetized with ketamine (90mg/kg) and xylazine (10mg/kg). Vessel painting was performed by cardiac injection of DiI (0.3mg/mL in PBS containing 4% dextrose, total volume 500 μL) into the left ventricle followed by perfusion with 10ml of phosphate buffer saline (PBS) and then 20ml of 4% paraformaldehyde (PFA). Extracted brains were then post-fixed in 4% PFA for 24h and stored in PBS until imaging. Success of vessel painting was confirmed based on visualized inspection of the brain parenchyma where a uniform pink stain demonstrated vascular labeling providing excellent definition of large and small cortical and sub-cortical vessels. Animals with uneven staining of the vessels were excluded. Axial and coronal brain images were then obtained

using a BZ-X700 Keyence microscope (Keyence Corp, Osaka, Japan). Axial

views of the brain were obtained using 2x magnification and 1mm depth of field

(25.2 μm pitch, 40 slices). For coronal images, brains were sliced at the lesion

site, 5mm away from the olfactory bulbs and imaged using 2x magnification and

0.75 mm depth of field (25.2 μm pitch, 30 slices).

Vessel painting analysis

Quantitative analysis of the labeled vessels was performed as described

previously on whole brain axial and coronal views[233]. Regions of interest (ROI)

were drawn around the ipsilateral and contralateral hemisphere on 2x axial and

coronal images. Perilesional area analysis was performed using a 1.5 mm

diameter ROI encompassing the lesion. ROIs were drawn around each lesion

and then were expanded by 1.5 mm to encompass the perilesional area.

Angiotool analysis was performed on each ROI to assess vessel characteristics,

including vessel density, junction number, and average vessel length[225].

Western blotting

Western blot assays were performed using controls in lieu of Sham

animals as the craniotomy results in small alterations to the cortical surface[261]

and affects expression of β-catenin in the brain (data not shown). Mice were

assigned into 5 groups: Controls (n=13), TBI 0.5 (n=6), 1 (n=7), 3 (n=6), and 7

dpi (n=6) (31 total). The animals were sacrificed by transcardial perfusion with

PBS. Extracted brains were cut into 4 quadrants (between the midline and Bregma) and the quadrant containing the injury site were processed to extract cytoplasmic and nuclear proteins (Nuclear extraction kit, EMD Millipore, Temecula, CA). Protein concentration was determined using a Bradford assay (Thermo Scientific, Rockford, IL). 8 or 10µg of protein was subjected to electrophoresis on 4-12% Sodium Dodecyl Sulfate PolyAcrylamide Gel Electrophoresis gels and transferred onto PVDF membranes. Immunoblots were probed with the following antibodies: rabbit anti-β-catenin, rabbit anti-GAPDH, rabbit anti-Lamin B1 (1:2000), rabbit anti-Cyclin D1 (1:10000), or anti-Wnt5a (1:200) (all antibodies from Abcam, Cambridge, MA). Secondary incubations were performed with anti-rabbit DyLight 800 (1:2500, Thermo Fisher, Rockford, IL) and anti-mouse IRDye 680 (1:2500, LI-COR, Lincoln, NE) antibodies and incubated for 2h. Bands were visualized using an infra-red scanner (Odyssey, LI-COR). Image Studio Lite (LI-COR) was used for densitometry analysis and band intensities were normalized to their respective loading controls.

Immunohistochemistry

Mice were assigned into 3 groups: Controls, TBI 1 dpi, and TBI 7 dpi (n=3-4/group). All animals appeared healthy before sacrificing. C57BL/6 (12 total) and transgenic TCF/Lef:H2B-GFP (12 total) mice used for immunohistochemistry were sacrificed by transcardial perfusion with PBS and 4% PFA. Following post-fixation, brains were cryoprotected in 30% sucrose solution for 24h. Brains were

embedded in Tissue-Tek OCT compound (Sakura Finetek, Torrance, CA) and

frozen on dry ice. Coronal sections were obtained using a cryostat (Leica

Biosystems, Nussloch, Germany) at a 20 µm thickness and collected on

Superfrost Plus® (Fisher Scientific, Pittsburg, PA) microscope slides. Tissue

sections were blocked with 2% Bovine Serum Albumin (BSA, Sigma Aldrich, St

Louis, MO) solution for 1.5 h. Primary antibodies used were: anti-β-catenin

(1:100, Abcam, Cambridge, MA), anti-Sox17 (1:100, Abcam), anti-Von

Willebrand Factor (vWF, 1:200, Abcam), anti-GFAP (1:500, Millipore, Billerica,

MA), anti-NeuN (1:400, Millipore), and anti-Iba1 (1:400, Wako, Richmond, VA).

DyLight 594-labeled tomato-lectin (T-lectin, 1:200, Vector Laboratories,

Burlingame, CA) and Isolectin B4 (IB4, 1:50, Sigma Aldrich) were used to label

the blood vessels. Primary antibodies or markers were incubated in antibody

solution (0.5% BSA + 0.5% Triton X) overnight or for 72 h for IB4. Appropriate

secondary antibodies (all from Invitrogen, Eugene, OR) were incubated in

antibody solution for 1.5 h. Slides were cover slipped with Vectashield mounting

medium (Vector Laboratories, Burlingame, CA) containing DAPI as a nuclear

counterstain.

β-catenin and IB4 expression analysis

Mouse brain sections from control and TBI animals were labeled with β-

catenin antibody and T-lectin. Vessel painted brain sections (DiI) from sham and

TBI 7 dpi animals were labeled with IB4 antibody. Images were blinded before

analysis. For each animal, two images were randomly captured with a fluorescence microscope (Keyence BZ-X700) in the cortical tissue surrounding the injury site at 20x magnification. Images were converted to grayscale and background was reduced by adjusting threshold values using ImageJ software. Images were overlaid (Image calculator, multiply) or subtracted (Image calculator, subtract) in order to measure the amount of colocalized and non-colocalized signal of the β-catenin and T-lectin channels respectively. Total β-catenin, colocalized, and non-colocalized intensity was calculated and integrated density values were used for analysis. Total IB4 and IB4-DiI colocalized integrated density was also calculated.

Quantification of Wnt-GFP expressing cells and vessels

TCF/Lef:H2B-GFP mouse brain sections at the level of the injury were stained with T-lectin. Two images were randomly captured from the cortical tissue surrounding the injury site at 20x magnification. GFP-positive nuclei and vessel segments were counted using the cell counting plugin in ImageJ. GFP-positive vascular cells were selected according to their endothelial cell-like morphology (oval nuclei, scant cytoplasm, and elongated cell outline) and location in the vessel. A single vessel segment was selected if it was present between two vessel junction points, two open endpoints, or a junction and open endpoint. GFP-positive vascular cells, positive vessel segments and total vessel segments were calculated as a total of the two images. Immunohistochemical

106

analyses were performed blindly and interpreted independently by two experimenters.

<u>Statistics</u>

Investigators were blinded to experimental conditions for all analyses. All measurements and analysis were performed without knowledge of the groups. One-way analysis of variance (ANOVA), with a post-hoc Tukey test, was used for comparison of vessel characteristics between hemispheres and perilesional tissue. One-way ANOVA, with a post-hoc Tukey test, was used for comparison of β-catenin and Cyclin D1 protein levels at multiple time points. Student T-test was used for comparison of Wnt5a protein levels. The data for the parametric tests showed a normal distribution and passed the Shapiro-Wilk normality tests. Student T-test, with Mann-Whitney test, was used for comparison of IB4 and DiI expression, and one way ANOVA, with Kruskal-Wallis test, was used for comparison of Wnt-GFP cells and positive vessel segments at multiple time points. All analysis was performed using GraphPad Prism 5.0 (GraphPad, San Diego, CA). Outliers were identified if they were below or above 1.5 times the interquartile range. All error bars are presented as standard error of mean (SEM). Statistical significance was noted at * $p < 0.05$, ** $p < 0.01$, or *** $p < 0.001$.

Results

Assessment of the cortical vasculature

We developed a novel vessel painting protocol that labels the whole brain vasculature. Vessel painted brains revealed excellent staining of the cortical and subcortical vessels (Fig. 3.1a, 3.2a). Thus, we utilized this technique to visualize vessel alterations within the brain after a moderate TBI. All animals appeared healthy before the procedure. A craniotomy alone in the Sham group showed minimal disruption of the vessels. The 1 day post-injury (dpi) group showed clear vascular loss at the site of the injury which extended to the outer perimeters as previously reported[262] (Fig. 3.1b). Conversely, the 7 dpi group revealed revascularization around the injury site (Fig. 3.1b). The majority of these new vessels appeared to originate from the perilesional tissue, radiating towards the injury site (Fig. 3.7). Irregular, disorganized and clearly disrupted vessels were also evident within the base of the injury site.

In order to determine the degree of vessel alterations after TBI, we undertook a vascular analysis to evaluate vessel density, number of junctions, and average vessel length (Fig. 3.1c-f). The Sham group (n=6/6) showed a reduction in vessel density in the ipsilateral hemisphere compared to the contralateral hemisphere (not significant), which was the result of the craniotomy. Vessel density in the ipsilateral hemisphere was decreased at 1 dpi by 36.7% compared to Shams ($p < 0.05$), which was followed by a 118.9% increase at 7 dpi ($p < 0.001$) (Fig. 3.1c). The 1 dpi group (n= 5/6, 1 outlier) exhibited decreased total

vessel density of 11.69 +/- 2.08 (mean +/- SEM) compared to 25.59 +/- 0.93 in

the 7 dpi group (n=4/5, 1 outlier). Interestingly, the contralateral hemisphere

showed a similar 48% increase in vessel density at 7 dpi (p<0.05) compared to 1

dpi (Fig. 3.1c). The 1 dpi group had a total vessel density of 19.93 +/- 2.01

compared to 29.49 +/- 0.51 in the 7 dpi group.

We next examined the vessel differences in the perilesional tissue (Fig.

3.1a). The Sham group (n=6/6) showed no significant difference in any vessel

parameters when comparing both hemispheres. The 1 dpi group (n=5/6) showed

a reduction in vessel density compared to the Sham group but this did not reach

significance (no statistical differences appeared in any of the other parameters).

We observed a 97.1% increase in vessel density (p<0.01), 157.0% increase in

number of junctions (p<0.01), and 93.7% increase in average vessel length

(p<0.05) at 7 dpi (n=4/5, 1 outlier) compared to 1 dpi (Fig. 3.1d-f). Thus, these

results suggest that there is a global increase in the vasculature following TBI

across both hemispheres by 7 dpi.

Assessment of the subcortical vasculature

To further assess the effects of cortical injury to the vasculature, we

analyzed coronal sections of vessel painted brains (Fig. 3.2a). The 1 dpi group

revealed loss of the cortical vessels that extended to the corpus callosum (Fig.

3.2b) and similar to the whole brain axial data (see above), the 7 dpi group

exhibited increased vascularization around the injury site (Fig. 3.2b). Newly

formed vessels appeared to extend from the surrounding tissues radiating toward the injury site. Similar to the axial cortical findings Sham mice showed minor injury to the cortical vessels.

Vascular analysis was performed on the coronal sections to quantify vessel characteristics. There was no significant difference in vessel density between the hemispheres. Vessel density in the ipsilateral hemisphere exhibited a non-significant decrease at 1 dpi (p=0.12), followed by a significant 56.5% increase at 7 dpi (p<0.01) (Fig. 3.2c). The 1 dpi group (n=5/6, 1 outlier) exhibited a total cortical vessel density of 9.33 +/- 0.74 compared to 14.61 +/- 0.56 in the 7 dpi group (n=5/5). Vessel density in the contralateral tissue was increased by 41.6% at 7 dpi (p<0.05) compared to the Shams (Fig. 3.2c). The Sham group (n=6/6) had a total vessel density of 11.86 +/- 1.38 compared to 16.79 +/- 1.06 in the 7 dpi group.

Analysis of vascular features in the perilesional tissue (Fig. 3.2a) found that TBI caused a significant decrease in vessel density and number of junctions at 1 dpi (p<0.001, n=5/6, 1 outlier), followed by 77.9% and 143% increase at 7 dpi (n=5/5) (Fig. 3.2d-f). Interestingly, both parameters at 7 dpi were still significantly reduced compared to Shams (p<0.05, p<0.01, n=6/6). There was no significant difference in average vessel length. Thus, these results suggest that despite robust repair of the cortical vessels, there is a slower temporal repair of vessels within the deeper layers of the cortex.

<u>Newly formed, non-perfusing vessels</u>

While our vessel painting technique labels perfused vessels in the brain, this method does not identify directly identify new or immature vessels after injury that are non-perfusing. Undamaged and newly formed vessels can be distinguished according to endothelial tip cell morphology and their perfusion status[263]. To investigate this, we further examined our vessel painted brains and stained with Isolectin B4 (IB4) to label all the blood vessels, including endothelial tip and stalk cells. The 7 dpi group exhibited an increased number of IB4+/DiI- vessels in comparison to the Sham group (Fig. 3.3a). Along with having reduced or lack of DiI staining, these vessels appeared thinner and more elongated than normal sham vessels, suggesting that they are likely immature (Fig. 3.3b). Furthermore, we observed IB4+ endothelial tip cells extending their filopodia into the extracellular environment that often were not associated with DiI+ vascular components consistent with vascular sprout formation (Fig. 3.3c). Quantitative analysis of the perilesional tissue revealed an increase in IB4 expression in the 7 dpi ($p=0.09$) compared to the Sham group, but this did not reach significance. However, we observed a 31.0% reduction in DiI-expressing IB4+ vessels by 7 dpi ($p<0.05$) in compared to the shams, indicating that the new vessels are non-perfusing. The Sham group (n=3/4, 1 outlier) had a DiI/IB4 colocalized integrated density of 2463 +/- 63.69 while the 7 dpi group (n=4/4) had 1700 +/- 202.40. Thus, these data provide further evidence for vascular regrowth after TBI.

<u>Changes in β-catenin expression profile</u>

The Wnt/β-catenin signaling pathway is tightly regulated by the protein β-catenin. Upon activation, β-catenin escapes degradation where it accumulates in the cytoplasm and translocates into the nucleus where it complexes with T-cell specific transcription factor/lymphoid enhancer-binding factor (TCF/LEF) to promote transcription of Wnt target genes. We hypothesized that TBI activates the Wnt/β-catenin signaling pathway to initiate vascular repair. To test this hypothesis, we measured cytoplasmic and nuclear β-catenin protein levels in the injury site over the course of 7 days after injury. The animals in the control group showed no change in cytoplasmic and nuclear β-catenin levels over 7 days following anesthesia treatment. We found that cytoplasmic β-catenin protein levels were reduced 93.9% by 7 dpi ($p < 0.05$) in compared to 1 dpi (Fig. 3.4a-b). The 1 dpi group (n=5/7, 2 outliers) had a normalized cytoplasmic β-catenin level of 92.15 +/- 20.55 compared to 5.59 +/- 3.52 for the 7 dpi group (n=5/6, 1 outlier). Similarly, there was a 35.7% reduction in nuclear β-catenin protein levels by 7 dpi ($p < 0.05$) (Fig. 3.4a, 3.4c). The 1 dpi group had normalized nuclear β-catenin levels of 84.01 +/- 5.17 compared to 54.03 +/- 8.30 for the 7 dpi group.

To assess activation of Wnt genes, we measured expression of the down-stream Wnt target gene Cyclin D1. We found that cytoplasmic Cyclin D1 protein levels were increased at 1 dpi ($p < 0.01$) and peaked at 3 dpi ($p < 0.001$) in compared to 12hr group (Fig. 3.4d-e). The 3 dpi group (n=5/5) had a normalized Cyclin D1 levels of 203.20 +/- 17.2 compared to 80.67 +/- 9.37 for the 12hr group

(n=5/5) with an increase of 151.9%. Interestingly, Cyclin D1 protein levels were reduced at 7 dpi (p< 0.05) in compared to the 3 dpi group. We next tested the expression of non-canonical Wnt5a, which downregulates β-catenin-induced gene expression[264]. Wnt5a protein levels increased 141.9% at 7 dpi (p< 0.05) in compared to 1 dpi group (Fig. 3.4f-g). The 7 dpi group (n=5/5) had a normalized Wnt5a levels of 150.90 +/- 26.78 compared to 62.06 +/- 20.24 for the 1 dpi group (n=4/5, 1 outlier). Thus, these data suggest that β-catenin levels are reduced at the injury site at 7 dpi and are likely inhibited by the non-canonical Wnt pathway.

We investigated β-catenin expression in blood vessels in the injured cortical tissue by staining for β-catenin and the vascular marker T-lectin. The control group exhibited uniform β-catenin expression throughout the cortex where β−catenin-expressing cells were primarily non-vascular and seen adjacent to the vessels (Fig. 3.5a). After TBI at 1 dpi and 7 dpi we observed a dramatic reduction in β-catenin expression around the injured cortex. Interestingly, β-catenin expression was specifically up-regulated in cortical vessels (Fig. 3.5a). Quantitative analysis revealed a gradual reduction in β-catenin expression over the course of 7 days after injury (p<0.001, control n=4/4. TBI 7 dpi n=4/5, 1 outlier) (Fig. 3.5b), consistent with our earlier findings (Fig. 3.4a-c). Despite the local decrease, β-catenin expression in T-lectin+ vessels was significantly increased by 1 and 7 dpi (p<0.05, TBI 1 dpi n=4/4, p<0.001) in comparison to controls (Fig. 3.5c). Furthermore, TBI groups showed a reduction in T-lectin density compared to control groups. Together, these data indicate that while

there is a gradual decrease in β-catenin expression after TBI, there is dramatic

shift from non-vascular to expression within vascular elements in the cortical

tissue.

Expression of Wnt target genes

To assess Wnt gene expression, we utilized a transgenic reporter mouse

line (TCF:LEF1:H2B-GFP) that expresses Histone 2B-GFP fusion protein under

the control of TCF/LEF response elements. Similar to wild types, TCF:LEF1:H2B-

GFP mice showed an identical reduction in β-catenin expression at 7 dpi ($p<0.05$,

n=4/4) in compared controls (n=3/3) (Fig. 3.8). Mouse brain sections from control

and TBI groups were stained with T-lectin and the perilesional tissue was

assessed. The control group had few Wnt-GFP vascular cells inside vessels with

most positive cells adjacent to the vessel wall. In contrast, TBI 1 dpi and 7 dpi

groups revealed a profound increase in Wnt-GFP vascular cells inside cortical

vessels (Fig. 3.6a-b). Quantitative analysis confirmed a 110.7% increase in Wnt-

GFP vascular cells within vessels at 1 dpi ($p<0.05$, n=4/4) followed by a decline

to control levels by 7 dpi (p=0.07, n=4/4) (Fig. 3.6c). Control mice (n=3/3) had

42.00 +/- 14.01 GFP-positive cells whereas the 1 dpi group had 88.50 +/- 10.65.

We also quantified the number of vessel segments that showed Wnt-GFP

positivity. Analysis revealed a 126.7% increase in Wnt-GFP-positive vessel

segments at 7 dpi (n=4/4) compared to the controls (n=3/3) (Fig. 3.6d). Controls

had 0.15 +/- 0.05 GFP-positive vessels whereas the 7 dpi group had 0.34 +/-

0.05. There was an increase in Wnt-GFP-positive vessel segments at 1 dpi

(n=3/4, 1 outlier) but this did not reach significance. We also observed increased

GFP expression in neurons (NeuN+) and astrocytes (GFAP+) in the injured

cortex (Fig. 3.9), which confirms findings from previous studies[206, 207].

We stained with the vascular marker von Willebrand factor (vWF), which

preferentially labels activated vessels and has previously been shown to identify

newly formed vessels in tumors[265] and in transplanted islets[266]. The control and 1

dpi groups showed heterogeneous vWF expression throughout the cortex with

limited staining in vascular structures (data not shown for 1 dpi group).

Conversely, vWF expression was enhanced in perilesional vessels by 7 dpi.

Furthermore, we observed Wnt-GFP-vascular cells in and around vWF+ vessels

(Fig. 3.6e). We next examined the expression of the Wnt target gene, sex

determining region Y-box 17 (Sox17)[203] after TBI. Compared to the controls,

Sox17 expression was increased in vascular structures at 7 dpi and co-localized

with Wnt-GFP-positive vessels (Fig. 3.6f). Together, these results strongly

suggest that Wnt gene expression is specifically enhanced in the vasculature

after TBI and it may participate in vascular repair.

Discussion

In this study, we sought to understand how the cerebral vasculature

responds after TBI and if Wnt/β-catenin signaling could play a role in vascular

repair. We report the following novel findings: 1) TBI results in vascular loss at 1

dpi which was followed by a subsequent increase in vascular features at 7 dpi, 2) immature, non-perfusing vessels were evident around the site of injury at 7 dpi, 3) β-catenin protein levels were reduced in the injury site at 7 dpi, 4) β-catenin expression was increased in perilesional vessels at 1 and 7 dpi, and 5) the number of Wnt-GFP+ vessel segments was increased after trauma. Our findings suggest that Wnt/β-catenin expression contributes to the vascular repair process after TBI.

Preclinical studies using a variety of animal models of TBI have reported repair of injured vessels, albeit abnormal. Park et al.[9] demonstrated that injured cortical vessels were repaired by 14 days after fluid percussion injury. Interestingly, the repaired vasculature in moderate and severely injured animals was abnormal compared to Sham animals. Mice that received multiple blast exposures had occluded vessels and narrowed lumens at 6 months after injury[72]. Similarly, Hayward et al.[70] revealed that vessel density in the ipsilateral cortex was restored by 14 days after fluid percussion injury but with altered cerebral blood flow. We found that there was a decrement at 1 dpi followed by an increase in vessel features at 7 dpi. Our data reveals a more gradual repair of the subcortical vessels within the brain in compared to the cortical vessels on the dorsal surface. The repaired vessels around the injury site appeared irregular and were clearly morphologically different from the uninjured vessels in the Sham group. These malformed vessels likely affect how the brain tissue undergoes repair, for example they could impede delivery of oxygen and neurovascular

substrates that are necessary for neurogenesis[267]. Additionally, these malformed

vessels may prevent clearance of fluid and waste products from the injured

tissue and be more susceptible for hemorrhagic progression and other secondary

complications[253]. Our results and the work from others suggest that the repaired

vasculature is abnormal after TBI, but more work is needed to assess the

functionality of these abnormal vessels and how they affect functional outcome.

While previous studies have provided some evidence of vascular repair at

the TBI lesion site, they have not assessed changes in the whole brain

(hemispheric)[9, 70, 72]. We are the first to report an increase in vascular features in

both hemispheres by 7 dpi. These findings strongly suggest a diaschisis effect in

which blood vessels from undamaged regions of the brain are activated and have

the potential to influence vascular repair. One possible explanation for this effect

is up-regulation of angiogenic factors within the blood circulation. Patients with

severe TBI have been reported to have increased expression of serum VEGF

and Angiopoietin-1, two key factors involved in sprouting angiogenesis, by 7-14

dpi[98, 144]. These circulating factors likely activate blood vessels throughout the

brain and lead to increased vascularization. Another explanation could be diffuse

hypoxia, which has been reported in clinical TBIs and can last up to 1 week after

injury[268]. Hypoxia is one the many inducers of sprouting angiogenesis after injury.

Studies have shown that chronic hypoxia increases vessel growth in both

hemispheres of the rodent brain[269, 270]. Thus, angiogenic factors may be up-

regulated in diffuse regions of the brain after TBI through a hypoxic-mediated response.

Many studies have utilized a variety of protocols to stain the vasculature in rodents, but these techniques have low efficiency rates, do not effectively stain all the vessels in the whole brain, and have minimal fluorescence[9, 271]. In our study, we utilized a novel vessel painting technique to visualize the cerebral vasculature after a moderate TBI. While our technique provides excellent staining of all the blood vessels in the mouse brain (including micro-vessels), it was difficult to acquire consistent staining across animals. We found that 65% (20 of 31) of mice showed excellent vessel staining, using very stringent criteria (uniform pink staining of entire brain parenchyma and staining of large and small vessels in cortical and deep compartments of the brain) that underwent analysis. We previously utilized a similar staining procedure in the adult rat after a moderate TBI and found that 70% of rat brains showed excellent vessel staining[233]. An issue with labeling of the vessels may be the result of the high alcohol content (10%) in the DiI solution. Another limitation with our technique is the preferentially labeling of DiI to arteries. Previous protocols that used DiI reported high staining of arteries with veins only weakly stained[220].

Sprouting angiogenesis, or the formation of new capillaries from existing vessels, is an important repair response that is activated after injury. This process is driven by endothelial tip and stalk cells where tip cells migrate into the hypoxic tissue and lead to vessel sprouts whereas stalk cells proliferate to form

the vessel lumen and extend the sprout[88]. Together, these cells form an immature non-perfusing vessel which is later remodeled and matured to form a functional, perfusing vessel[88]. The 7 dpi group showed vessels with narrowed lumens, elongated shapes, and sprouting endothelial tip cells. One interesting finding was that 31.0% of the vessels appeared to have reduced DiI staining which may be a reflection of their immaturity. While these findings suggest that sprouting angiogenesis is occurring around the lesion site, the possibility still exists that these vessels are not *de novo* but existing vessels that were constricted. We believe that this is unlikely since most instances of vasospasms are transient and occur early after injury, i.e. part of hemostasis[43, 44, 272]. Severe vasospasms can last for several weeks after severe TBI and blast injuries but are likely not present in our moderate model at this time point[44]. Another possibility is the obstruction of vessels by microthrombi. Schwarzmaier et al.[272] observed the formation of microthrombi in pial vessels early after moderate TBI (<2 hours) leading to reductions in blood flow to the peri-lesional tissue. The incidence of microthrombi are highest in the acute phases of injury and tend to resolve by 1-2 weeks[273]. While we cannot rule out of the possibility of microthrombi occluding vessels early after TBI, it is unlikely that this is occurring at our later time points.

Activation of the Wnt/β-catenin pathway has reported after TBI. However, studies have shown contrasting results with regards to β-catenin expression after TBI[191, 208, 260]. The expression profile of β-catenin appears to be dependent on the injury model. We found a reduction in global β–catenin protein levels in the

injured brain tissue at 7 dpi. Our results are consistent with Yi-Min and colleagues[260], which found a down-regulation of β-catenin protein levels between 3-14 days after weight drop injury. Interestingly, despite a reduction in nuclear β-catenin we noticed increased expression of Cyclin D1 at 1 and 3 dpi, indicating that even low levels of nuclear β-catenin can induce gene activation. It has been suggested that β-catenin fold-changes, as opposed to absolute levels, controls Wnt/β-catenin pathway activation[274]. Moreover, when β-catenin is present in the nucleus, it can interact with TCF/LEF family of transcription factors along with a multitude of other transcription factors to enhance or inhibit Wnt/β-catenin signaling[182]. One key inhibitor is the non-canonical Wnt pathway, which can inhibit β-catenin/TCF activity[264]. Others have reported that non-canonical Wnts directly modulate β-catenin by inducing its degradation[275] or redirecting it to the cell membrane[276]. In support of this, we observed increased Wnt5a expression at 7 dpi indicating that non-canonical Wnt pathway may be involved in suppressing Wnt/β-catenin pathway.

The Wnt/β-catenin signaling pathway is critical in the formation of blood vessels in the Central Nervous System (CNS)[198, 202]. The Wnt/β-catenin pathway is robustly activated in CNS vessels during development, but its activity declines in the adult[199, 200]. Emerging research suggests that the Wnt/β-catenin pathway is reactivated in blood vessels following CNS injuries and diseases. Lengfeld et al.[277] demonstrated that Wnt/β-catenin pathway partially repairs the blood brain

barrier following Multiple Sclerosis. Dysfunctional Wnt/β-catenin signaling has also been implicated in aberrant angiogenesis in Huntington's disease[278]. Additionally, this pathway possesses many angiogenic functions in non-CNS injuries. In a vascular balloon injury, β-catenin induces vascular remodeling after injury[258], and Kim et al.[259] showed that β-catenin modulates angiogenesis and improves vascular function in a mouse hindlimb ischemia model. Our results extend these early observations wherein we report increased β-catenin expression and enhanced Wnt gene expression in the cerebral vessels at 1 and 7 days after TBI. Together, our findings suggest that Wnt/β-catenin expression likely has a role in vascular repair and represents a potential target for future therapeutics for TBI and other brain injuries.

Numerous angiogenic factors are up-regulated after TBI and have distinct expression profiles and functions. One such molecule is VEGF, which plays a role in post-stroke angiogenesis[279]. Experimental studies using animal models of TBI have reported up-regulation in VEGF expression at 3-7 dpi[89, 280, 281]. An important finding was the rapid up-regulation of β-catenin expression in the cortical vessels, indicating that β-catenin may be the driving force for vascular repair by regulating the expression of VEGF and other putative angiogenic factors. The VEGF promoter contains seven binding sites for β-catenin/TCF[282], and β-catenin has been shown to increase VEGF expression after hindlimb ischemic injury[259]. Thus, β-catenin may directly regulate VEGF expression or act in parallel with VEGF to promote vascular repair after TBI.

In summary, the cerebral vasculature participates in the pathogenesis of TBI and treatments that can enhance vascular repair and restore vascular function are critical for functional outcome. This study provides quantitative morphometric information on the vascular network in acute and subacute stages of TBI. The Wnt/β-catenin signaling pathway has been studied in the context of regeneration, neuronal and glial cell populations, after TBI[206-208]. The present study is the first to examine this pathway in the context of vascular repair after TBI. We are the first to report increased β-catenin expression and activation of Wnt genes in the vasculature early after TBI, suggesting that Wnt/β-catenin signaling may be a key player in the initiation of vascular repair. Our results open up the possibility of targeting the Wnt/β-catenin signaling pathway to enhance vascular repair as a therapeutic target for TBI. The Wnt/β-catenin signaling pathway may work in conjunction with Notch signaling to activate vascular repair genes after injury. Ongoing research will be needed to discover the molecular mechanisms underlying Wnt/β-catenin-mediated vascular repair.
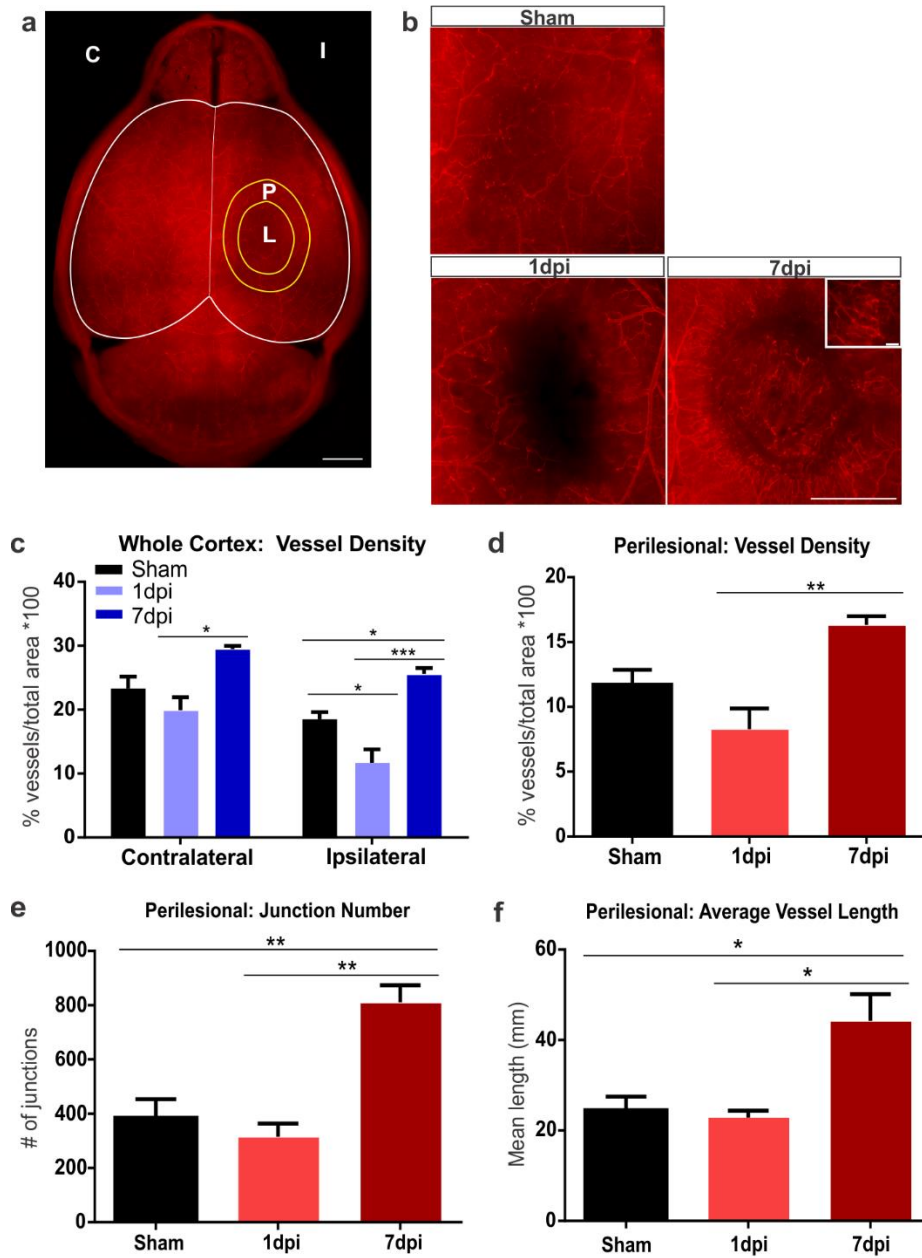
Figure legends

Figure 3.1. TBI results in vascular injury followed by repair. A) Axial view of a

vessel painted brain from a Sham animal illustrating the dense vascular plexus.

Analysis on the ipsilateral (I), contralateral (C) hemispheres, and perilesional

tissue (P) around the lesion (L) was undertaken. Scale bar = 1000µm. B) Representative images from Sham, 1 dpi, and 7 dpi groups. Sham animals exhibited minor vascular disruptions due to the craniotomy. In the 1 dpi group there was a clear disruption of the vessels that extended beyond the impact site. In contrast, the 7 dpi group showed the presence of newly formed vessels around the impact site. The inset illustrates these new vessels at high magnification. Scale bar = 1000µm, 100µm (insert). C) Vascular analysis of the ipsilateral hemisphere demonstrated a reduction in vessel density (one-way ANOVA, $p<0.05$) in 1 dpi group compared to Shams, while the 7 dpi group showed a significant increase in vessel density (one-way ANOVA, *** $p< 0.001$, * $p< 0.05$) compared to the 1 dpi and Sham groups. The contralateral hemisphere also exhibited a reduction in vessel density (not significant) at 1 dpi compared to the Sham group. Interestingly, the 7 dpi group showed a significant increase in vessel density (one-way ANOVA, * $p< 0.05$) compared to the 1 dpi group with no change compared to Shams. D) Vascular analysis of perilesional tissue revealed a significant increase in vessel density (one-way ANOVA, ** $p< 0.01$) in the 7 dpi compared to the 1 dpi group. E) Analysis of the perilesional tissue revealed a significant increase in the number of junctions (one-way ANOVA, ** $p< 0.01$) in the 7 dpi compared to 1 dpi and Sham groups. F) Similarly, we observed a significant increase in average vessel length (one-way ANOVA, * $p< 0.05$) in the 7 dpi compared to 1 dpi and Sham groups
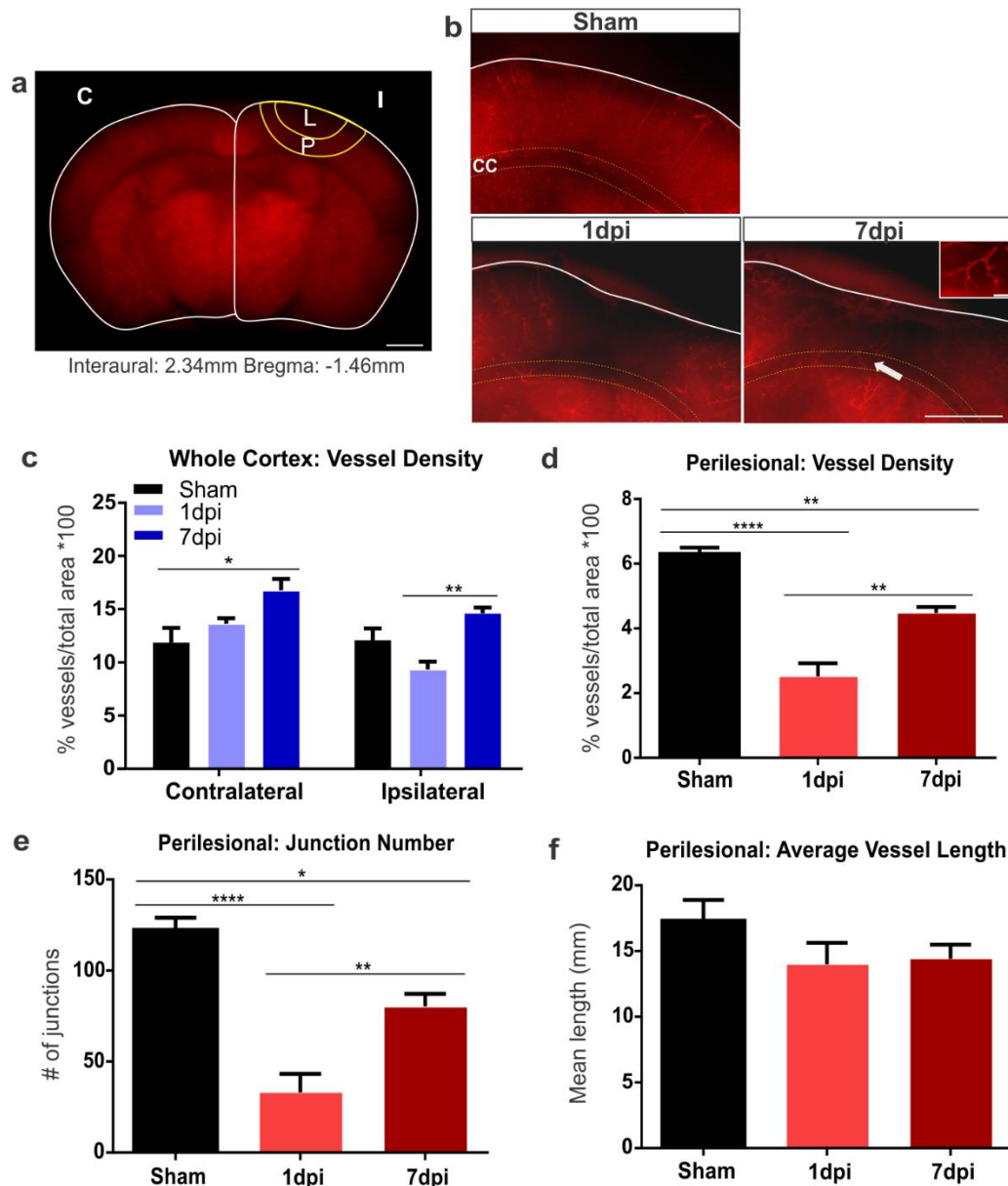
Figure 3.2. Coronal assessment of vessel painted vasculature. A) Coronal view

of a vessel painted Sham animal illustrating staining of the cortical and

subcortical vasculature. ROIs in the ipsilateral (I), contralateral (C) hemispheres,

and perilesional tissue (P) encompassing the lesion (L) were undertaken. Scale

bar = 1000µm. B) Representative images of Sham, 1 dpi, and 7 dpi animals. The

Sham group exhibited minor loss of vessel density, whereas the 1 dpi group had

extensive vascular loss of the cortical vessels that extended to the corpus callosum (CC, yellow dotted line). The 7 dpi group revealed newly formed vessels radiating toward the impact site (arrow). High magnification image of designated vessel is present in the insert. Scale bar = 200µm, 100µm (insert). C) Vascular analysis of the ipsilateral hemisphere demonstrated a reduction in vessel density (not significant) at 1 dpi while the 7 dpi group showed a significant increase in vessel density (one-way ANOVA, ** $p < 0.01$) compared to the 1 dpi group. Analysis of the contralateral hemisphere demonstrated an increase in vessel density (one-way ANOVA, *$p < 0.05$) in 7 dpi group compared to Shams. D) Vascular analysis of the perilesional tissue revealed a significant increase in vessel density (one-way ANOVA, ** $p < 0.01$) in the 7 dpi compared to the 1 dpi group. Vessel density in the 7 dpi group (one-way ANOVA, ** $p < 0.01$) was significantly reduced compared to the Sham group. E) Similarly, we observed a significant increase in the number of junctions (one-way ANOVA, ** $p < 0.01$) in the 7 dpi compared to the 1 dpi group. Number of junctions in the 7 dpi group (one-way ANOVA, * $p < 0.05$) was significantly reduced compared to the Sham group. F) Vessel length at 1 and 7 dpi showed a reduction compared to the Shams, but it did not reach significance
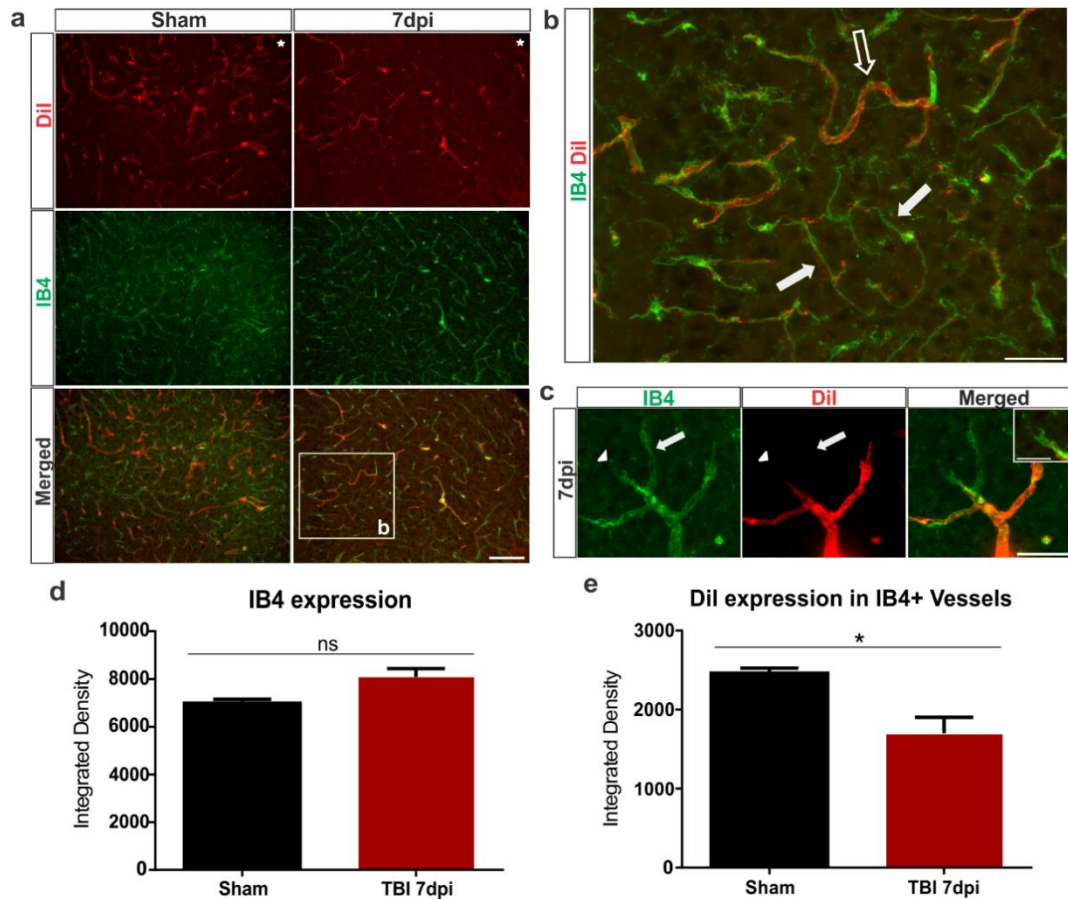
Figure 3.3. Identification of perfused and newly formed vessels in the cortex. A)
Sham animals showed uniform vessel staining with DiI in coronal sections (see
Fig. 3.2) whereas the 7 dpi group exhibited a reduction in labeled vessels
adjacent to the injury site (top panel). Similarly, in Shams there was a uniform
staining of IB4+ vessels with an apparent reduction in the 7 dpi group.
Interestingly, there appeared to be an increase in co-localized DiI and IB4+
vessels in the Sham group, with little co-localization in the 7 dpi group. The
boxed area is enlarged in B. Star indicates region of impact. Scale bar = 100µm.
B) A IB4+/DiI+ vessel from a 7 dpi mouse (open arrow) that is perfused (DiI+).
Immature vessels, IB4+/DiI-, appear narrower and elongated in shape and are

likely not fully formed nor perfused (solid arrow). Scale bar = 50µm. C) High

magnification image of a newly forming vessel branching from an existing vessel.

A new vessel is seen sprouting from a pre-existing vessel (arrow). IB4+

endothelial tip cells extend their filopodia into the cortex (arrowhead). Insert

illustrates the filopodia of an endothelial tip cell. Scale bar = 25µm, 15µm (insert).

D) Analysis of the perilesional tissue revealed an increase in IB4 expression in

the 7 dpi (Student T-test, p=0.09) compared to the Sham group. E) Analysis

revealed a significant decrease in DiI-expressing IB4+ vessels in the 7 dpi

(Student T-test, * p< 0.05) in compared to the Sham group.
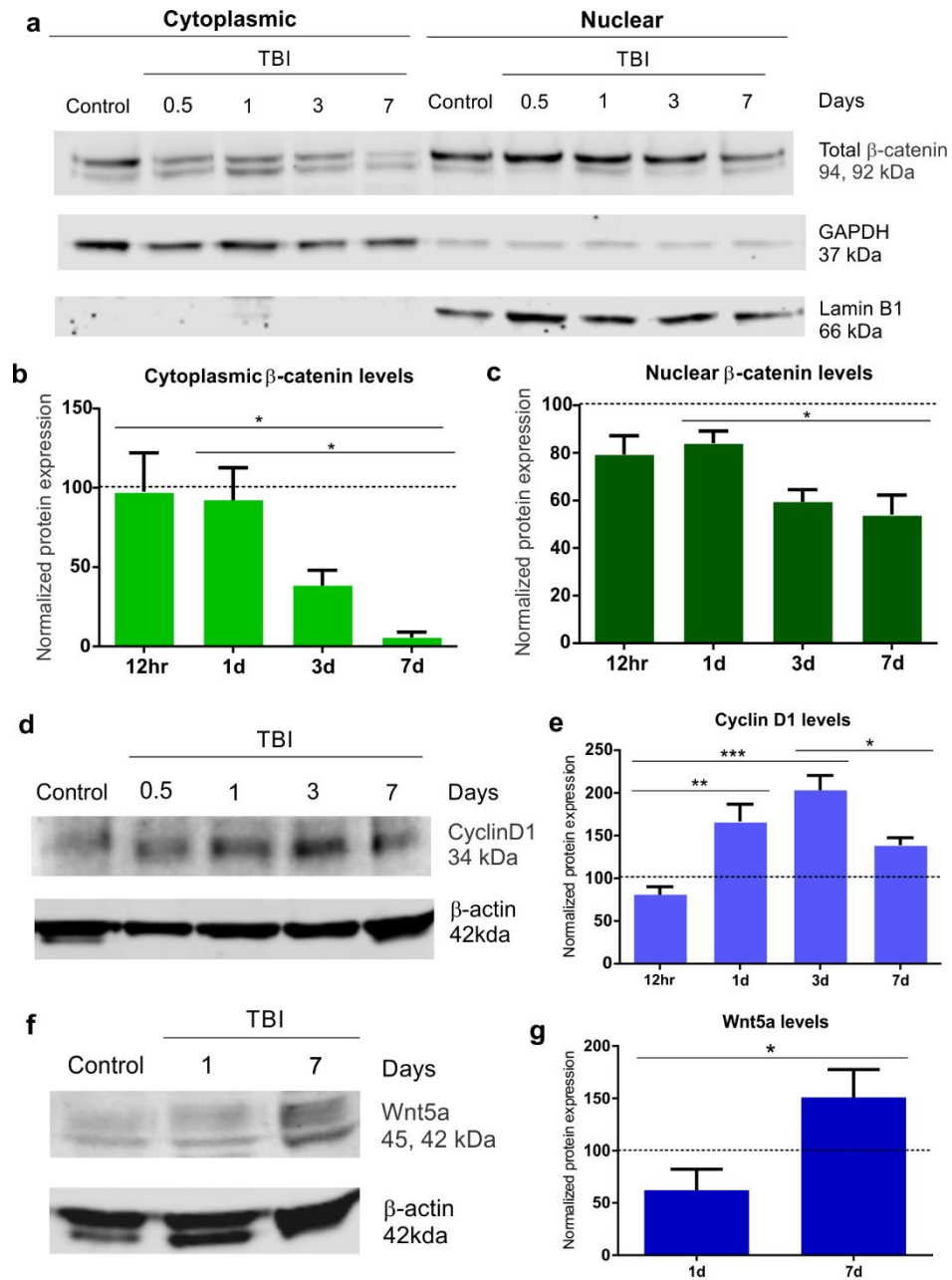
Figure 3.4. Temporal decrease in beta-catenin levels after TBI. A) Western blots reveal a gradual decrease in cytoplasmic and nuclear β-catenin protein levels over a time course of 7d after injury. Control animals showed no changes in β-catenin expression during the 7d time frame. GAPDH was used as cytoplasmic

loading control. Lamin B1 was used as a nuclear loading control. 8µg loaded per well. B) Densitometric analysis showed a significant decrease in cytoplasmic β-catenin levels (one-way ANOVA, * p< 0.05) at 7 dpi compared to the 12hr and 1 dpi groups. C) Similarly, there was a significant decline in nuclear β-catenin levels (one-way ANOVA. * p< 0.05) in the 7 dpi compared to 1 dpi group. Control (n=13), TBI 12hr (n=6), 1dpi (n=7), 3dpi (n=6), and 7dpi (n=6) group. D) Western blot revealed that Cyclin D1 protein levels peak by 3 dpi followed by reduction at 7 dpi. β-actin was used as cytoplasmic loading control. 10µg loaded per well. E) Densitometric analysis demonstrated a significant increase in Cyclin D1 levels at 1 and 3 dpi (one-way ANOVA, ** p<0.01, *** p<0.001) in compared to the 12hr group. Expression peaked at 3 dpi. There was a significant decline in Cyclin D1 levels at 7 dpi (one-way ANOVA, * p<0.05) compared to the 3 dpi. F) Western blot revealed an increase in Wnt5a protein levels at 7 dpi compared to 1 dpi. β-actin was used as cytoplasmic loading control. 10µg loaded per well. G) Densitometry analysis showed a significant increase in Wnt5a levels at 7 dpi (Student T-test, * p<0.05) in compared to 1 dpi group.
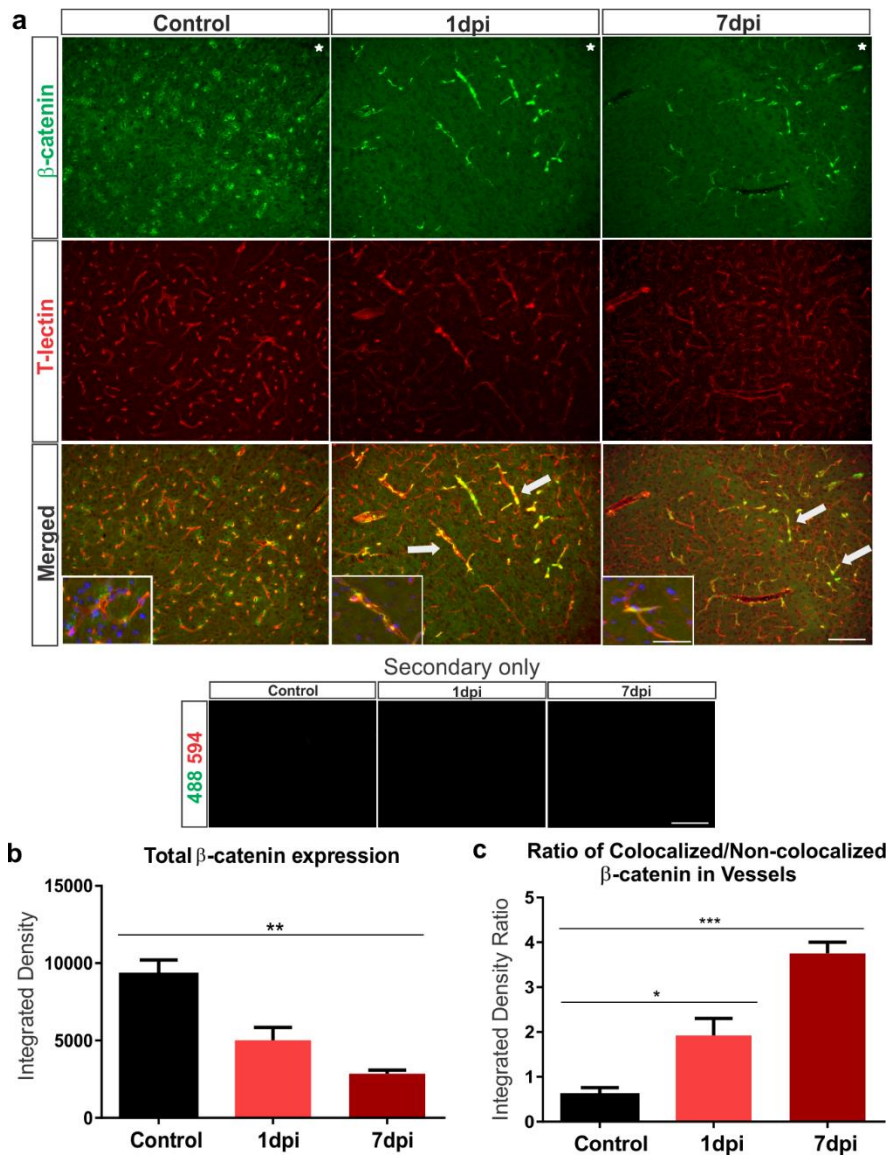
Figure 3.5. Beta-catenin is up-regulated in cortical vessels after TBI. A)

Immunohistochemical images from control, 1 and 7 dpi groups. The controls

exhibited β-catenin uniform expression in the cortex whereas there was a

dramatic loss of expression in the 1 and 7 dpi animals. Vascular loss relative to

controls was also observed in the 1 and 7 dpi groups (T-lectin). Interestingly, in

the control animals β-catenin expression was observed adjacent to vessels

stained with T-lectin whereas 1 and 7 dpi animals clearly demonstrated β-catenin expression inside vascular structures. Note the increased number of β-catenin+/T-lectin+ vessels in the 1 and 7 dpi groups (arrows). No auto fluorescence was observed in the 594 and 488 channels in any of the tissues. High magnification insert with DAPI illustrates β-catenin-expressing cells adjacent to the vessels in the controls groups and β-catenin+ vessels in the 1 and 7dpi groups. Star indicates region of impact. Scale bar = 100µm, 50µm (insert). B) Densitometric analysis of β-catenin expression in the ipsilateral cortex revealed a significant reduction at 7 dpi compared to controls (one-way ANOVA, ** $p < 0.01$). C) Analysis of β-catenin localization revealed a significant increase in β-catenin expression in T-lectin+ vessels (increased colocalized/non-colocalized ratio) at 1 and 7 dpi compared to the controls (one-way ANOVA, * $p < 0.05$, *** $p < 0.001$)
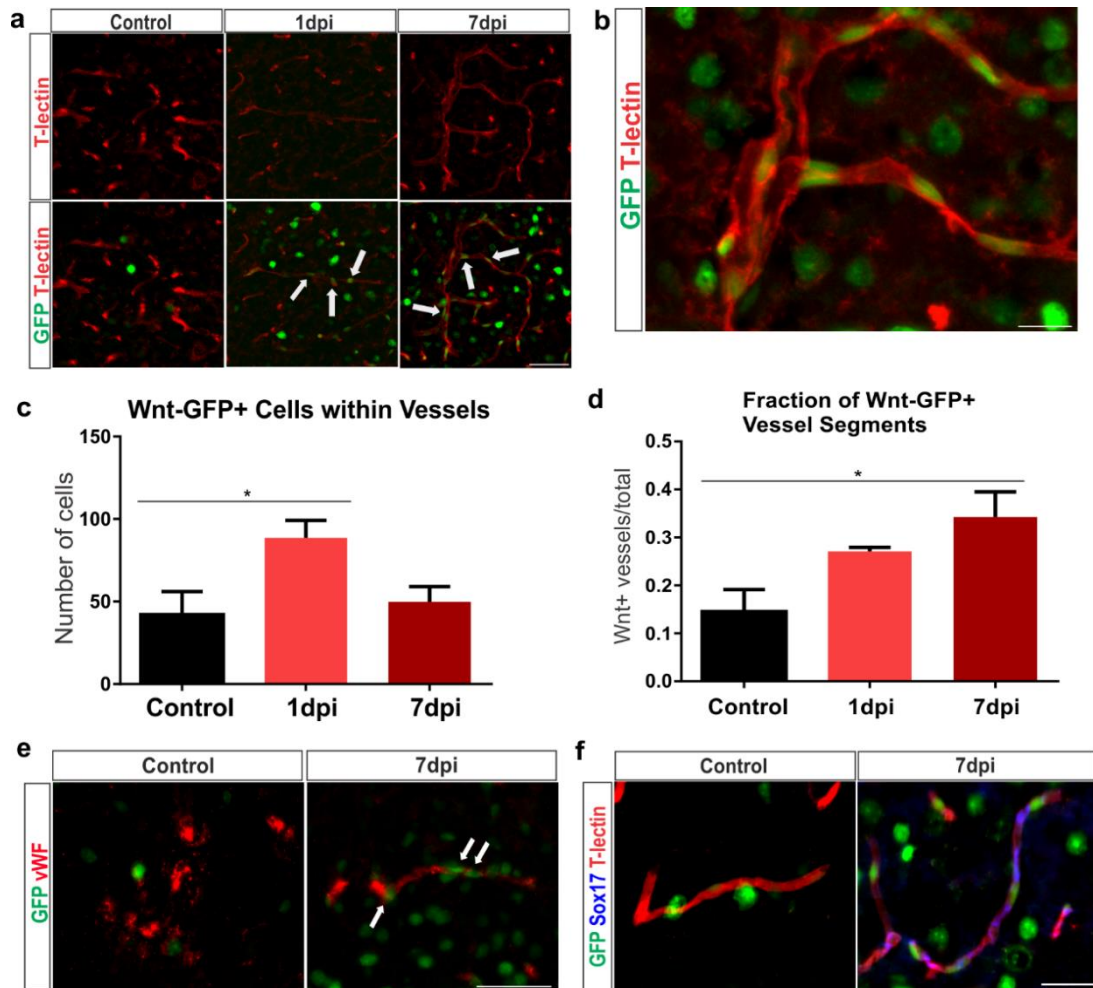
Figure 3.6. Wnt-GFP-expressing cells are increased inside vascular structures after TBI. A) We utilized a transgenic mouse line (TCF/LEF:H2B-GFP) to track individual cells with Wnt gene expression. Representative images of control, 1, and 7 dpi groups from the ipsilateral cortex. Few Wnt-GFP vascular cells were seen inside the vessels (T-lectin) in the control group, whereas there was an increase in the 1 and 7 dpi groups (arrows). Scale bar = 50μm. B) A vessel from a 7 dpi animal showing Wnt-GFP vascular cells inside blood vessels. Scale bar = 15μm. C) Quantitative analysis revealed a significant increase in the number of Wnt-GFP vascular cells at 1 dpi (one-way ANOVA, * p< 0.05) which was followed

by decrease at 7 dpi (one-way ANOVA, p=0.09). D) Quantitative analysis revealed a significant increase in Wnt-GFP-positive vessel segments at 7 dpi compared to the controls (one-way ANOVA, * p<0.05). E) Immunofluorescence of GFP (green) and von Willebrand Factor (vWF; red) in control and 7dpi group. The control group exhibited heterogeneous vWF expression throughout the brain. In contrast, 7 dpi group showed vWF expression in blood vessels around the impact site. Wnt-GFP vascular cells were found in and around most of these vessels (arrows). Scale bar = 50µm. F) Immunofluorescence of Sox17 (blue), GFP (green), and T-lectin (red) in control and 7 dpi group. Sox17 expression is up-regulated in vessels after 7 dpi and colocalizes with GFP+ vessels in Wnt reporter mice. Scale bar = 50µm
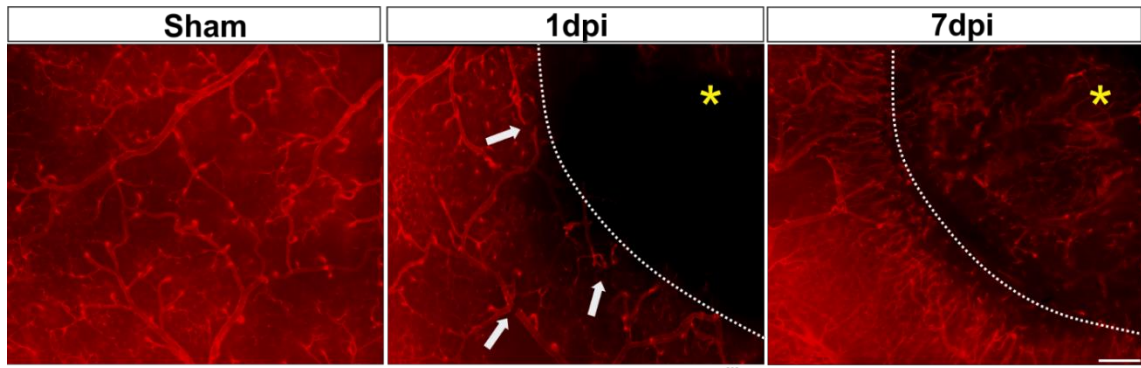
Figure 3.7. Temporal evolution of vascular repair in the peri-lesional tissues after TBI. Representative axial images from Sham, 1 dpi, and 7 dpi groups. We observed that a moderate TBI elicits a loss of the vasculature that extended beyond the impact site (yellow asterisk). Note the fragmented vessels in the peri-lesional tissue at 1 dpi (arrows). Over the ensuing 7 dpi there is repair of the injured vessels along with new vessels radiating toward the impact site. New vessels are also evident in the base of the impact site. White dotted line is the lesion border. Scale bar = 200µm
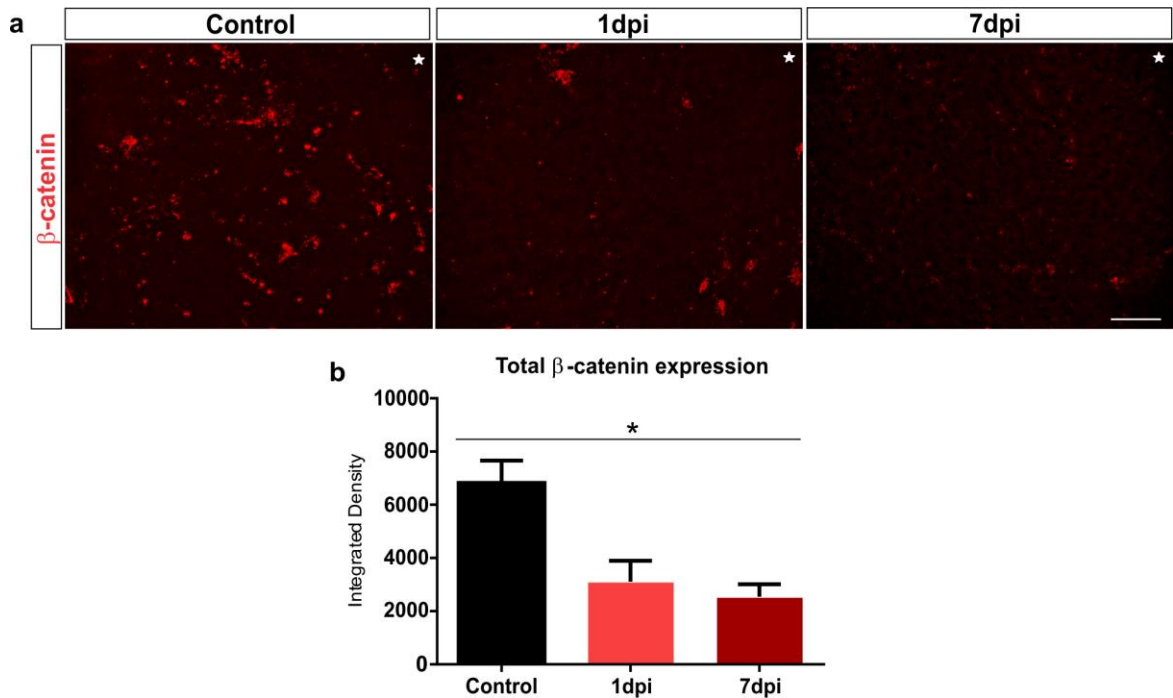
Figure 3.8. β-catenin expression was reduced in the peri-lesional tissue in

TCF/LEF:H2B-GFP mice. A) Immunohistochemistry of brain sections labeled

with β-catenin from control, 1 and 7 dpi TCF/LEF:H2B-GFP mice. The control

group exhibited high β-catenin expression while the 1 and 7 dpi groups revealed

a dramatic reduction in β-catenin expression. Star indicates region of impact.

Scale bar = 100µm. B) Densitometric analysis revealed a significant reduction in

β-catenin expression at 7 dpi compared to controls (one-way ANOVA, * $p < 0.05$).
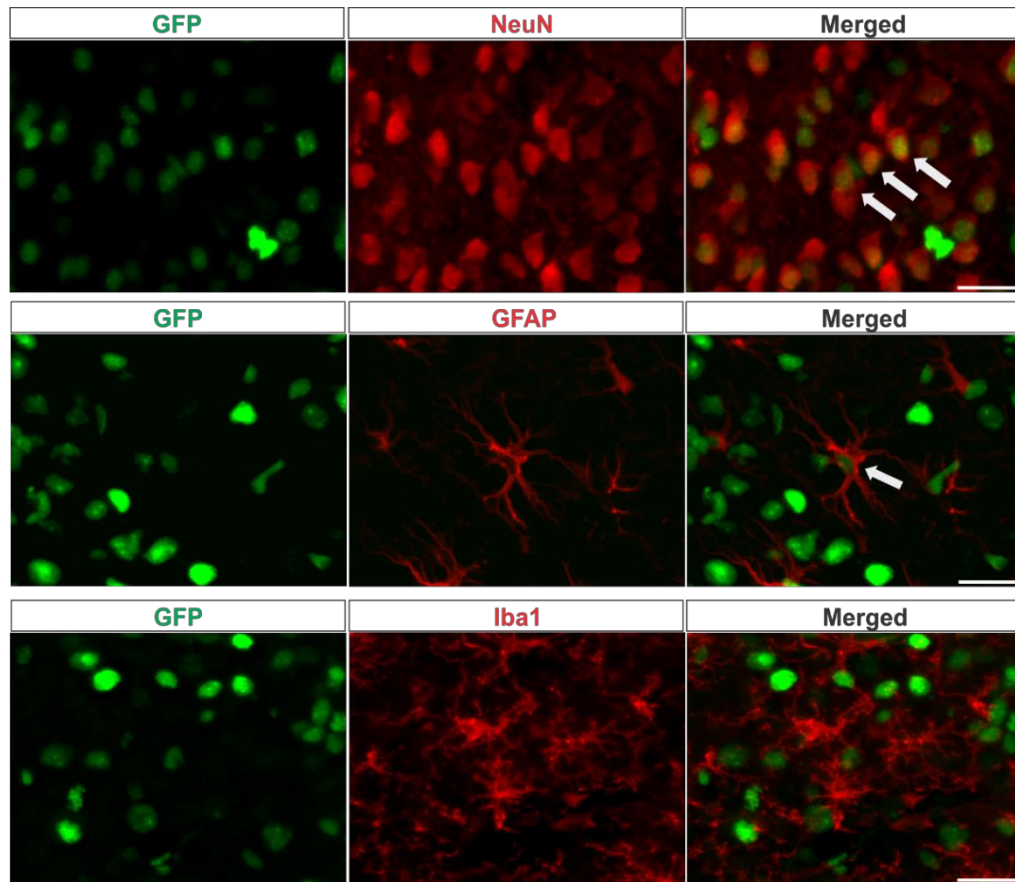
Figure 3.9. Astrocytes and neurons but not microglia have high Wnt-GFP expression after TBI. Characterization of the Wnt-GFP expressing cells outside the vessels by staining with a neuronal (NeuN), astrocyte (GFAP), and microglia (Iba1) marker. TBI 1 and 7 dpi groups revealed the presence of GFP+/NeuN+ cells throughout the injured cortex (arrows). A small subset of GFP+/GFAP+ cells were also evident (arrow). No GFP+/Iba-1+ cells were observed. Scale bar = 25μm

Chapter 4

Wnt/Beta-catenin Participates in Vascular Repair after Traumatic Brain Injury

Preface

This chapter discusses how increasing or decreasing beta-catenin protein following moderate traumatic brain injury affects vascular repair, long-term remodeling of the repaired vasculature, and development of hemorrhage and edema

Abstract

Cerebral vascular injury is a defining feature of traumatic brain injuries (TBI) which leads to secondary injury and influences clinical outcomes. There is an urgent need to develop new therapies to repair and restore cerebral vessels. β-catenin promotes blood vessel formation during embryonic development, but its role in vascular repair after TBI remains unclear. We previously reported that TBI leads to an early increase in β-catenin in cerebral vessels which coincides with vascular repair at 7 days post injury (dpi). Here, we tested the hypothesis that β-catenin regulates new vessel formation and long-term remodeling of the cerebral vasculature after TBI. We utilized Lithium to enhance β-catenin and JW74 to reduce β-catenin and evaluated its effects on vascular repair after TBI. Using a novel vessel painting (VP) technique, we found that Lithium treatment enhanced vascular repair and led to elongated vessels at 7 dpi whereas JW74 treatment reduced vascular repair and lead to truncated vessels. The repaired vasculature of Lithium and JW74 treated mice showed increased branching and elongated vessels at 14 dpi. *Ex vivo* magnetic resonance imaging of VP brains at 7 dpi revealed a reduction in hemorrhage following Lithium treatment and increased edema following JW74 treatment. Our findings suggest that β-catenin represents a potential target for future therapies to promote vascular repair and restoration.

Introduction

Traumatic brain injury (TBI) is a significant public health problem that can elicit cognitive, emotional, and behavioral deficits in individuals[14]. At present, there are no effective clinical treatments to assist in recovery of long-term outcomes. One potential target is the cerebral vasculature. TBI often results in injury to the cerebral vessels which leads to altered blood flow, edema, and hemorrhage[253]. The cerebral vasculature is a key focus of research in many neurological disorders (stroke, epilepsy, Parkinson's disease, and Alzheimer's disease) and it has been suggested that a dysfunctional vasculature is the cause of neurodegeneration in these brain disorders[283]. Thus, repairing the injured cerebral vessels after TBI is critical for neuroprotection and improving outcomes.

We have recently shown that a moderate TBI using controlled cortical impact (CCI) injury results in vascular loss followed by vessel formation at 7 days post injury (dpi)[74]. Furthermore, several studies revealed that blood flow is returned to the perilesional tissue by 14-21 dpi[70, 79, 80]. Given that a reduction in cerebral blood flow and tissue oxygenation is linked to poor neurological outcomes following TBI[37, 284], our results suggest that delayed vascular repair contributes to secondary injury after TBI. Another key finding from our study is that the repaired vessels are morphologically abnormal[74]. This is in agreement with studies in rodent models of fluid percussion injury and blast injury[9, 72, 73]. The irregular morphology and patterning of the repaired vasculature is associated with hypoperfusion 4 weeks after moderate TBI using a CCI model[71]. Thus, this

suggests that vascular abnormalities are likely a contributing factor to persistent neurological complications after TBI.

Although blood vessel formation increases in the perilesional cortex following TBI[9, 70, 80], it is unclear which pathways mediate its repair. One such molecule is vascular endothelial growth factor (VEGF). While VEGF induces angiogenesis in tumors and ischemic stroke (largely driven by hypoxia)[285, 286], it is unclear what role VEGF plays in vascular repair following TBI. Studies reported reduced VEGF levels early after Marmarou's acceleration impact[287] while other studies reported increased VEGF levels late (>7 dpi) after cortical cold injury and weight drop injury[89, 288]. Plasma VEGF were reduced at 7 and 30 dpi in rats given a mild fluid percussion injury[289] whereas serum VEGF were increased at 7-14 days in patients with severe TBI which correlated with increased circulating endothelial progenitor cells[98, 144]. It should be noted that delayed VEGF treatment after TBI (>7 dpi) increased vessel density[137] and capillary diameter[73], but it can increase vessel permeability[255]. Based on these studies and the non-angiogenic roles of VEGF[210, 290], it is likely that VEGF plays a minimal role in acute vascular repair after TBI.

One alternative and unexplored factor is β-catenin, which is a transcriptional regulator of the Wnt/β-catenin pathway and an adaptor protein of the adherens junctions. We previously reported that TBI results in an acute increase in expression of β-catenin in cerebral vessels which coincides with vascular repair at 7 dpi, indicating that β-catenin is a strong candidate in vascular

repair[74]. There are several lines of evidence in support of β-catenin in vascular repair after TBI. First, the Wnt/β-catenin pathway promotes blood vessel formation during embryonic development and controls angiogenesis, vascular sprouting, tip and stalk cell specification, vascular integrity, and blood brain barrier formation[198-200, 202]. Second, Wnt 7a, not VEGF, is a migratory factor in the mouse brain endothelial cell line, bEND3.0 cells[198]. Third, in cancer studies, β-catenin regulates expression of angiogenic factors including VEGF[291, 292]. Lastly, studies have reported an upregulation of β-catenin and Wnt genes in neuronal and glial cells after TBI and it has been suggested that Wnt/β-catenin pathway participates in neural stem and progenitor cell proliferation, neuronal cell apoptosis, and glial cell proliferation[191, 207, 208].

In this regard, we investigated the role of β-catenin in vascular repair by using Lithium (β-catenin agonist) to enhance β-catenin expression and JW74 (β-catenin antagonist) to reduce β-catenin expression. A key advantage in targeting β-catenin with small molecules is that it provides temporal control of β-catenin expression after TBI. To examine the cerebral vessels and its repair after injury, we used a novel vessel painting (VP) and analysis protocol that can visualize the cerebral vasculature at the whole brain level and can identify and analyze pial, penetrating, and parenchymal vessels including capillaries[74]. This study will focus on the superficial (~50 micrometer depth) cerebral vessels which are injured after TBI and which have not been studied in vascular repair. The first objective of this study was to evaluate how increasing and decreasing β-catenin affects vascular

repair at 7 dpi. The second objective was to assess how modulating β-catenin affects the new, repaired vasculature at 14 dpi. The third objective was to examine how enhancing and inhibiting vascular repair modulates hemorrhage and edema formation.

Material and methods

Animals

All animal experiments and care complied with federal regulations and were approved by the Institutional Animal Care and Use Committee of Loma Linda University according to Guide For the Care and Use of Laboratory Animals (Eighth edition). Adult male C57BL/6J mice (8-10 weeks, 25-30 grams) were purchased from Jackson Laboratory (Sacramento, CA). Mice were group housed and kept in a temperature controlled animal facility on a 12-hour light and dark cycle with free access to food and water.

Mice received a moderate TBI, drugs were injected 1 hour after TBI followed by injections once daily for 6 days, and thereafter drugs were discontinued for 8 days. Mice underwent vessel painting (VP) and *ex vivo* magnetic resonance imaging (MRI) at 7 or 14 dpi (Fig. 4.7a). In another cohort, mice were sacrificed for western blot at 7 or 14 dpi (Fig. 4.7b). The number of mice in each group are presented in Table 1 (Table 4.1). Only 2 mice were removed from the study: 1 mouse experienced a >15% reduction in weight and

did not recover following supportive care and 1 mouse died immediately following the TBI due to cardiac arrest.

Traumatic brain injury

A controlled cortical impact (CCI) model of moderate brain injury was utilized as previously described[31]. Briefly, mice were anesthetized with isoflurane (3% induction, 2% maintenance) using isoflurane vaporizer (VetEquip Inc., Pleasanton, CA). Anesthetized mice were placed in a stereotaxic frame and body temperature was maintained at $38\pm1°C$ with a heating pad during the surgery. A midline incision of the skin was made to expose the skull and a 5 mm craniotomy was carefully performed over the right parietal cortex between lambda and bregma sutures. A moderate CCI (1.5 mm depth, 3 mm diameter, 2.0 m/s speed, 200 ms dwell time) was delivered using an electromagnetically driven piston (Leica Microsystems Company, Richmond, IL). CCI procedure resulted in visible bleeding at the injury site that stopped in a few minutes. The bone flap was not re-inserted at the craniotomy site and skin was sutured. Buprenorphine (0.01mg/kg, intramuscular) was administered several minutes after the surgery. Mice were monitored daily following the procedure.

Drug administration

Lithium chloride (84.8 mg/kg dissolved in saline, Sigma-Aldrich, St. Louis, MO) or an equal volume of saline were injected intraperitoneal (I.P.). The dose of

lithium was based on previous studies using a mouse model of CCI[193, 194]. JW74 (75 mg/kg dissolved in 50% dimethyl sulfoxide and 50% polyethylene glycol 400, Tocris Biosciences, Minneapolis, MN) or an equal volume of dimethyl sulfoxide and polyethylene glycol 400 (both reagents are from Sigma-Aldrich, St. Louis, MO, referred to as vehicle) were administered orally via gavage. Since JW74 had not been used in TBI studies previously, we undertook a dose range study at 3 doses and found that a 75 mg/kg dose significantly reduced cytoplasmic and nuclear β-catenin protein in TBI-injured mice at 1 dpi (Fig. 4.10, *p<0.05, Mann-Whitney test). JW74 and vehicle were well tolerated in mice without any apparent adverse symptoms. There was no significant change in mouse weight after 14 days of treatments (Fig. 4.9, mixed effects ANOVA).

VP procedure and microscopy

VP was performed as previously described[74]. Mice were anesthetized with ketamine (90 mg/kg) and xylazine (10 mg/kg) and the following sequential injections were delivered: 1) intracardiac injection of 500 µL DiI solution (0.3 mg/mL in PBS containing 4% dextrose) into the left ventricle over 10 seconds, 2) 10 ml of phosphate buffer saline (PBS), and 3) 20 ml of 4% paraformaldehyde (PFA). Brains were carefully removed from the cranium and the dura mater was gently removed from the brain surface. Extracted brains were post fixed in 4% PFA for 24 hours and stored in PBS until imaging. Successful VP was defined as uniform pink staining of the surface of the brain and clear staining of anterior,

middle, and posterior cerebral arteries assessed by wide-field fluorescence microscopy. Brains that did not meet these criteria were excluded (29/80 mice). Acquisition of wide-field axial images were obtained by positioning the brain between two glass slides and gently flattening the dorsal surface of the brain. Brains were gently compressed on the glass slides until a compression ring was in the outer edge of the brain leading to clear visualization of the middle cerebral artery trunk and its branching vessels. Wide-field axial images were obtained using a BZ-X700 Keyence microscope (Keyence Corp, Osaka, Japan). Axial views of the brain were obtained using 2x magnification and 1 mm depth of field (25.2 μm pitch, 40 slices) in order to get clear visualization of the outer perimeters of the brain. The fluorescent microscope used in this study was able to image at a depth of 50 μm in vessel painted tissue.

Classical vessel and fractal analysis

Quantitative analysis of the labeled vessels was performed as previously described[74]. The raw fluorescent images were processed for black balance and haze reduction using BZ-X700 Analyzer software (version 1.2.0.1). Regions of interests (ROI) were drawn around the ipsilateral and contralateral hemisphere on 2x axial images (Fig. 4.8a). For the perilesional area, ROIs were drawn around the lesion (defined here as the cavity), expanded by 1.5 mm to encompass the perilesional area, and the lesion ROI was removed from the analysis image (Fig. 4.8b, 4.8c). The lesion-perilesion boundary was identified by

146

a black border and the appearance of morphologically new vessels which were typically aligned in the direction of the lesion while lesional vessels appeared more disarranged (Fig. 4.8d).

For classical vascular analysis, ROIs were imported to Angiotool software[225] and analysis was performed on each ROI to assess vessel density (percent vessels/area of ROI *100), branch points (number of branches/area of ROI), and average vessel length (average length of each vessel segment). Values were normalized to the total number of pixels in the image. Classical vascular analysis generated a colorized AngioTool image that displays vessels in red and branch points in blue.

Fractal geometric analysis was performed using the ImageJ plugin, Fraclac[237]. A local fractal dimension (LFD) analysis was performed at each pixel using the box counting method. LFD distributions result in histograms with local fractal dimensions (complexity) in the x-axis and frequency (vessel number) in the y-axis. Kurtosis, skewness, peak local fractal dimension, and peak fractal frequency were also extracted from the fractal histograms.

Laser confocal microscopy

A Zeiss LSM 710 NLO laser scanning confocal microscope (Jena, Germany) was used to acquire axial images from the perilesional area at 5x, 10x, and 20x magnification (wave length absorbance: 549 nm, emission: 565 nm). Z-stack acquisition were obtained at 10 μm step for 5x images, 6.7 μm step for 10x

images, and 2 µm step for 20x images. Images were processed for maximum intensity projections and 3D volumetric rendering using Zeiss Zen software (Zeiss Zen 2010 version 1.0, Jena, Germany).

Vessel diameter analysis

Four axial images (2 anterior and 2 posterior side) were acquired of the perilesional area at 10x magnification and 280 µm depth of field (7 µm pitch, 40 slices). Images encompassed the lesion, lesion-perilesion boundary and perilesion. The raw fluorescent images were converted to binary, smoothed (Gaussian blur, sigma: 2), and edge detection (Mexican hat filter, radius: 4) using Fiji software (http://fiji.sc/). ROI were drawn around the lesion and expanded by 400 µm and 800 µm to obtain two boundaries (Fig. 4.12a). All vessel segments that crossed along the boundary were counted. A vessel segment was defined as any vessel between two open end points, two branch points, or an open end point and a branch point. For each vessel segment, a line was drawn perpendicular to the vessel lumen and an intensity histogram was obtained. A horizontal line was draw across the base of the intensity histogram to obtain the vessel diameter. 90-120 vessel segments were counted for each animal.

MRI

High resolution MRI was undertaken on vessel painted brains to assess edema and blood volumes. *Ex vivo* T2 weighted images (T2WI; TR/TE=2395

ms/10 ms, 15 x 1 mm slices) and susceptibility weighted images (SWI; TR/TE=693.8 ms/7 ms, 30 x 0.5 mm slices) were collected with a 256 x 256 matrix and a 1.5 cm field of view, on an 11.7 T Bruker Avance Instrument (Bruker Biospin, Billerica, MA) run with the Paravision software (version 5.1, Bruker Biospin). *Ex vivo* data was collected at room temperature.

MRI data analysis

Blood and edema volumes were identified by using Hierarchical Regional Splitting (HRS) computational method (U.S. patent: 8731261; European patent: 11748009.5-1265), based on T2 relaxation times. T2 value ranges for blood, edema, and normal-appearing brain matter (NABM) containing pixels were determined by taking the average T2 value of manually segmented blood, edema, and NABM pixels in 14 random animals (3-4 animals per group) where a T2 value of <47 ms was considered blood, >70 ms was considered edema, and 48-69 ms was considered NABM. Blood and edema pixels in the perilesional cortex and hippocampus (right of midline and above the thalamus) were included in analysis. No mice showed edema or blood in the contralateral hemisphere and 3 mice had trace amounts of blood in the thalamus. The presence of blood on T2WI slices was confirmed on corresponding SWI scans. Analysis was performed on brain slices between bregma 3 mm and bregma -4 mm.

<u>Western blot</u>

Mice were sacrificed by transcardial perfusion with PBS. Extracted brains were cut into 4 quadrants (between the midline and Bregma) and the quadrant containing the injury site were processed to extract cytoplasmic and nuclear proteins (Nuclear extraction kit, EMD Millipore, Temecula, CA). Protein concentration was determined using a Bradford assay (Thermo Scientific, Rockford, IL). 8 or 14µg of protein was subjected to electrophoresis on 4-12% Sodium Dodecyl Sulfate PolyAcrylamide Gel Electrophoresis gels and transferred onto polyvinylidene difluoride membranes. Immunoblots were probed with the following antibodies: rabbit anti-β-catenin (1:2000), rabbit anti-Lamin B1 (1:2000), rabbit anti-Cyclin D1 (1:10000), rabbit anti-VEGF (1:2000) (antibodies from Abcam, Cambridge, MA), rabbit anti-non-phosphorylated β-catenin (1:2000) (Cell Signaling Technology, Danvers, MA), or mouse anti-β-actin (1:10000) (EMD Millipore, Burlington, MA). Secondary incubations were performed with anti-rabbit DyLight 800 (1:5000, Thermo Fisher, Rockford, IL) and anti-mouse IRDye 680 (1:5000, LI-COR, Lincoln, NE) antibodies and incubated for 2 hours. Immunoblots were stripped by incubation with Restore Fluorescent Western Blot Stripping Buffer (Thermo Scientific, Rockford, IL). Bands were visualized using an infra-red scanner (Odyssey, LI-COR). Image Studio Lite was used for densitometry analysis and band intensities were normalized to their respective loading controls. Lamin B1 was used as a nuclear loading control and β-actin was used as a cytoplasmic loading control.

All measurements and analysis were performed without knowledge of the treatment groups. Student's t-test, two-way analysis of variance (ANOVA) followed by Sidak's post-hoc test, and one-way ANOVA followed by Tukey's post-hoc test used GraphPad Prism 5.0 (GraphPad, San Diego, CA). Mixed effects ANOVA was used to analyse repeated measures data. Two-tailed Pearson correlation analyses utilized matching data. The data for the parametric tests showed a normal distribution and passed the Kolmogorov-Smirnov or Shapiro-Wilk normality tests. Outliers were identified if they were below or above 1.5 times the interquartile range. Error bars are presented as standard error of mean (SEM). Statistical significance was noted at $*p < 0.05$, $**p < 0.01$, $***p < 0.001$, or $****p < 0.0001$.

Results

Modulating β-catenin perturbs vascular repair at 7 dpi

To investigate whether β-catenin regulates vascular repair following TBI, we modulated β-catenin expression in the early phase (1-6 dpi) to study how timed manipulation alters new vessel formation at 7 dpi and subsequent vessel maturation at 14 dpi. Pharmacological modulation of β-catenin was achieved by timed injections of Lithium (β-catenin agonist) and JW74 (β-catenin antagonist). Since JW74 has not been used in TBI studies, we first confirmed that JW74 reduces β-catenin expression after TBI. We extracted brain tissue from the injury

151

site and quantified expression of total and non-phosphorylated β-catenin and Wnt

target gene Cyclin D1 by Western blot. JW74 significantly reduced cytoplasmic β-

catenin by 42.3% and nuclear β-catenin by 36.3% at 1 dpi compared to the

vehicle (cytoplasmic, 5.46 ± 0.46 vs. 9.47 ± 0.80, *p<0.05, Mann-Whitney test,

nuclear, 21.39 ± 1.17 vs. 33.60 ± 1.57, *p<0.05, Mann-Whitney test) (Fig. 4.10).

JW74 reduced cytoplasmic β-catenin by 50.2% and significantly reduced

cytoplasmic non-phosphorylated β-catenin by 40.3% at 7 dpi (total, 7.54 ± 1.40

vs. 15.13 ± 3.06, p=0.054, t=2.26 df=8, non-phosphorylated, 5.39 ± 0.27 vs. 9.03

± 1.18, *p<0.05, Mann-Whitney test) (Fig. 4.1a). However, nuclear β-catenin and

Cyclin D1 were unaffected at 7 dpi (Fig. 4.1a). The VEGF promoter contains

seven binding sites for T-cell factor/lymphoid enhancer-binding factor[282], and β-

catenin has been shown to regulate VEGF expression in hindlimb ischemia[259].

However, we found that JW74 had no effect on VEGF expression at 7 dpi (Fig.

4.1a). Overall, we observed that treatment with JW74 for 7 days resulted in

reduced cytosolic β-catenin at 7 days after TBI.

We next asked the question whether reducing β-catenin influences new

vessel formation at 7 dpi. Vehicle and JW74 TBI mice underwent VP to stain the

cerebral vessels and axial images were acquired of the brain surface. Compared

to the Vehicle TBI mice, JW74 TBI mice showed reduced vessels in and around

the injury site (Fig. 4.1b). Images of the perilesional tissue demonstrated sparsity

of vessel structures and reduced number of branch points in JW74 TBI mice.

Confocal imaging of VP brain tissues in the perilesional tissue revealed reduced

and fragmented vessels in JW74 TBI mice (Fig. 4.1c). Classical vascular analysis of the perilesional tissue was performed to assess vessel features[74] and we found no difference in vessel density between the Vehicle and JW74 TBI mice (Fig. 4.1d, Fig. 4.8). It is important to note that the lack of vessel density changes may be due to changes in vessel branching and concomitant new vessel segments, vessel lengths, vessel diameter, or a combination of these factors. To investigate this, we determined the number of vascular branch points, length of vessel segments, and diameter of the vessel lumens in Vehicle and JW74 TBI mice. JW74 TBI mice showed a 15.7% reduction in branch points (0.00096 ± 0.000057 vs. 0.0011 ± 0.000048,*$p<0.05$, t=2.33 df=9) (Fig. 4.1e) and a 53.4% reduction in average vessel length (0.17 ± 0.022 mm vs. 0.37 ± 0.036 mm, ***$p<0.001$, t=4.93 df=10) (Fig. 4.1f) compared to the Vehicle TBI mice. Vessel diameters at either the 400 μm or 800 μm boundary showed no statistical differences between the Vehicle and JW74 TBI mice (Fig. 4.12a, 4.12b). To assess the entire injury site, we performed classical vascular analysis of the ipsilateral hemisphere and obtained similar reductions in branch points in JW74 TBI mice (0.0011 ± 0.00015 vs. 0.0016 ± 0.000040, *$p<0.05$, t=2.45 df=10) (Fig. 4.1g, Fig. 4.8). Surprisingly, the contralateral hemisphere also exhibited a significant reduction in branch points in the JW74 TBI mice compared to the Vehicle TBI mice (0.0017 ± 0.00016 vs. 0.0025 ± 0.000071, *$p<0.01$, t=4.12 df=10) (Fig. 4.1g), indicating that JW74 can modify vessels remote from the site of injury. Group analysis of ipsilateral and contralateral hemisphere revealed a

significant increase in branch points in the contralateral hemisphere compared to ipsilateral hemisphere of Vehicle TBI mice (**p<0.01, f=16.78, one-way ANOVA) and contralateral hemisphere compared to ipsilateral hemisphere of JW74 TBI mice (*p<0.05, f=16.78, one-way ANOVA) (Fig. 4.1g). These results were expected given that contralateral hemisphere had higher baseline levels of vessels compared to the ipsilateral hemisphere and we have previously shown an increase in vessel density in the contralateral hemisphere at 7 dpi[75]. In summary, this suggests that JW74 treatment following TBI results in reduced vascular repair and leads to fragmented vessels at 7 dpi.

We confirmed that Lithium increases β-catenin expression after TBI using Western blot. Lithium did not change cytoplasmic β-catenin, but significantly increased nuclear β-catenin by 96.7% and nuclear non-phosphorylated β-catenin by 182.6% at 7 dpi (total, 52.46 ± 3.86 vs. 26.68 ± 2.00, **p<0.01, Mann-Whitney, non-phosphorylated, 46.57 ± 9.15 vs. 16.54 ± 2.52, *p<0.05, t=2.52 df=11) (Fig. 4.2a). We observed a 53.5% increase in cytoplasmic Cyclin D1 at 7 dpi (55.99 ± 5.71 vs. 36.47 ± 6.19, *p<0.05, t=2.32 df=8) (Fig. 4.2a). Lithium did not change VEGF expression at 7 dpi (Fig. 4.2a). Thus, this suggests that Lithium increased β-catenin expression leading to an increased expression of Cyclin D1, consistent with other studies[188-190].

We examined whether increasing β-catenin modulates new vessel formation at 7 dpi. In compared to Saline TBI mice, Lithium TBI mice showed increased vessels in and around the injury site (Fig. 4.2b). Confocal imaging of

the perilesional tissue clearly demonstrated elongated vessel segments in the

Lithium TBI mice compared to the shorter vessels in the Saline TBI mice (Fig.

4.2c). Classical vascular analysis of the perilesional tissue revealed a 19.5%

increase in vessel density in the Lithium TBI mice compared to the Saline TBI

mice (17.21 ± 0.91% vs. 14.40 ± 0.61%, *p<0.05, t=2.57 df=10) (Fig. 4.1d).

Lithium TBI mice showed no differences in branch points (Fig. 4.1e), but a 38.4%

increase in average vessel length compared to the Saline TBI mice (0.24 ± 0.018

mm vs. 0.17 ± 0.016 mm, *p<0.05, t=3.09 df=10) (Fig. 4.1f). Vessel diameter at

the 400 μm and 800 μm boundary showed no statistical differences between the

Saline and Lithium TBI mice (Fig. 4.12a, 4.12c). Vascular analysis of the

ipsilateral hemisphere demonstrated a non-significant increase in average vessel

length in the Lithium TBI mice (0.17 ± 0.0094 mm vs. 0.13 ± 0.017 mm, p=0.065,

Mann-Whitney) (Fig. 4.1g). However, the contralateral hemisphere exhibited a

significant increase in average vessel length in the Lithium TBI mice compared to

the Saline TBI mice (0.21 ± 0.012 mm vs. 0.16 ± 0.021, *p<0.05, t=2.28 df=9)

(Fig. 4.1g), indicating that Lithium enhanced vessel length remote from the site of

injury. Taken together, this suggests that Lithium treatment after TBI enhanced

vascular repair, leading to elongated vessel segments at 7 dpi.

Modulating β-catenin has long-term effects on the cerebral vasculature at 14 dpi

Previous studies have shown that repaired vasculature of non-treated

rodents is morphologically abnormal after TBI[9, 72, 73, 75, 78]. We asked whether

increasing β-catenin in early phase (1-6 dpi) has an influence on the perilesional

vasculature at 14 dpi. Classical vascular analysis revealed a significant increase

in branch points in the Lithium 14 dpi mice compared to the Saline 14 dpi mice

(0.0017 ± 0.00032 vs. 0.00077 vs. 0.00013, *p<0.05, t=2.33, df=10, student t-

test) (Fig. 4.3a). There was a significant increase in average vessel length in the

Lithium 14 dpi mice compared to the Saline 14 dpi mice (0.18 ± 0.0048 mm vs.

0.12 ± 0.023 mm, *p<0.05, t=3.09, df=9, student t-test) (Fig. 4.3b).

Dense and complex vessel networks can be challenging to analyze using

traditional vascular analysis methods. Thus, we employed fractal analyses to

measure vascular complexity in the perilesional tissue[74]. The fractal features that

we assessed were skewness, kurtosis, local fractal dimension (LFD), and

frequency. Histogram distribution of the LFD and frequency revealed a

pronounced increase in complexity (rightward LFD shift) and frequency (increase

in amplitude) in Lithium 14 dpi mice compared to the Saline 14 dpi mice (Fig.

4.3c), suggesting that Lithium increased complexity and number of vessels at 14

dpi. Analysis of the distribution of the LFD histograms revealed an increase in

skewness (2.01 ± 0.16 vs. 1.60 ± 0.063, p=0.060, t=2.13, df=10, student t-test)

and a significant increase in kurtosis (2.97 ± 0.63 vs. 1.20 ± 0.25, *p<0.05,

t=2.25, df=10, student t-test) and peak frequency (0.033 ± 0.0028 vs. 0.025 ±

0.0011, *p<0.05, t=2.27, df=10, student t-test) in the Lithium 14 dpi mice

compared to the Saline 14 dpi mice (Fig. 4.3d). These results are in line with the

increased branch points and average vessel length from the classical vascular

analysis (Fig. 4.3a, 4.3b). To determine whether the vessels are proliferating or are quiescent, we assessed Cyclin D1 at the injury brain tissue but found no difference in Cyclin D1 between Saline and Lithium 14 mice (Fig. 4.11), indicating that cerebral vessels are in a quiescent state at 14 dpi.

We next investigated whether decreasing β-catenin in early phase (1-6 dpi) has an influence on the perilesional vasculature at 14 dpi. Classical vascular analysis of the perilesional tissue revealed a significant increase in branch points in the JW74 14 dpi mice compared to the Vehicle 14 dpi mice (0.0014 ± 0.00022 vs. 0.00075 ± 0.00011, *p<0.05, t=2.61 df=11, student t-test) (Fig. 4.3e). We observed a significant increase in average vessel length in the JW74 14 dpi mice compared to the Vehicle 14 dpi mice (0.23 ± 0.036 mm vs. 0.11 ± 0.0098 mm, **p<0.01, Mann-Whitney) (Fig. 4.3f).

Vascular complexity in the perilesional tissue was analyzed. Histogram distribution of the LFD and frequency revealed an increase in complexity (rightward LFD shift) and frequency (increase in amplitude) in the JW74 14 dpi mice compared to the Vehicle 14 dpi mice (Fig. 4.3g), suggesting that JW74 increased complexity and number of vessels at 14 dpi. Analysis revealed an increase in kurtosis (2.37 ± 0.43 vs. 1.35 ± 0.10, p=0.054, t=2.16, df=11, student t-test) and a significant increase in skewness (1.90 ± 0.10 vs. 1.60 ± 0.032, *p<0.05, t=2.39, df=10, student t-test) and peak frequency (0.030 ± 0.0016 vs. 0.025 ± 0.00045, *p<0.05, t=2.54, df=11, student t-test) (Fig. 4.3h). These results are in line with the increased branch points and average vessel length from the

classical vascular analysis (Fig. 4.3e, 4.3f). We also measured Cyclin D1 at the injury brain tissue but found no difference in Cyclin D1 between Vehicle and JW74 14 mice (Fig. 4.11). Together, these data suggest that Lithium and JW74 treatment after TBI resulted in more elongated and branched vessels and complex vascular network at 14 dpi.

Modulating β-catenin results in alterations in the cerebral vasculature between 7 and 14 dpi

We examined the changes in branch points and average vessel length in Saline and Lithium TBI mice between 7 and 14 dpi. While Saline and Lithium TBI mice had similar numbers of branch points at 7 dpi, Lithium TBI mice had a significant increase in branch points at 14 dpi compared to the Saline TBI mice (*p<0.05, f=5.64, two-way ANOVA) (Fig. 4.4a). Lithium TBI mice showed a significant increase in average vessel length at 7 and 14 dpi compared to the Saline TBI mice (*p<0.05, f=18.99, two-way ANOVA) (Fig. 4.4b). Additionally, there was a reduction in average vessel length between the Saline 14 dpi mice compared to the Saline 7 dpi mice (p=0.087, f=10.40, one-way ANOVA) and Lithium 14 mice compared to the Lithium 7 dpi mice (p=0.066, f=10.40, one-way ANOVA), indicating regression of the vasculature at 14 dpi. Thus, this suggests that Lithium results in new elongated vessels that are maintained and become more branched at 14 dpi.

We next examined the changes in branch points and average vessel length in Vehicle and JW74 TBI mice between 7 and 14 dpi. While Vehicle and JW74 TBI mice had similar number of branch points at 7 dpi, JW74 TBI had a significant increase in branch points at 14 dpi compared to the Vehicle TBI mice ($**p<0.01$, f=2.91, two-way ANOVA) (Fig. 4.4c). JW74 TBI mice showed a significant reduction in average vessel length at 7 dpi ($***p<0.001$, two-way ANOVA) but a significant increase at 14 dpi ($*p<0.05$, f=2.03, two-way ANOVA) compared to the Vehicle TBI mice (Fig. 4.4d). Additionally, there was a significant reduction in average vessel length between the Vehicle 14 dpi mice compared to the Vehicle 7 dpi mice ($****p<0.0001$, f=14.76, one-way ANOVA), indicating regression of the vasculature at 14 dpi. Thus, this indicates that JW74 results in truncated vessels that are maintained and become more branched at 14 dpi.

Enhancing or inhibiting vascular repair affects edema and blood

To assess alterations in edema and blood composition around the TBI lesion site following treatment, we performed *ex vivo* MRI and quantified edema and blood volumes using an automated and unbiased segmentation tool called Hierarchical Region Splitting (HRS)[293]. VP brains at 7 dpi underwent T2 weighted imaging (T2WI) to assess edema and blood and susceptibility weighted imaging (SWI) to confirm the presence of blood. SWI was acquired due to its exquisite sensitivity to extravascular blood and the blooming artifact of SWI can detect the presence of minute extravascular blood[294]. HRS analysis revealed a significant

reduction in blood volume in Lithium TBI mice in compared to the Saline TBI mice (0.20 ± 0.055% vs. 0.96 ± 0.23%, *p<0.05, t=2.97 df=9) (Fig. 4.5a). These results were confirmed on the SWI magnitude images (Fig. 4.5a) and photographs taken of the cranial surface that showed minimal bleeding in the Lithium TBI mice (Fig. 4.5c) relative to Saline mice. Edema volumes were also increased in the Lithium TBI mice compared to the Saline TBI mice (1.02 ± 0.32% vs. 0.40 ± 0.13% p=0.10, t=1.80 df=10) (Fig. 4.5a). We found no significant difference in total (blood and edema) volume between Saline and Lithium TBI mice. Automated analysis revealed a significant increase in edema volume in JW74 TBI mice compared to Vehicle TBI mice (1.20 ± 0.14% vs. 0.56 ± 0.14%, *p<0.05, t=3.34 df=8) (Fig. 4.5b). These findings were confirmed on T2WI images that showed increased edema in the perilesional tissue. We observed an increase in blood and total volume which did not reach significance. The lack of significance was partially the result of the heterogeneity in bleeding in the JW74 TBI mice. Thus, this suggests that Lithium treatment reduced blood while JW74 treatment increased edema at 7 dpi.

High magnification confocal images of VP brains in the perilesional tissue exhibited elongated vessels of Lithium TBI mice (Fig. 4.5d). Conversely, we observed fragmented vessels and punctate DiI aggregates or DiI-stained cells in the extravascular space of JW74 TBI mice indicating that JW74 resulted in leaky vessels (Fig. 4.5e). These findings are in agreement with the increased volume of edema that was observed in the JW74 TBI mice (Fig. 4.5b). Furthermore,

correlations were performed to determine if vascular features in the ipsilateral hemisphere were predictive of edema and blood volumes. Correlational analysis found no significant correlations between average vessel length and blood volume in Saline and Lithium TBI mice at 7 dpi (Fig. 4.13a). However, there was one trend toward a significant correlation between vessel density and edema volume in the Lithium TBI mice at 7 dpi (p=0.093, r=0.74, two-tailed Pearson correlation) (Fig. 4.13b), indicating that in the Lithium 7 dpi mice increased edema volumes may be associated with increased vessel density.

Discussion

The current study revealed three novel findings related to the vascular response to treatments to assess Wnt/β-catenin's role in vessel repair. First, at 7 dpi JW74 treatment resulted in reduced vessel branching and length and fragmented neovessels. Second, at 7 dpi Lithium treatment resulted in increased vessel density and elongated neovessels. Third, JW74 and Lithium treatment resulted in increased vessel branching and length at 14 dpi. Fourth, JW74 treatment increased edema volume while Lithium treatment reduced blood volume at 7 dpi. Together, these findings suggest that β-catenin is a key regulator of new vessel formation and long-term remodeling of the cerebral vasculature after TBI (Fig. 4.6).

The Wnt/β-catenin signaling pathway plays an important role in blood vessel formation during development. Numerous studies have shown a robust

161

upregulation of Wnt genes in central nervous system (CNS) blood vessels during embryo development which rapidly declines after birth[198-200]. Emerging research and our own studies[75] revealed that β-catenin and Wnt genes are increased in blood vessels after CNS injuries and diseases[277, 278, 292, 295-297]. In the context of CNS injuries, we previously reported that TBI results in increased expression of β-catenin in perilesional vessels at 1 dpi followed by a decline in expression levels as new vessels start to form at 7 dpi[75]. Here we provide evidence that β-catenin participates in vascular repair after TBI. We found that at 7 dpi JW74 treatment after TBI reduced vascular repair and led to reduced and truncated neovessels, whereas Lithium treatment enhanced vascular repair and lead to elongated neovessels. Critically, and in contrast to other studies[259, 298], we show that treatment with Lithium and JW74 did not change VEGF expression. Together, these findings suggest that TBI results in damage of the cerebral vasculature leading to an increase in β-catenin and its downstream molecules to enhance vascular repair.

Studies have reported reduced VEGF levels after TBI[287, 289] and a late VEGF response (>7dpi)[89, 288], indicating that VEGF plays a small role in acute vascular repair after TBI. We found that Lithium and JW74 did not affect VEGF expression in the injury site at 7 dpi. This is unexpected as the VEGF promoter contains seven binding sites for T-cell factor/lymphoid enhancer-binding factor[282], and β-catenin increased VEGF expression after hindlimb ischemia[259]. Additionally, Lithium increased VEGF expression in the hippocampus of rats with

162

chronic mild stress[299]. One possible reason is that the changes in VEGF protein were undetectable in our brain samples. We extracted and processed brain tissue sections that encompassed the injury site and undamaged subcortical tissue and this may have prevented us from detecting changes in VEGF protein through Western blot. Collecting a more defined brain region, as shown by other studies[259, 299], may lead to different results. Another reason could be the severity of the injury. Studies that reported an upregulation of VEGF induced milder brain injuries than in our study[89, 288]. Our own unpublished results showed no noticeable change in VEGF protein levels at 1 and 7 dpi (data not shown). Thus, moderate-severe brain injuries may not initiate a VEGF response. Overall, our results suggest that β-catenin and its downstream molecules are key regulators of vascular repair after TBI that works by not affecting VEGF protein levels.

Our own work and several other studies have suggested that the injured cerebral vasculature is repaired by 14-28 dpi, but repair results in irregular and torturous vessels[9, 70-73]. Despite blood flow returning to the perilesional tissue by 14-21 days[70, 79, 80], some studies report hypoperfusion in the repaired vasculature indicating abnormalities in the repaired vasculature[70, 71, 81]. We hypothesized that Lithium treatment would "normalize" the repaired vasculature and form larger-diameter vessels that resembled the naive vessels. Contrary to our hypothesis, we found that Lithium treatment after TBI resulted in more elongated and branched vessels at 14 dpi. The results from fractal analyses were similar and in concert with classical vascular analysis which showed increased vessel

complexity and vessel numbers in the Lithium 14 dpi mice. Additionally, vessel diameters were not different between the Saline and Lithium 14 dpi mice. This suggests that Lithium administered in the acute phase (1-6 dpi) after TBI formed a more abnormal vasculature with increased numbers of small-diameter vessels and increased branching at 14 dpi. Consistent with this idea is a study by Kim et al. [300], which revealed that chronic Lithium treatment after middle cerebral artery occlusion resulted in increased microvascular density in the peri-infarct tissue at 14 dpi. In the study, the vessels appeared more elongated and complex in the Lithium-treated rats than the saline-treated rats. Given that Lithium promotes proliferation and migration of brain endothelial cells[190], our results suggest that Lithium treatment after TBI increased proliferation and migration of endothelial cells leading to the formation of elongated neovessels at 7 dpi. Discontinuation of Lithium resulted in maintenance of the vessels which become more branched and complex at 14 dpi, possibly through actions of VEGF and Angiopoetin-1. It is important to note that the 14 dpi time point to assess the repaired vasculature is not sufficient as there is evidence of vessel pruning at later time points[301].

One key question is whether these morphological changes in the repaired vasculature lead to improved behavioral outcomes. Lithium has been shown to have protective effects in TBI models. Daily lithium pre-treatment for 14 days before the onset of TBI resulted in improved spatial learning and memory performance between 14-16 days after moderate CCI[192] and daily lithium post treatment after moderate CCI resulted in reduced anxiety like behavior at 10 dpi

and improved long-term motor coordination at 14-21 dpi[193]. In the case of

Lithium, increased vessel length and branching of the repaired vasculature likely

leads to improved behavioral outcomes. This study is the first to use JW74 after

TBI. We hypothesized that JW74 treatment would form a more abnormal

vasculature at 14. We speculate that TBI mice treated JW74 would initially

perform worse in behavioral tests and then show long-term functional

improvements (possibly increased neuroplasticity) attributed to the

enhancements in the repaired vasculature.

Magnetic resonance imaging for brain injury can assess patient outcome

in the clinic. We used *ex vivo* MRI and highly sensitive HRS analysis to measure

edema and hemorrhage following treatment and found that JW74 treatment

increased edema volumes at 7 dpi. Given that β-catenin is a component of the

adheren junctions, downregulation of β-catenin may lead to defects in the

endothelial cell junctions and vessel leakage after TBI. Consistent with this idea

are multiple findings that reduced endothelial cell β-catenin affects the

endothelial junctions during development: Liebner et al.[200] showed that

endothelial cell deletion of β-catenin resulted in a reduction of Claudin-5 protein

expression and increased vessel permeability at postnatal day 14 and Cattelino

et al.[201] showed that endothelial cell deletion of β-catenin resulted in increased

vessel permeability and hemorrhage at embryonic day 9.5 and 10.5 which was

due to a reduction in α-catenin and an increase in desmoplakin protein

expression. Thus, our results are consistent with the possibility that JW74 altered

the adheren and tight junctions leading to increased vessel permeability and edema. Overall, this highlights that β-catenin plays an important role in the endothelial cell junctions and therapeutic that target β-catenin need to evaluate vessel integrity.

Additionally, we found that Lithium treatment non-significantly increased edema volumes at 7 dpi. This is in contrast to a study by Yu et al.[193], which found that Lithium (84.8 mg/kg) reduced matrix metalloproteinase-9 expression and reduced Evans blue extravasation 3 days after moderate CCI. While Lithium at a lower dose (56.5 mg/kg) had no effect on vessel permeability 3 days after moderate CCI[194], Lithium pre-treatment (42.4 mg/kg) for 14 days before the onset of TBI reduced cerebral edema 1 day after moderate CCI[192]. These differences in findings can be attributed to the time point that was analyzed (3 dpi vs. 7 dpi) and it appears that Lithium treatment after TBI reduces vessel permeability at early time points (<3dpi) and may increase vessel permeability and delay closure of the blood brain barrier at later time points. Thus, this highlights the importance of timing of treatments following TBI and acute treatment of a β-catenin agonist may be the most efficacious in reducing vessel permeability.

Moderate and severe head injuries result in hemorrhagic lesions that often expand or form new hemorrhagic lesions (hemorrhagic progression). While the molecular mechanisms underlying hemorrhagic progression is unclear, numerous reports by the Simard group suggest that this phenomenon is

attributed to delayed, progressive endothelial cell death[302-304]. Our results

showed that Lithium treatment reduced blood volume at 7 dpi, which is consistent

with the possibility that Lithium attenuates endothelial cell degeneration.

However, given the off target effects of Lithium, it is likely that other mechanisms

may be in play and account for the reduction in blood. Further research on

Lithium's role in endothelial cell degeneration should be conducted.

There are several limitations to this study. First, while a pharmacological

approach provides great temporal control of β-catenin protein levels, they have

potential off-target effects. In animal models of TBI, β-catenin and Wnt genes are

detected not only in endothelial cells, but also in neuronal and glial cells[191, 206].

Survivin and serum- and glucocorticoid-regulated kinases are GSK3-β inhibitors

and were upregulated in neuronal cells after TBI[207, 208]. The Wnt/β-catenin

pathways likely has pleiotropic roles in neural stem and progenitor cell

proliferation, neuronal cell apoptosis, and glial cell proliferation[191, 206-208].

Likewise, Cyclin D1 also regulates neuronal cell apoptosis and glial cell

proliferation after TBI[305]. Thus, Lithium and JW74 likely affect a multitude of

repair processes unrelated to angiogenesis and could impact our findings.

Second, while VP was used due to its excellent staining of vascular structures

(including micro-vessels) and the ability to perform wide field fluorescent

microscopy, this procedure is reliant on blood flow to circulate the DiI solution

throughout the brain. Thus, compressed and collapsed vessels can affect the

quality of the vessel staining and lead to poorly labeled vessels. Given the

increase in edema in the JW74 and Lithium TBI mice, the possibility exists that vessels were compressed and not all vessels were labeled. Endothelial cell reporter lines, such as the Tie2-GFP mice, are available[306] and these could be combined with our VP procedure to assess perfusing and non-perfusing vessels. Third, for the Vehicle and JW74 groups, mice were orally administered a mixture of dimethyl sulfoxide and polyethylene glycol 400 and this vehicle may had unintended consequences on vascular repair. This vehicle was used because it maintained JW74 solubility and promoted drug absorption into the blood circulation[307]. We don't believe the vehicle had an effect on vascular repair because the Vehicle and Saline TBI mice showed similar values in nearly all vessel parameters from the classical and fractal analysis. Interestingly, Vehicle 7 dpi mice had a significant increase in average vessel length compared to the Saline 7 dpi mice (***$p<0.001$, $t=5.245$, $df=9$, student t-test). This could be credited to increased staining vessel sprouts and filopodia processes.

In summary, this study employed a dual pharmacological approach to investigate the role of β-catenin in new vessel formation and vessel maturation. The novel VP and analysis methods provide exceptional examination of brain and region wide vascular network. Our findings suggest that signaling molecules involved during embryonic development become re-activated after TBI to promote vascular repair. Given the rapid increase in β-catenin in vessels after TBI, this suggests that Wnt/β-catenin signaling is involved in the initiating of vascular repair. These results suggest that at least part of the protective effects

of activation of Wnt/β-catenin signaling in TBI animal models *in vivo* can be credited to enhanced vascular repair. Furthermore, therapies to enhance β-catenin activity may be an effective therapeutic option for TBI. VEGF treatment can induce angiogenesis and ameliorate functional deficits[73, 137, 308], but it also increases vessel permeability[255, 309]. Acute treatment of a β-catenin agonist followed by delayed VEGF may help in reducing adverse side effects and improving treatment efficacy.

Figure 4.1. JW74 treatment reduced vascular repair and lead to truncated

vessels at 7 dpi. a) Western blot and quantification of total and non-

phosphorylated β-catenin, Cyclin D1, and VEGF for Vehicle and JW74 TBI mice

at 7 dpi. JW74 TBI mice revealed a reduction in cytoplasmic total β-catenin

(p=0.054, student t-test) and significant reduction in non-phosphorylated β-

catenin (*p<0.05, Mann-Whitney test) compared to the Vehicle TBI mice. Nuclear

total β-catenin, cytoplasmic Cyclin D1, and VEGF were not different between the

Vehicle and JW74 TBI mice. b) Axial VP images (top panel) and Angiotool

images of the perilesional tissue (bottom panel) of Vehicle and JW74 TBI mice.

Vehicle TBI mice showed new vessels at the injury site (white circle), while the

JW74 animal showed reduced vessels. Note the reduced numbers of vessel

segments (red) and branch points (blue) in the JW74 TBI mice. c) Confocal

images of the perilesional tissue (dashed box is enlarged in the bottom panel).

JW74 TBI mice showed reduced and fragmented vessels compared to the

Vehicle TBI mice. d) Vessel density in the perilesional tissue was not different

between the Vehicle and JW74 TBI mice. e) Branch points was significantly

reduced in the JW74 TBI mice compared to the Vehicle TBI mice ($*p<0.05$,

student t-test). f) Average vessel length was significantly reduced in the JW74

TBI mice compared to the Vehicle TBI mice ($***p<0.001$, student t-test). g)

Branch points in the ipsilateral and contralateral hemisphere was significantly

reduced in the JW74 TBI mice compared to the Vehicle TBI mice ($*p<0.05$,

$**p<0.01$ student t-test).

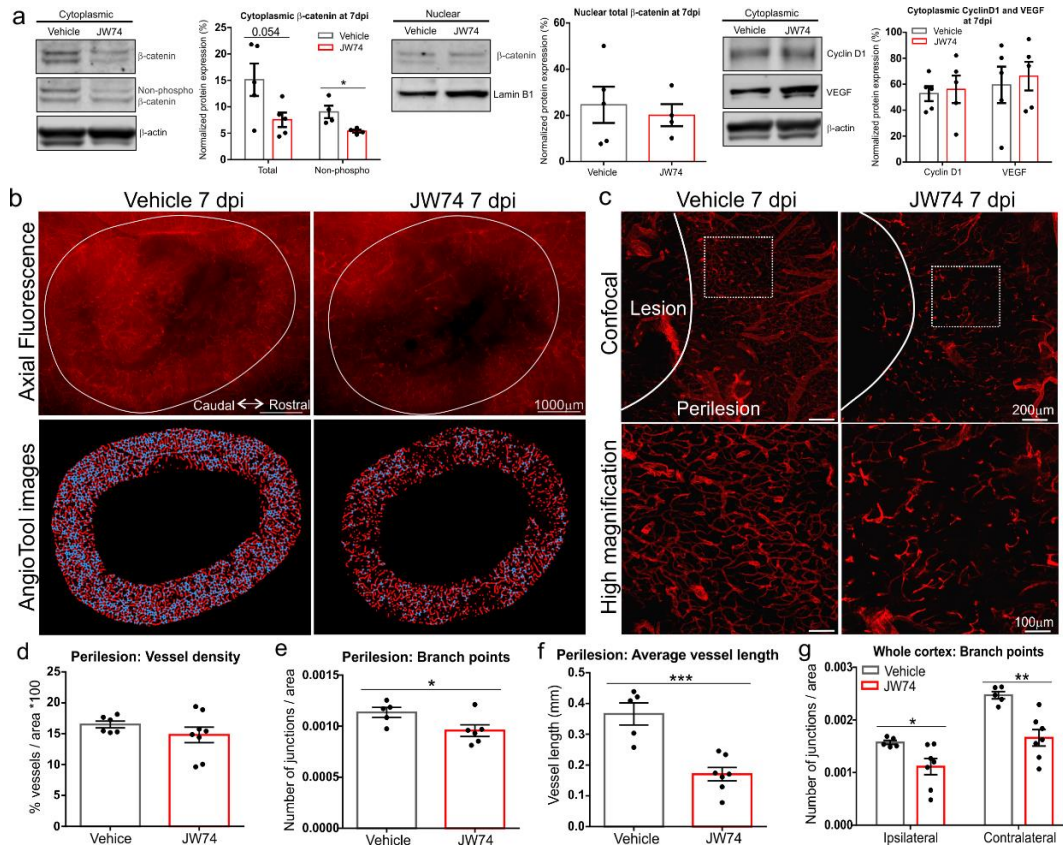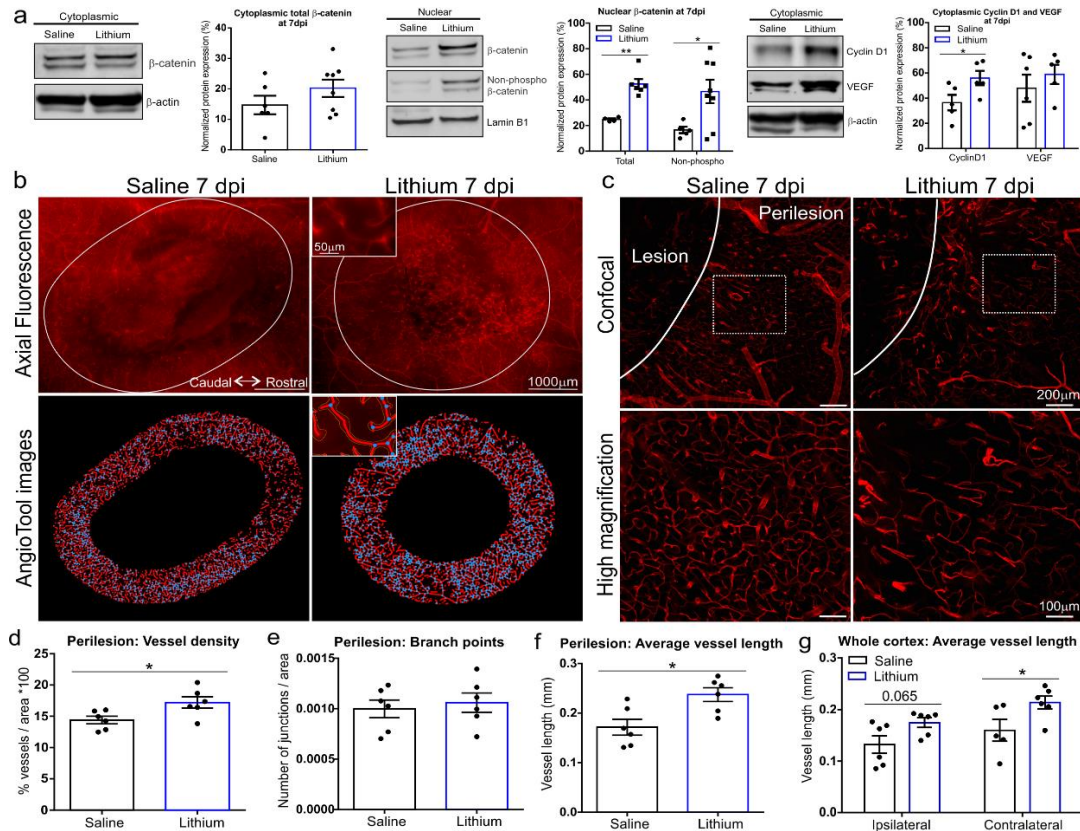**Figure 4.2.** Lithium treatment enhanced vascular repair and lead to elongated vessels at 7 dpi. a) Western blot and quantification of total and non-phosphorylated β-catenin, Cyclin D1, and VEGF for Saline and Lithium TBI mice at 7 dpi. Lithium TBI mice revealed no difference in cytoplasmic total β-catenin but a significant increase in nuclear total and non-phosphorylated β-catenin (**$p<0.01$, Mann-Whitney; *$p<0.05$, student t-test) and cytoplasmic Cyclin D1 (*$p<0.05$, student t-test) compared to the Saline TBI mice. Cytoplasmic VEGF was not different between the two groups. b) Axial VP images (top panel) and Angiotool images of the perilesional tissue (bottom panel) of Saline and Lithium TBI mice. Saline TBI mice showed new micro-vessels at the injury site (white

circle), while the Lithium TBI mice showed increased vessels. Note the subtle increase in vessel segments and branch points in the Lithium TBI mice. Inserts illustrate elongated vessel segments. c) Confocal images of the perilesional tissue (dashed box is enlarged in the bottom panel). Lithium TBI mice showed elongated vessel segments compared to the Saline TBI mice. d) Vessel density in the perilesional tissue was significantly increased in Lithium TBI mice compared to the Saline TBI mice (*$p < 0.05$, student t-test). e) Branch points was not different between Saline and Vehicle TBI mice. f) Average vessel length was significantly increased in the Lithium TBI mice compared to the Saline TBI mice (*$p < 0.05$, student t-test). g) Average vessel length in the ipsilateral and contralateral hemisphere was increased in the Lithium TBI mice compared to the Saline TBI mice ($p = 0.065$, Mann-Whitney; *$p < 0.05$, student t-test)
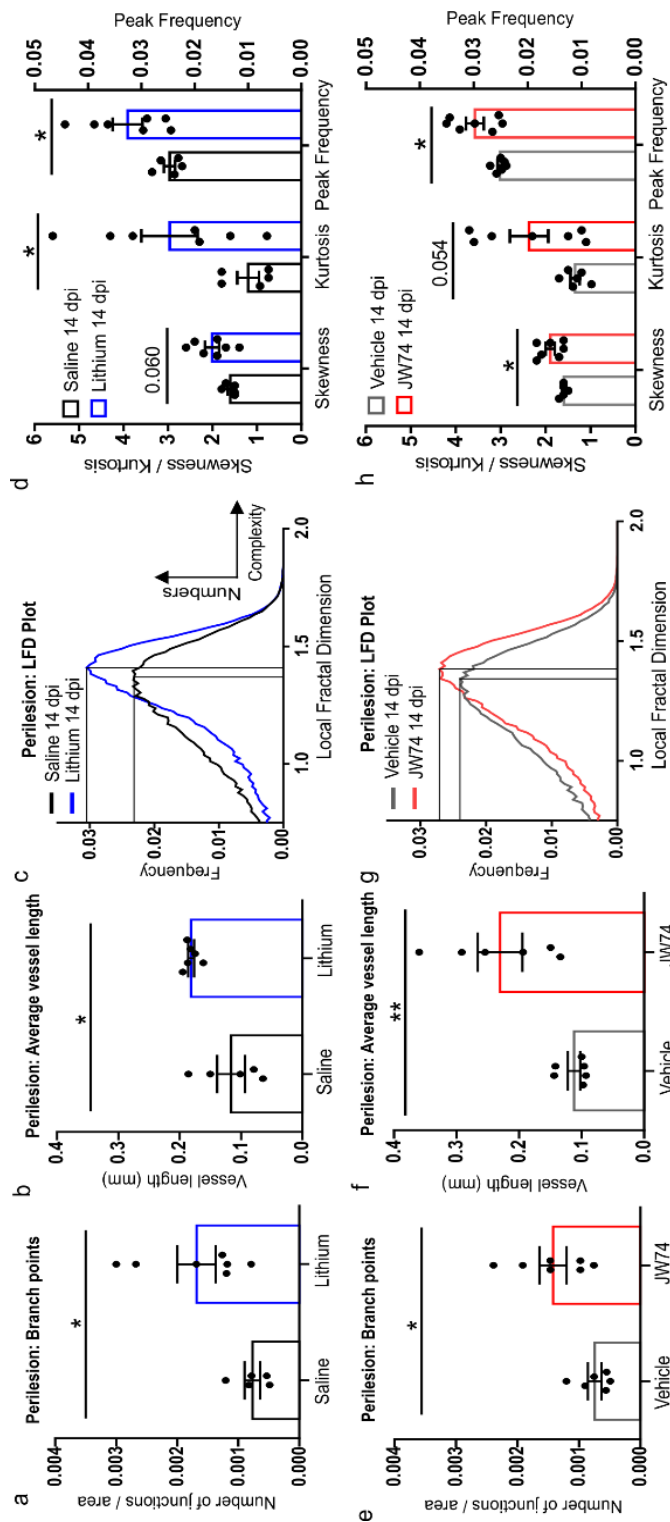
Figure 4.3. Lithium and JW74 treatment increased branching, average vessel length, and vessel complexity at 14 dpi. a) Branch points was significantly increased in the Lithium 14 dpi mice compared to the Saline 14 dpi mice (*p<0.05, student t-test). b) Average vessel length was significantly increased in the Lithium 14 dpi mice compared to the Saline 14 dpi mice (*p<0.05, student t-test). c) Histogram distribution of the local fractal dimension (LFD) and frequency from Saline 14 dpi and Lithium 14 dpi mice. The Lithium 14 dpi histogram (blue line) showed a pronounced increase in vessel complexity (rightward LFD shift) and frequency (increased vessel numbers) compared to the Saline 14 dpi histogram (black line). d) Lithium 14 dpi mice showed an increase in skewness (p=0.060, student t-test) and a significant increase in kurtosis (*p<0.05, student t-test) and peak frequency (*p<0.05, student t-test) compared to the Saline 14 dpi mice. e) Branch points was significantly increased in the JW74 14 dpi mice compared to the Vehicle 14 dpi mice (*p<0.05, student t-test). f) Average vessel length was significantly increased in the JW74 14 dpi mice compared to the Vehicle 14 dpi mice (**p<0.01, student t-test). g) Histogram distribution of the LFD and frequency from Vehicle 14 dpi and JW74 14 dpi mice. The JW74 14 dpi histogram (red line) showed an increase in vessel complexity (rightward LFD shift) and frequency (increased vessel numbers) compared to the Vehicle 14 dpi mice. h) JW74 14 dpi mice showed an increase in kurtosis (p=0.054, student t-test) and a significant increase in skewness (*p<0.05, student t-test) and peak frequency (*p<0.05, student t-test) compared to the Vehicle 14 dpi mice.
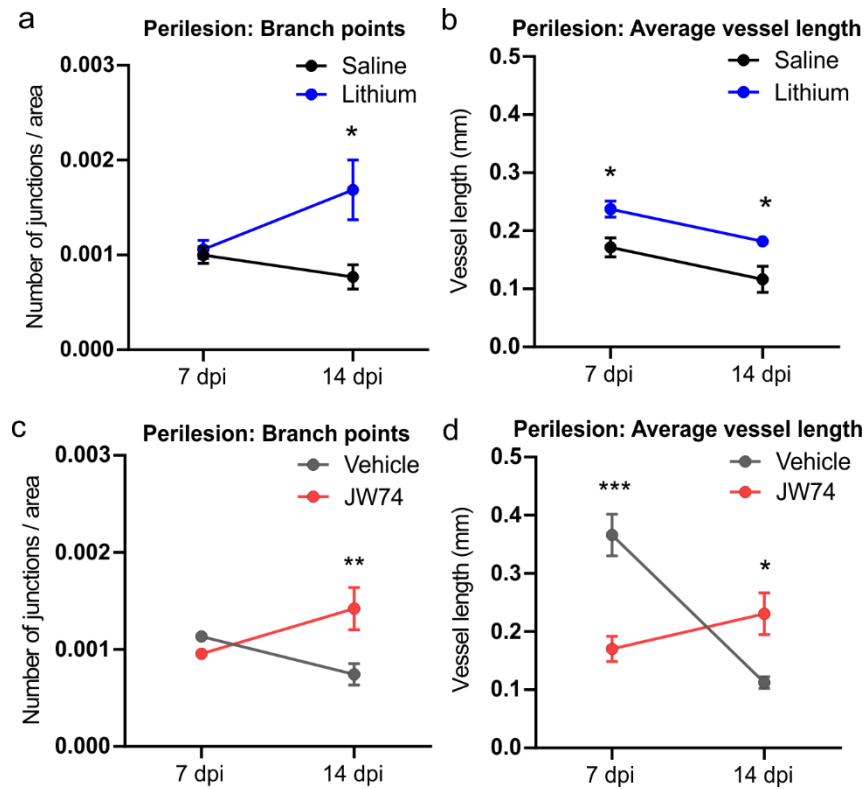
Figure 4.4. Lithium and JW74 treatment modulates the perilesional vasculature between 7 and 14 dpi. a) Saline and Lithium TBI mice showed no difference in branch points at 7 dpi. However, Lithium TBI mice showed a significant increase in branch points at 14 dpi compared to the Saline TBI mice (*$p<0.05$, two-way ANOVA). b) Lithium TBI mice showed a significant increase in average vessel length at 7 and 14 dpi compared to the Saline TBI mice (*$p<0.05$, two-way ANOVA). There was a reduction in average vessel length between the Saline 14 dpi mice compared to the Saline 7 dpi mice ($p=0.087$, f=10.40, one-way ANOVA) and Lithium 14 mice compared to the Lithium 7 dpi mice ($p=0.066$, f=10.40, one-way ANOVA). c) Vehicle and JW74 TBI mice showed no difference in branch points at 7 dpi. However, JW74 TBI mice showed a significant increase in branch

points at 14 dpi compared to the Vehicle TBI mice (**p<0.01, two-way ANOVA).

d) JW74 TBI mice showed a decrease in average vessel length at 7 dpi compared to the Vehicle TBI mice (***p<0.001, two-way ANOVA). However, JW74 TBI mice showed a significant increase in average vessel length at 14 dpi compared to the Vehicle TBI mice (*p<0.05, two-way ANOVA). There was a significant reduction in average vessel length between the Vehicle 14 dpi mice compared to the Vehicle 7 dpi mice (****p<0.0001, f=14.76, one-way ANOVA).
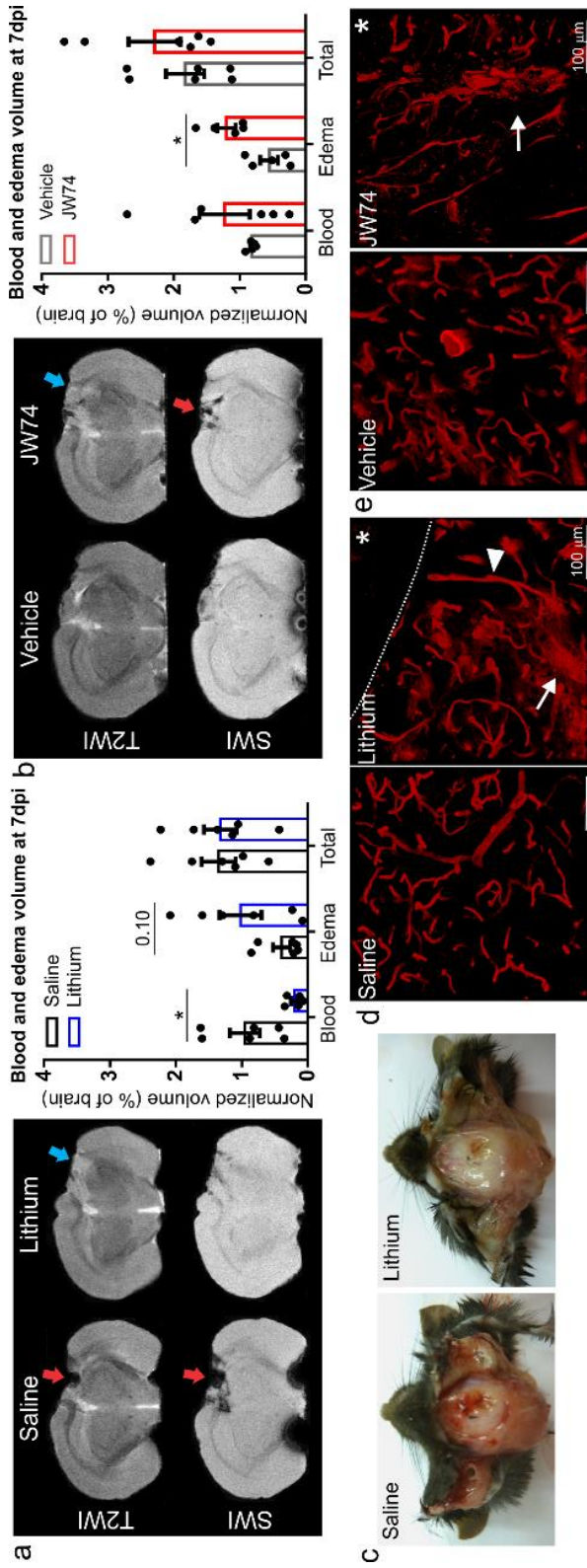
Figure 4.5. Lithium treatment reduced blood while JW74 treatment increased edema at 7 dpi. a) Representative coronal slices and blood and edema volumetric analysis for Saline and Lithium TBI mice. Lithium TBI mice showed a significant reduction in blood volume (*p<0.05, student t-test) but an increase in edema volume (p=0.10, student t-test). Note the reduced bleeding (red arrow) on susceptibility weighted imaging (SWI) and increased edema (blue arrow) on T2 weighted imaging (T2WI) in the Lithium TBI mice. b) Representative coronal slices and blood and edema volumetric analysis for Vehicle and JW74 TBI mice. JW74 TBI mice showed a significant increase in edema volume (*p<0.05, student t-test) compared to the Vehicle TBI mice. Note the increased edema (blue arrow) on T2WI and increased bleeding (red arrow) on SWI in the JW74 TBI mice. c) Images of the cranial surface for Saline and Lithium TBI mice. The Saline TBI mice showed bleeding on the surface of the cranium while the Lithium animal showed minimal bleeding. d) 3D volumetric rendering of perilesional vessels in Saline and Lithium TBI mice. Lithium TBI mice showed elongated vessels (arrowhead), but diffuse DiI staining in the extravascular space (arrow). Lesion-perilesion boundary (dotted line). e) 3D volumetric rendering of perilesional vessels in Vehicle and JW74 TBI mice. JW74 TBI mice showed fragmented vessels and punctate DiI staining in the extravascular space (arrow). *= injury site.
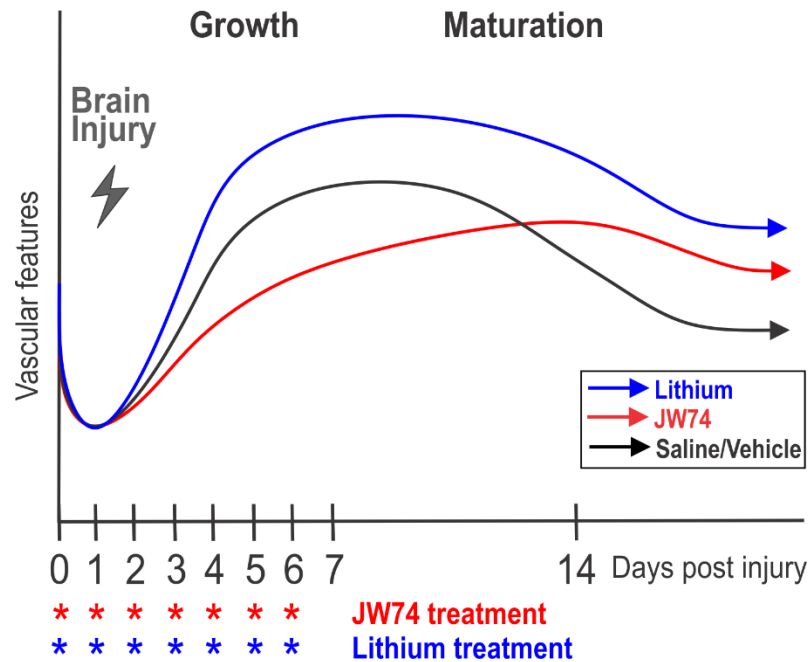
Figure 4.6. Schematic illustrating how modulating β-catenin in blood vessels affects vascular repair. TBI results in vascular loss which is followed by vessel formation (growth phase) and maturation (maturation phase) (black line). β-catenin increase in vessels results in elongated neovessels in the growth phase which are maintained and become more complex in the maturation phase (blue line). β-catenin reduction in vessels results in truncated neovessels which are maintained and become more complex in the maturation phase (red line).
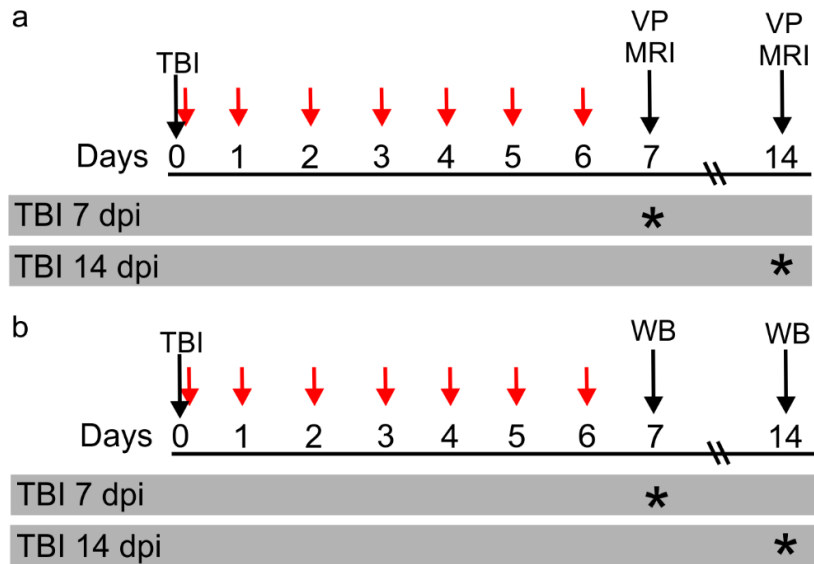
Figure 4.7. Experimental design. Mice received a moderate TBI on day 0. All mice were administered Saline, Lithium, Vehicle, or JW74 1 hour after TBI followed by daily injections every 24 hours until day 6. Drugs were then discontinued until day 14. a) Mice underwent vessel painting (VP) and *ex vivo* magnetic resonance imaging (MRI) on day 7 or 14. b) Mice were sacrificed for Western blot (WB) on day 7 or 14. Red arrows = injections. * = sacrifice days.

a

C

I

1000μm

b

Lesion-perilesion
boundary

1000μm

c

Lesion
(Deep vessels at
base of lesion)

Perilesion
(Superficial vessels)

1000μm

d

Perilesion

Lesion

200μm
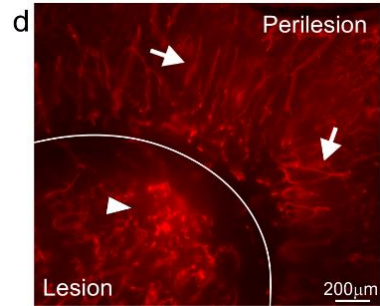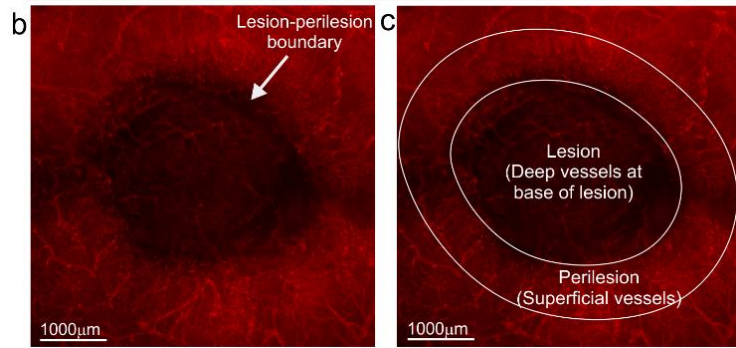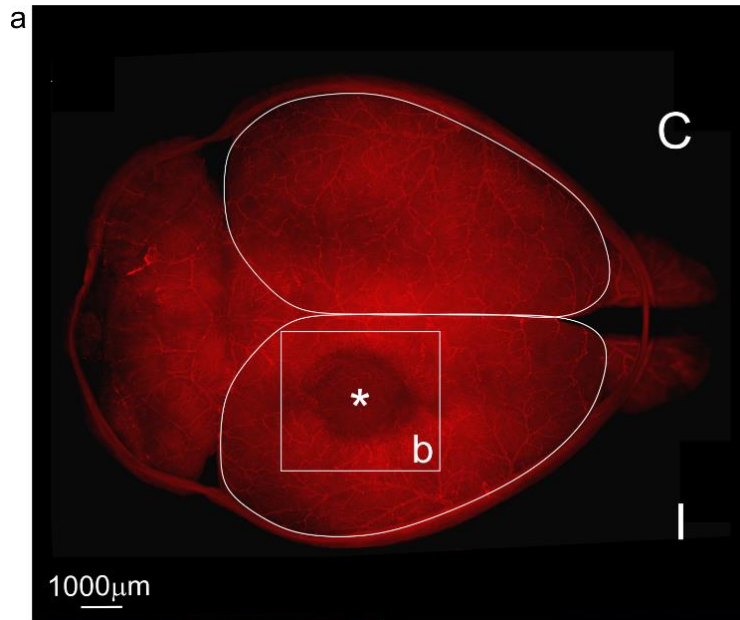
Figure 4.8. Region of interests for vascular analysis. a) Axial view of a VP brain from a TBI mouse. ROIs of the ipsilateral (I) and contralateral (C) hemisphere were undertaken. The injury site (*) is magnified in Fig. 4.8b. b) The lesion-perilesion boundary was characterized by a faint black border. c) The injury site had vessels at the base of the lesion (defined as lesion) and superficial vessels on the brain surface (perilesion). The perilesion boundary was formed by drawing an ROI around the lesion and expanding it by 1.5 millimeters. d) The lesion and perilesion tissue showed a distinct vessel morphology: perilesional vessels were typically aligned in the direction of the lesion (arrows) while lesional vessels appeared more disarranged (arrowhead). The lesion-perilesion boundary is outlined by a white line.
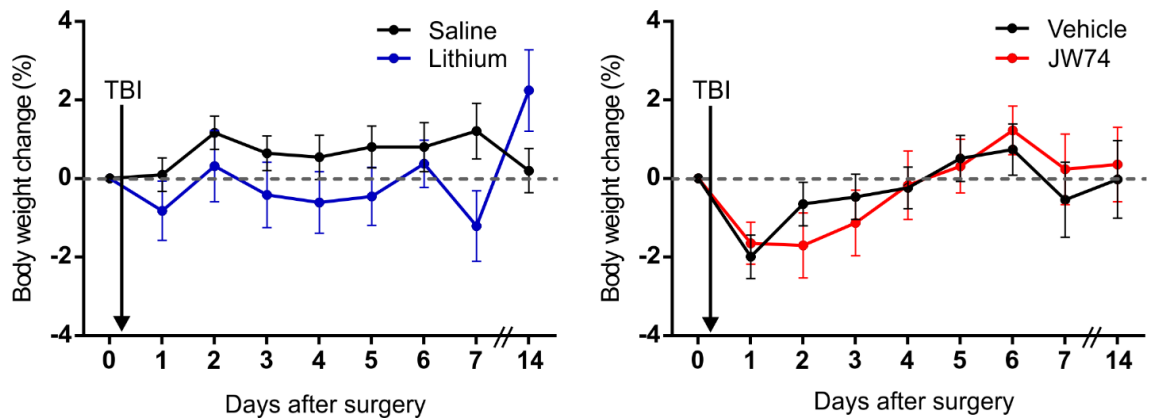
Figure 4.9. Drug treatments had no effect on mouse weight after TBI. There was no significant difference in mouse weight between the Saline and Lithium TBI mice and Vehicle and JW74 TBI mice. Mice were weighed prior to the TBI on day 0. Graphs include all mice from the study, including unsuccessful VP mice. TBI 7 dpi: Saline (n=13), Lithium (n=24), Vehicle (n=12), JW74 (n=17). TBI 14 dpi: Saline (n=16), Lithium (n=17), Vehicle (n=17), JW74 (n=19).
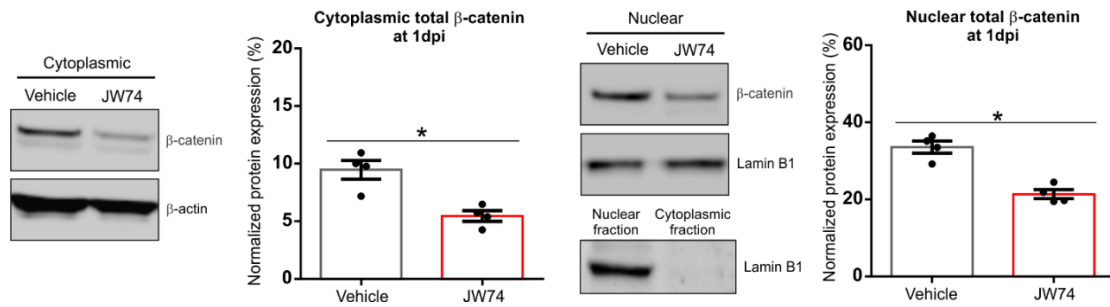
Figure 4.10. JW74 treatment reduced cytoplasmic and nuclear β-catenin protein at 1 dpi. Western blot and quantification for total β-catenin for Vehicle and JW74 TBI mice at 1 dpi. JW74 TBI mice showed a significant reduction in cytoplasmic total β-catenin and nuclear total β-catenin compared to the Vehicle TBI mice (*p<0.05, Mann-Whitney test). Lamin B1, a nuclear protein, is not present in the cytoplasmic fraction indicating that the protein extracts were not contaminated.
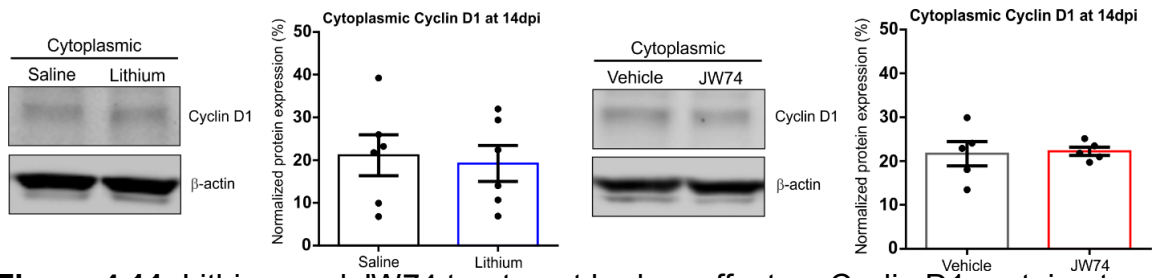
Figure 4.11. Lithium and JW74 treatment had no effect on Cyclin D1 protein at

14 dpi. Western blot and quantification for Cyclin D1 for Saline, Lithium, Vehicle,

and JW74 TBI mice. Cytoplasmic Cyclin D1 protein was not significantly different

between the Saline, Lithium TBI mice and Vehicle, JW74 TBI mice.
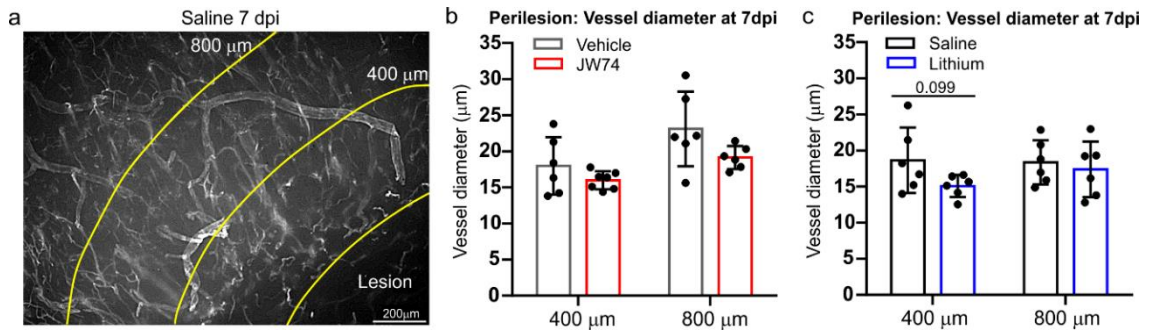
Figure 4.12. Lithium and JW74 treatment had no influence on vessel diameter in the perilesional tissue. a) Representative axial image from the perilesional tissue of Saline 7 dpi mouse that was processed to enhance the edges of the vessels. The lesion-perilesional boundary, 400 μm, and 800 μm boundary are outlined (yellow lines). Vessel segments that crossed the 400 μm and 800 μm boundary were counted in analysis. b) Vessel diameter at the 400 μm and 800 μm boundary was not significantly different between the Vehicle and JW74 TBI mice. c) Vessel diameter at the 400 μm boundary showed a reduction in the Lithium TBI mice compared to the Saline TBI mice (p=0.099, student t-test).
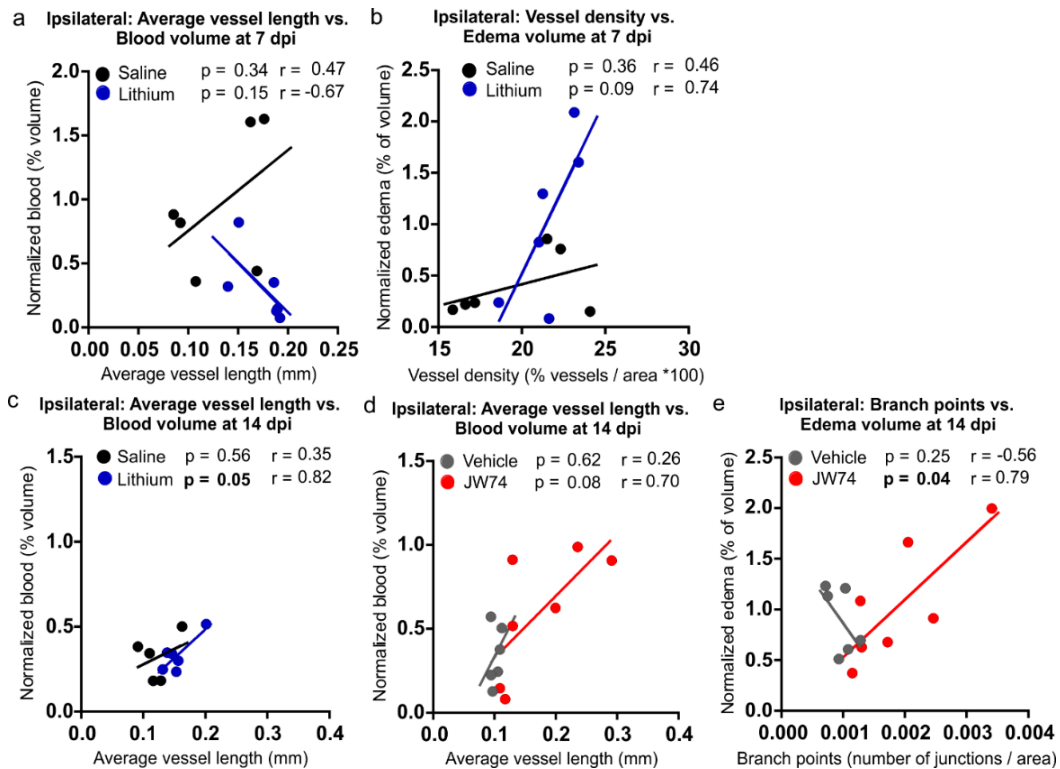
Figure 4.13. Correlations between vascular features and blood and edema volumes at 7 and 14 dpi. a) There were no significant correlations between average vessel length and blood volume in the Saline and Lithium TBI mice at 7 dpi. Note the divergent trend between the two groups. b) Average vessel length correlated to edema volume in the Lithium TBI mice at 7 dpi and approached significance (p=0.093, two-tailed Pearson correlation). c) Average vessel length significantly correlated to blood volume in the Lithium TBI mice at 14 dpi (*p<0.05, two-tailed Pearson correlation). d) Average vessel length correlated to blood volume in the JW74 TBI mice at 14 dpi and approached significance (p=0.080, two-tailed Pearson correlation). e) Branch points significantly correlated with edema volume in the JW74 TBI mice at 14 dpi (*p<0.05, two-

188

tailed Pearson correlation). Again, note the divergent trend between the two

groups.
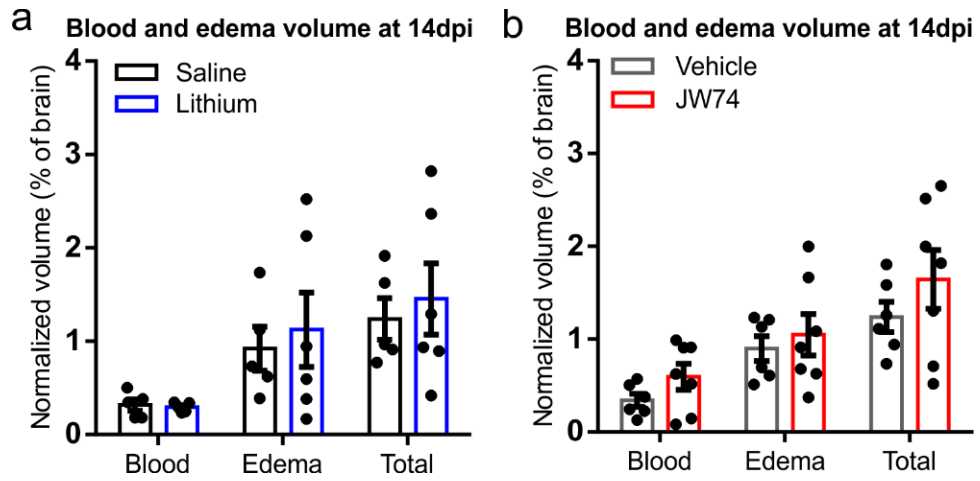
Figure 4.14. Lithium and JW74 TBI mice exhibited no difference in blood and edema volumes at 14 dpi. a-b) Blood, edema, and total (blood and edema) volumes were not significantly different between the Saline and Lithium TBI mice and Vehicle and JW74 TBI mice (Student t-test).

Table 4.1. Number of mice that underwent VP and *ex vivo* MRI or Western blot

Groups	VP and *ex vivo* MRI	Western blot
Saline 7 dpi	6	6
Lithium 7 dpi	6	9
Vehicle 7 dpi	6	5
JW74 7 dpi	8	5
Saline 14 dpi	5	6
Lithium 14 dpi	7	6
Vehicle 14 dpi	6	6
JW74 14 dpi	7	6

The table summarizes the number of mice in each group. One cohort of mice were sacrificed for VP and *ex vivo* MRI at 7 or 14 dpi and a second cohort was sacrificed for western blot at 7 or 14 dpi.

Chapter 5

Conclusion

This dissertation investigated the response of the cerebral vasculature to TBI, how vessels undergo repair after injury and the role of β-catenin in vascular repair. We report three novel findings: 1) we developed a novel protocol to stain, visualize, and analyze the cerebral vasculature in the entire rodent brain, 2) using this novel vessel staining and analysis protocol, we found that TBI results in vascular loss followed by repair of the blood vessels at 7 dpi. Simultaneously, we observed an acute increase in expression of β-catenin in cerebral vessels after TBI, and 3) that β-catenin contributes to new vessel formation at 7 dpi and long-term remodeling of the cerebral vasculature at 14 dpi.

Staining of blood vessels in the rodent brain can be achieved by various inks, resins, or dyes[9, 263, 271, 310-312], but many of these techniques have limitations. Space occupying materials, such as silicone rubber[9], Evans blue[263], Microfil contrast agent[312], and fluorescent dye-conjugated dextran[313], fill the vessels but remain unbound to vessels allowing the materials to freely move and potentially leading to extravasation when the vessels are damaged, compressed or after injury with leaky BBB. Many of these materials also require the tissue to be cleared for visualization, resulting in loss of critical anatomical landmarks. Other methods using space occupying materials are corrosion casting techniques that use low viscosity resins to form casts of the blood vessels[314-316],

but these are technically difficult to prepare and the resultant casts often require image acquisition using a scanning electron microscope or similar types of instruments. Methods using viscous reagents, such as gelatin and white ink[317], latex with carbon black ink[318], and latex and black inks[319], stain large blood vessels, but do not typically stain capillaries. Several methods have been developed to label the cerebral vasculature by fluorescent microscopy, but have reported wide variation in efficiency of vessel labeling with different types of fluorescently labeled lectins[320-322]. We have previously stained cerebral vessels by cardiac perfusion with DyLight 594 labeled tomato-lectin, but whole brain axial and coronal images showed high background staining and micro-vessels were not clearly visible.

Our novel VP technique utilizes a lipophilic, fluorescent carbocyanine dye (DiI) that directly binds to the vessel lumen. The DiI molecules incorporate into the endothelial cell lipid membranes and are able to laterally diffuse in the lipid membrane providing uniform staining of blood vessels. VP stains cerebral vessels with a bright red fluorescence which can be imaged using wide-field fluorescence microscopy for whole brain imaging and subsequent confocal microscopy for regional imaging. As we have reported in the previous chapters and our recent publications[78, 233, 323, 324], VP effectively labels pial, penetrating, and parenchymal vessels (including capillaries) across rodent species, ages, and pathological conditions. Additionally, we introduce two complimentary analysis methods to assess vessel morphology and complexity in the whole brain.

We found that treatment with JW74 (β-catenin antagonist) after TBI reduced vascular repair and lead to fragmented vessels while treatment with Lithium (β-catenin agonist) enhanced vascular repair and lead to elongated vessels. This work suggests that endogenous developmental factors, such as β-catenin, become activated after TBI to initiate vascular repair and treatment strategies to enhance activation of β-catenin represents a potential target for future therapeutics. Lithium is a FDA approved drug for bipolar disease[325] and our exciting findings raise the possibility that Lithium could be repurposed as a drug that can be used in the clinical settings to enhance vascular repair after TBI. Lithium could also be used in combination with Becaplemin (recombinant human platelet derived growth factor), which is an FDA approved drug for diabetic skin ulcers. Since platelet derived growth factor promotes vessel maturation through recruitment of mural cells to the nascent vessels[326], co-application of Lithium and Becaplemin may form stable and functional vessels. Additionally, we have unpublished data showing mural cells in contact with perilesional vessels at 14 dpi, suggesting that early administration of Lithium followed by delayed Becaplemin may be an effective therapeutic strategy. Thus, Lithium and Becaplemin need be considered in the development of new angiogenic therapies.

While it is well established that VEGF induces angiogenesis in tumors and ischemic stroke[285, 286], our evidence suggests that VEGF does not play a critical role in initiating vascular repair in our TBI model; we did not observe increased

VEGF protein levels within the injured brain tissue at 1 and 7 dpi or in response to increasing or decreasing β-catenin levels also did not affect VEGF protein expression. However, VEGF may be involved in maturation of the vascular network. Wnt/β-catenin and VEGF signaling may have coordinated actions with Wnt/β-catenin signaling initiating vascular repair in the early phase and VEGF signaling promoting vessel maturation and pruning in the later phase. Future investigations are warranted to understand how Wnt/β-catenin and VEGF signaling mediate vascular regrowth and restoration after TBI.

Other endogenous vascular developmental factors may become activated after TBI and also participate in the vascular repair process. Our unpublished data demonstrated increased expression of Wnt 7a and Wnt 7b as well as Cyclin D1, Sox17, and Notch Intracellular Domain that are co-localized within vessel structures at 1 and 7 dpi, which suggests that the β-catenin may work with Sox17 and Notch signaling to promote blood vessel formation after TBI. Thus, Wnt 7a, Wnt 7b, Cyclin D1, Sox17, and Notch signaling components are potential molecular targets that could be used in the development of new therapies. Moving forward, it is critical to understand the molecular mechanisms of β-catenin-mediated vascular repair and how β-catenin coordinates with down-stream angiogenic factors (Fig. 5.1).

In conclusion, this dissertation was the first to investigate β-catenin in the context of vascular repair after TBI and we uncovered a new reparative role that has not been previously reported. Our findings suggest that β-catenin is a novel

molecular target that can be used for the development of therapies to repair and restore the cerebral vasculature after injury. Additionally, this work may have broad implications for a host of vascular-related brain injuries such as ischemic stroke, subarachnoid hemorrhage, and intracerebral hemorrhage.

Future Directions

Future work will be focused on extending the ideas explored in this dissertation to address other relevant vascular phenomena after TBI. While VP stains functional, perfusing vessels, it does not stain vessels that are not perfusing after injury, including compressed, collapsed vessels or new vessels with an immature vessel lumen. We performed VP in the endothelial cell reporter line Tie2-GFP mice[306] to examine the time course of functional perfused vessels as they undergo repair. Our preliminary data show that TBI results in a clear loss of vessels and non-perfused vessels at 1 dpi (Fig. 5.2). At 7 dpi, there is increased vessel density and a concomitant increase in the number of perfused and non-perfused vessels within and adjacent to the injury site. Previous reports have also noted hypoperfusion in the repaired vasculature between 14-28 dpi in CCI, fluid percussion injury, and blast injury models of TBI[70, 71, 81]. Going forward, we plan to extend our preliminary findings to investigate the perfused and non-perfusing vessels in the repaired vasculature at 14 and 30 dpi.

One of the more important future extensions of this work will involve the use of blood flow imaging techniques to monitor cortical blood flow during

vascular repair and restoration after brain injury. Laser speckle imaging (LSI) is a real time, non-invasive technique that permits high resolution mapping of tissue blood perfusion. Unlike other imaging techniques, LSI does not require a contrast agent or fluorescent marker, provides clear visualization of pial surface vessels, and captures wide field images (at low magnification) of the entire brain surface[327]. LSI has been used to measure relative changes in blood flow and create flow maps in implanted engineered tissue [328, 329] and cardiac arrest model [330], but has not been used to study cortical blood flow following TBI. In collaboration with Dr. Bernard Choi at the Beckman Laser Institute at University of California Irvine, in preliminary data we have shown marked reduction in the vessel network and dramatic loss of cerebral blood flow at 2 dpi that gradually increased at 7 dpi, which is consistent with our previously published work on vascular regrowth after TBI[75]. Additionally, we obtained blood flow measurements in TBI mice treated with JW74 and Lithium to assess the perfusion capability of the repaired vessels.

Behavioral testing in this dissertation was not acquired but will be addressed in ongoing work. It is important to determine whether stimulation or inhibition of angiogenesis after brain injury leads to improved neurological recovery. We expect that increased vessel density will result in improved behavioral outcomes, whereas reduced vessel density results in poorer behavioral outcomes. We are currently in the process of performing open field and foot fault tests in TBI-injured mice treated with Lithium and JW74 and the

results from these behavioral tests will be combined with the vascular

morphological results in Chapter 5 at the time of publication.
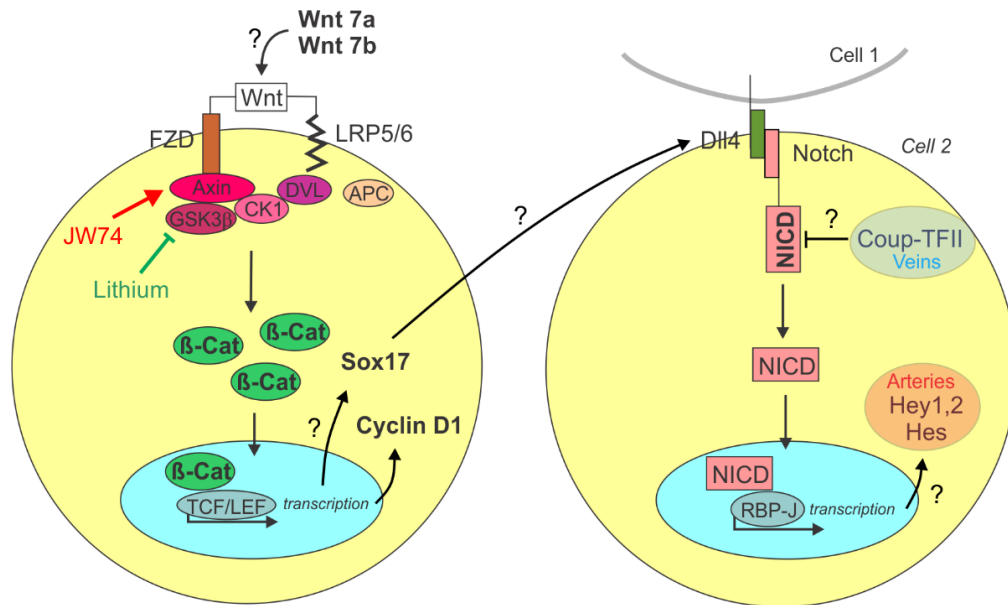
Figure 5.1. Possible mechanism of β-catenin-mediated vascular repair. The dissertation reported novel findings that are shown in bold. We reported that after TBI perilesional vessels have 1) increased β-catenin protein levels, 2) increased TCF/LEF activity, 3) increased Sox17 protein levels, 4) increased Cyclin D1 protein levels (unpublished data), and 5) increased active NICD protein levels (unpublished data). We reported increased extracellular Wnt7a and Wnt7b protein in the perilesional tissue (unpublished data). Additionally, we reported that Cyclin D1 protein levels are increased following Lithium treatment. Possible interactions between signaling molecules are denoted by a question mark (?) and require additional research. Binding of Wnt7a and Wnt7b to the FZD and LRP5/6 receptors leads to dissociation of the β-catenin destruction complex consisting of APC, Axin, CK1, and GSK3β. β-catenin escapes degradation where it

accumulates in the cytoplasm and translocates to the nucleus and complexes with TCF and LEF to promote transcription of Wnt target genes such as Cyclin D1. One possible gene regulated by β-catenin/TCF/LEF is Sox17, a transcription factor that induces vessel formation by regulating transcription of Notch signaling components including Dll4. Binding of Dll4 to the Notch receptor results in dissociation of the NICD where it translocates to the nucleus and complexes with RBP-J to promote transcription of Notch target genes. Notch target genes, such as Hey1, Hey2, and Hes, activate arterial genes and induces arterial specification. COUP-TFII prevents cleavage of NICD which activates venous genes and induces venous specification. Lithium, a GSK3 inhibitor, prevents β-catenin degradation and increases β-catenin levels. JW74 increases Axin levels leading to β-catenin degradation and reduction in β-catenin levels.

Abbreviations: APC, adenomatous polyposis coli; CK1, casein kinase 1; β-cat, β-catenin; DVL, Dishevelled; FZD, Frizzled; GSK3β, glycogen synthase kinase 3 β; LRP, low-density lipoprotein receptor-related protein; TCF, T cell factor; LEF, lymphoid enhancer binding factor; Dll4, Delta-like ligand 4; NICD, Notch intracellular domain; Coup-TFII, Coup transcription factor 2; RBP-J, Recombination Signal Binding Protein For Immunoglobulin Kappa *J* Region
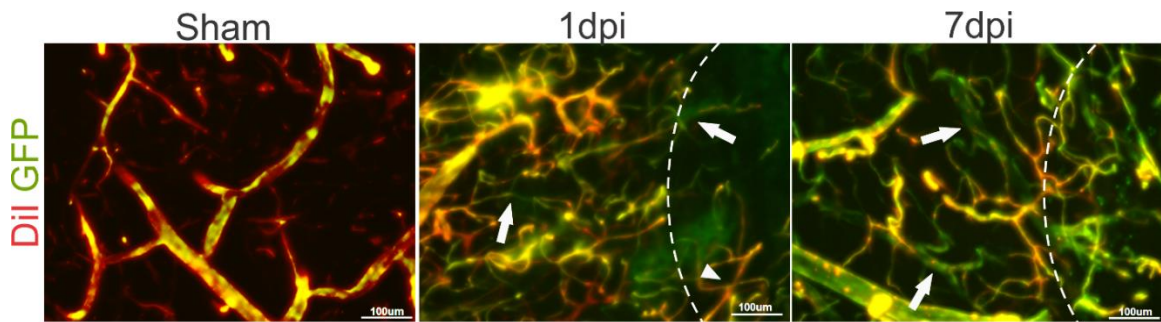
Figure 5.2. TBI results in an increase in the number of non-perfused vessels at 1 and 7 dpi. Sham animals showed Tie2-GFP colocalized with vessels stained with DiI. At 1 dpi there is clear reduction of vessels in the injury site with non-perfused vessels (solid arrow) and newly perfused vessel that are DiI+GFP⁻ (arrowhead). At 7 dpi there is increase in the number of perfused and non-perfused vessels (arrow) within and adjacent to the injury site. There is increased density and tortuosity of the new vessels at 7 dpi compared to the sham animals.

References

1.   Kabadi SV and Faden AI. Neuroprotective strategies for traumatic brain injury: improving clinical translation. *Int J Mol Sci*. 2014; 15: 1216-36.

2.   Logsdon AF, Lucke-Wold BP, Turner RC, Huber JD, Rosen CL and Simpkins JW. Role of Microvascular Disruption in Brain Damage from Traumatic Brain Injury. *Compr Physiol*. 2015; 5: 1147-60.

3.   Kenney K, Amyot F, Haber M, et al. Cerebral Vascular Injury in Traumatic Brain Injury. *Exp Neurol*. 2016; 275 Pt 3: 353-66.

4.   Jullienne A, Obenaus A, Ichkova A, Savona-Baron C, Pearce WJ and Badaut J. Chronic cerebrovascular dysfunction after traumatic brain injury. *J Neurosci Res*. 2016; 94: 609-22.

5.   Zhang JH, Badaut J, Tang J, Obenaus A, Hartman R and Pearce WJ. The vascular neural network--a new paradigm in stroke pathophysiology. *Nat Rev Neurol*. 2012; 8: 711-6.

6.   Jullienne A and Badaut J. Molecular contributions to neurovascular unit dysfunctions after brain injuries: lessons for target-specific drug development. *Future Neurol*. 2013; 8: 677-89.

7.   Morgan R, Kreipke CW, Roberts G, Bagchi M and Rafols JA. Neovascularization following traumatic brain injury: possible evidence for both angiogenesis and vasculogenesis. *Neurol Res*. 2007; 29: 375-81.

8.   Frontczak-Baniewicz M and Walski M. New vessel formation after surgical brain injury in the rat's cerebral cortex I. Formation of the blood vessels proximally to the surgical injury. *Acta Neurobiol Exp (Wars)*. 2003; 63: 65-75.

9.   Park E, Bell JD, Siddiq IP and Baker AJ. An analysis of regional microvascular loss and recovery following two grades of fluid percussion trauma: a role for hypoxia-inducible factors in traumatic brain injury. *J Cereb Blood Flow Metab*. 2009; 29: 575-84.

10.   Rosenbaum BP, Kelly ML, Kshettry VR and Weil RJ. Neurologic disorders, in-hospital deaths, and years of potential life lost in the USA, 1988-2011. *J Clin Neurosci*. 2014; 21: 1874-80.

11.   Corrigan JD, Selassie AW and Orman JA. The epidemiology of traumatic brain injury. *J Head Trauma Rehabil*. 2010; 25: 72-80.

12.   Maas AI, Menon DK, Steyerberg EW, et al. Collaborative European NeuroTrauma Effectiveness Research in Traumatic Brain Injury (CENTER-TBI): a prospective longitudinal observational study. *Neurosurgery*. 2015; 76: 67-80.

13.   Vaishnavi S, Rao V and Fann JR. Neuropsychiatric problems after traumatic brain injury: unraveling the silent epidemic. *Psychosomatics*. 2009; 50: 198-205.

14.   Selassie AW, Zaloshnja E, Langlois JA, Miller T, Jones P and Steiner C. Incidence of long-term disability following traumatic brain injury hospitalization, United States, 2003. *J Head Trauma Rehabil*. 2008; 23: 123-31.

15.   Johnson VE, Meaney DF, Cullen DK and Smith DH. Animal models of traumatic brain injury. *Handb Clin Neurol*. 2015; 127: 115-28.

16.   Guskiewicz KM, Marshall SW, Bailes J, et al. Association between recurrent concussion and late-life cognitive impairment in retired professional football players. *Neurosurgery*. 2005; 57: 719-26; discussion -26.

17.   Yeh DD and Schecter WP. Primary blast injuries--an updated concise review. *World J Surg*. 2012; 36: 966-72.

18.   Benson RR, Gattu R, Sewick B, et al. Detection of hemorrhagic and axonal pathology in mild traumatic brain injury using advanced MRI: implications for neurorehabilitation. *NeuroRehabilitation*. 2012; 31: 261-79.

19.   Konrad C, Geburek AJ, Rist F, et al. Long-term cognitive and emotional consequences of mild traumatic brain injury. *Psychol Med*. 2011; 41: 1197-211.

20.   Obenaus A. Traumatic brain injury. *Encyclopedia of mental health, 2nd ed*. 2015: 329–40.

21.   Maas AI, Stocchetti N and Bullock R. Moderate and severe traumatic brain injury in adults. *Lancet Neurol*. 2008; 7: 728-41.

22.   Spitz G, Alway YJ, Gould K and Ponsford J. Disrupted white matter microstructure and mood disorders following traumatic brain injury. *J Neurotrauma*. 2016.

23.   Lozano D, Gonzales-Portillo GS, Acosta S, et al. Neuroinflammatory responses to traumatic brain injury: etiology, clinical consequences, and therapeutic opportunities. *Neuropsychiatr Dis Treat*. 2015; 11: 97-106.

24.   Pop V and Badaut J. A neurovascular perspective for long-term changes after brain trauma. *Transl Stroke Res*. 2011; 2: 533-45.

25.   Perel P, Roberts I, Bouamra O, Woodford M, Mooney J and Lecky F. Intracranial bleeding in patients with traumatic brain injury: a prognostic study. *BMC Emerg Med*. 2009; 9: 15.

26.   Hochstadter E, Stewart TC, Alharfi IM, Ranger A and Fraser DD. Subarachnoid hemorrhage prevalence and its association with short-term outcome in pediatric severe traumatic brain injury. *Neurocrit Care*. 2014; 21: 505-13.

27. Faust K, Horn P, Schneider UC and Vajkoczy P. Blood pressure changes after aneurysmal subarachnoid hemorrhage and their relationship to cerebral vasospasm and clinical outcome. *Clin Neurol Neurosurg*. 2014; 125: 36-40.

28. Park JH, Park SW, Kang SH, Nam TK, Min BK and Hwang SN. Detection of traumatic cerebral microbleeds by susceptibility-weighted image of MRI. *J Korean Neurosurg Soc*. 2009; 46: 365-9.

29. Gaasch JA, Lockman PR, Geldenhuys WJ, Allen DD and Van der Schyf CJ. Brain iron toxicity: differential responses of astrocytes, neurons, and endothelial cells. *Neurochem Res*. 2007; 32: 1196-208.

30. Glushakova OY, Johnson D and Hayes RL. Delayed increases in microvascular pathology after experimental traumatic brain injury are associated with prolonged inflammation, blood-brain barrier disruption, and progressive white matter damage. *J Neurotrauma*. 2014; 31: 1180-93.

31. Donovan V, Bianchi A, Hartman R, Bhanu B, Carson MJ and Obenaus A. Computational analysis reveals increased blood deposition following repeated mild traumatic brain injury. *Neuroimage Clin*. 2012; 1: 18-28.

32. Marmarou A. Pathophysiology of traumatic brain edema: current concepts. *Acta Neurochir Suppl*. 2003; 86: 7-10.

33. Ewing-Cobbs L, Prasad M, Kramer L, et al. Acute neuroradiologic findings in young children with inflicted or noninflicted traumatic brain injury. *Childs Nerv Syst*. 2000; 16: 25-33; discussion 4.

34. Badaut J, Ashwal S and Obenaus A. Aquaporins in cerebrovascular disease: a target for treatment of brain edema? *Cerebrovasc Dis*. 2011; 31: 521-31.

35. Nirula R, Millar D, Greene T, et al. Decompressive craniectomy or medical management for refractory intracranial hypertension: an AAST-MIT propensity score analysis. *J Trauma Acute Care Surg*. 2014; 76: 944-52; discussion 52-5.

36. Bouma GJ, Muizelaar JP, Stringer WA, Choi SC, Fatouros P and Young HF. Ultra-early evaluation of regional cerebral blood flow in severely head-injured patients using xenon-enhanced computerized tomography. *Journal of neurosurgery*. 1992; 77: 360-8.

37. Soustiel JF, Glenn TC, Shik V, Boscardin J, Mahamid E and Zaaroor M. Monitoring of cerebral blood flow and metabolism in traumatic brain injury. *J Neurotrauma*. 2005; 22: 955-65.

38. Bouma GJ, Muizelaar JP, Choi SC, Newlon PG and Young HF. Cerebral circulation and metabolism after severe traumatic brain injury: the elusive role of ischemia. *Journal of neurosurgery*. 1991; 75: 685-93.

39.   Ostergaard L, Engedal TS, Aamand R, et al. Capillary transit time heterogeneity and flow-metabolism coupling after traumatic brain injury. *J Cereb Blood Flow Metab*. 2014; 34: 1585-98.

40.   Doshi H, Wiseman N, Liu J, et al. Cerebral hemodynamic changes of mild traumatic brain injury at the acute stage. *PLoS One*. 2015; 10: e0118061.

41.   Inoue Y, Shiozaki T, Tasaki O, et al. Changes in cerebral blood flow from the acute to the chronic phase of severe head injury. *J Neurotrauma*. 2005; 22: 1411-8.

42.   Kramer DR, Winer JL, Pease BA, Amar AP and Mack WJ. Cerebral vasospasm in traumatic brain injury. *Neurol Res Int*. 2013; 2013: 415813.

43.   Oertel M, Boscardin WJ, Obrist WD, et al. Posttraumatic vasospasm: the epidemiology, severity, and time course of an underestimated phenomenon: a prospective study performed in 299 patients. *Journal of neurosurgery*. 2005; 103: 812-24.

44.   Alford PW, Dabiri BE, Goss JA, Hemphill MA, Brigham MD and Parker KK. Blast-induced phenotypic switching in cerebral vasospasm. *Proc Natl Acad Sci U S A*. 2011; 108: 12705-10.

45.   Izzy S and Muehlschlegel S. Cerebral vasospasm after aneurysmal subarachnoid hemorrhage and traumatic brain injury. *Curr Treat Options Neurol*. 2014; 16: 278.

46.   Dore-Duffy P, Owen C, Balabanov R, Murphy S, Beaumont T and Rafols JA. Pericyte migration from the vascular wall in response to traumatic brain injury. *Microvasc Res*. 2000; 60: 55-69.

47.   Ho KM, Honeybul S, Yip CB and Silbert BI. Prognostic significance of blood-brain barrier disruption in patients with severe nonpenetrating traumatic brain injury requiring decompressive craniectomy. *Journal of neurosurgery*. 2014; 121: 674-9.

48.   Tomkins O, Shelef I, Kaizerman I, et al. Blood-brain barrier disruption in post-traumatic epilepsy. *J Neurol Neurosurg Psychiatry*. 2008; 79: 774-7.

49.   Yeoh S, Bell ED and Monson KL. Distribution of blood-brain barrier disruption in primary blast injury. *Ann Biomed Eng*. 2013; 41: 2206-14.

50.   Kolaczkowska E and Kubes P. Neutrophil recruitment and function in health and inflammation. *Nat Rev Immunol*. 2013; 13: 159-75.

51.   Abdul-Muneer PM, Chandra N and Haorah J. Interactions of oxidative stress and neurovascular inflammation in the pathogenesis of traumatic brain injury. *Mol Neurobiol*. 2015; 51: 966-79.

52.   Harhangi BS, Kompanje EJ, Leebeek FW and Maas AI. Coagulation disorders after traumatic brain injury. *Acta Neurochir (Wien)*. 2008; 150: 165-75; discussion 75.

53.   Yuan Q, Sun YR, Wu X, et al. Coagulopathy in Traumatic Brain Injury and Its Correlation with Progressive Hemorrhagic Injury: A Systematic Review and Meta-Analysis. *J Neurotrauma*. 2016; 33: 1279-91.

54.   de Oliveira Manoel AL, Neto AC, Veigas PV and Rizoli S. Traumatic brain injury associated coagulopathy. *Neurocrit Care*. 2015; 22: 34-44.

55.   Lustenberger T, Talving P, Kobayashi L, et al. Time course of coagulopathy in isolated severe traumatic brain injury. *Injury*. 2010; 41: 924-8.

56.   Midura EF, Jernigan PL, Kuethe JW, et al. Microparticles impact coagulation after traumatic brain injury. *The Journal of surgical research*. 2015; 197: 25-31.

57.   Ploplis VA, Donahue DL, Sandoval-Cooper MJ, et al. Systemic platelet dysfunction is the result of local dysregulated coagulation and platelet activation in the brain in a rat model of isolated traumatic brain injury. *J Neurotrauma*. 2014; 31: 1672-5.

58.   Laroche M, Kutcher ME, Huang MC, Cohen MJ and Manley GT. Coagulopathy after traumatic brain injury. *Neurosurgery*. 2012; 70: 1334-45.

59.   Nakae R, Takayama Y, Kuwamoto K, Naoe Y, Sato H and Yokota H. Time Course of Coagulation and Fibrinolytic Parameters in Patients with Traumatic Brain Injury. *J Neurotrauma*. 2016; 33: 688-95.

60.   Schnuriger B, Inaba K, Abdelsayed GA, et al. The impact of platelets on the progression of traumatic intracranial hemorrhage. *The Journal of trauma*. 2010; 68: 881-5.

61.   Lorente L. New Prognostic Biomarkers in Patients With Traumatic Brain Injury. *Archives of trauma research*. 2015; 4: e30165.

62.   Shen X, Dutcher SK, Palmer J, et al. A Systematic Review of the Benefits and Risks of Anticoagulation Following Traumatic Brain Injury. *J Head Trauma Rehabil*. 2015; 30: E29-37.

63.   Kumar A and Loane DJ. Neuroinflammation after traumatic brain injury: opportunities for therapeutic intervention. *Brain Behav Immun*. 2012; 26: 1191-201.

64.   Hinson HE, Rowell S and Schreiber M. Clinical evidence of inflammation driving secondary brain injury: a systematic review. *J Trauma Acute Care Surg*. 2015; 78: 184-91.

65.   Gentleman SM, Leclercq PD, Moyes L, et al. Long-term intracerebral inflammatory response after traumatic brain injury. *Forensic Sci Int*. 2004; 146: 97-104.

66.   Johnson VE, Stewart JE, Begbie FD, Trojanowski JQ, Smith DH and Stewart W. Inflammation and white matter degeneration persist for years after a single traumatic brain injury. *Brain*. 2013; 136: 28-42.

67.	Smith C, Gentleman SM, Leclercq PD, et al. The neuroinflammatory response in humans after traumatic brain injury. *Neuropathol Appl Neurobiol*. 2013; 39: 654-66.

68.	Block ML, Zecca L and Hong JS. Microglia-mediated neurotoxicity: uncovering the molecular mechanisms. *Nat Rev Neurosci*. 2007; 8: 57-69.

69.	Hernandez-Ontiveros DG, Tajiri N, Acosta S, Giunta B, Tan J and Borlongan CV. Microglia activation as a biomarker for traumatic brain injury. *Front Neurol*. 2013; 4: 30.

70.	Hayward NM, Tuunanen PI, Immonen R, Ndode-Ekane XE, Pitkanen A and Grohn O. Magnetic resonance imaging of regional hemodynamic and cerebrovascular recovery after lateral fluid-percussion brain injury in rats. *J Cereb Blood Flow Metab*. 2011; 31: 166-77.

71.	Steinman J, Cahill LS, Koletar MM, Stefanovic B and Sled JG. Acute and chronic stage adaptations of vascular architecture and cerebral blood flow in a mouse model of TBI. *bioRxiv*. 2018: 479626.

72.	Gama Sosa MA, De Gasperi R, Janssen PL, et al. Selective vulnerability of the cerebral vasculature to blast injury in a rat model of mild traumatic brain injury. *Acta Neuropathol Commun*. 2014; 2: 67.

73.	Siddiq I, Park E, Liu E, et al. Treatment of traumatic brain injury using zinc-finger protein gene therapy targeting VEGF-A. *J Neurotrauma*. 2012; 29: 2647-59.

74.	Salehi A, Jullienne A, Wendel KM, et al. A Novel Technique for Visualizing and Analyzing the Cerebral Vasculature in Rodents. *Transl Stroke Res*. 2018.

75.	Salehi A, Jullienne A, Baghchechi M, et al. Up-regulation of Wnt/beta-catenin expression is accompanied with vascular repair after traumatic brain injury. *J Cereb Blood Flow Metab*. 2018; 38: 274-89.

76.	Obenaus A, Ng M, Orantes A, et al. Traumatic brain injury results in acute rarefication of the vascular network. *Scientific Reports*. 2016.

77.	Brickler TR, Hazy A, Guilhaume Correa F, et al. Angiopoietin/Tie2 Axis Regulates the Age-at-Injury Cerebrovascular Response to Traumatic Brain Injury. *J Neurosci*. 2018; 38: 9618-34.

78.	Jullienne A, Salehi A, Affeldt B, et al. Male and Female Mice Exhibit Divergent Responses of the Cortical Vasculature to Traumatic Brain Injury. *J Neurotrauma*. 2018; 35: 1646-58.

79.	Jia Y, Grafe MR, Gruber A, Alkayed NJ and Wang RK. In vivo optical imaging of revascularization after brain trauma in mice. *Microvasc Res*. 2011; 81: 73-80.

80.	Liu H, He J, Zhang Z, et al. Evolution of cerebral perfusion in the peri-contusional cortex in mice revealed by in vivo laser speckle imaging after traumatic brain injury. *Brain Res*. 2018; 1700: 118-25.

81.   Hayward NM, Immonen R, Tuunanen PI, Ndode-Ekane XE, Grohn O and Pitkanen A. Association of chronic vascular changes with functional outcome after traumatic brain injury in rats. *J Neurotrauma.* 2010; 27: 2203-19.

82.   Rodriguez-Baeza A, Reina-de la Torre F, Poca A, Marti M and Garnacho A. Morphological features in human cortical brain microvessels after head injury: a three-dimensional and immunocytochemical study. *Anat Rec A Discov Mol Cell Evol Biol.* 2003; 273: 583-93.

83.   Rafols JA, Kreipke CW and Petrov T. Alterations in cerebral cortex microvessels and the microcirculation in a rat model of traumatic brain injury: a correlative EM and laser Doppler flowmetry study. *Neurol Res.* 2007; 29: 339-47.

84.   Castejon OJ. Ultrastructural alterations of human cortical capillary basement membrane in human brain oedema. *Folia Neuropathol.* 2014; 52: 10-21.

85.   Danaila L, Popescu I, Pais V, Riga D, Riga S and Pais E. Apoptosis, paraptosis, necrosis, and cell regeneration in posttraumatic cerebral arteries. *Chirurgia (Bucur).* 2013; 108: 319-24.

86.   Jullienne A, Roberts JM, Pop V, et al. Juvenile traumatic brain injury induces long-term perivascular matrix changes alongside amyloid-beta accumulation. *J Cereb Blood Flow Metab.* 2014; 34: 1637-45.

87.   Lynch CE, Crynen G, Ferguson S, et al. Chronic cerebrovascular abnormalities in a mouse model of repetitive mild traumatic brain injury. *Brain injury.* 2016; 30: 1414-27.

88.   Carmeliet P and Jain RK. Molecular mechanisms and clinical applications of angiogenesis. *Nature.* 2011; 473: 298-307.

89.   Skold MK, von Gertten C, Sandberg-Nordqvist AC, Mathiesen T and Holmin S. VEGF and VEGF receptor expression after experimental brain contusion in rat. *J Neurotrauma.* 2005; 22: 353-67.

90.   Gajavelli S, Kentaro S, Diaz J, et al. Glucose and oxygen metabolism after penetrating ballistic-like brain injury. *J Cereb Blood Flow Metab.* 2015; 35: 773-80.

91.   Anderson J, Sandhir R, Hamilton ES and Berman NE. Impaired expression of neuroprotective molecules in the HIF-1alpha pathway following traumatic brain injury in aged mice. *J Neurotrauma.* 2009; 26: 1557-66.

92.   Hirota K and Semenza GL. Regulation of angiogenesis by hypoxia-inducible factor 1. *Crit Rev Oncol Hematol.* 2006; 59: 15-26.

93.   Krum JM, Mani N and Rosenstein JM. Angiogenic and astroglial responses to vascular endothelial growth factor administration in adult rat brain. *Neuroscience.* 2002; 110: 589-604.

94.   Krum JM and Khaibullina A. Inhibition of endogenous VEGF impedes revascularization and astroglial proliferation: roles for VEGF in brain repair. *Exp Neurol*. 2003; 181: 241-57.

95.   Balabanov R, Goldman H, Murphy S, et al. Endothelial cell activation following moderate traumatic brain injury. *Neurol Res.* 2001; 23: 175-82.

96.   Van Hove AH and Benoit DS. Depot-Based Delivery Systems for Pro-Angiogenic Peptides: A Review. *Front Bioeng Biotechnol*. 2015; 3: 102.

97.   Asahara T, Masuda H, Takahashi T, et al. Bone marrow origin of endothelial progenitor cells responsible for postnatal vasculogenesis in physiological and pathological neovascularization. *Circ Res*. 1999; 85: 221-8.

98.   Gong D, Zhang S, Liu L, et al. Dynamic changes of vascular endothelial growth factor and angiopoietin-1 in association with circulating endothelial progenitor cells after severe traumatic brain injury. *The Journal of trauma*. 2011; 70: 1480-4.

99.   Liu L, Wei H, Chen F, Wang J, Dong JF and Zhang J. Endothelial progenitor cells correlate with clinical outcome of traumatic brain injury. *Crit Care Med*. 2011; 39: 1760-5.

100.   Guo X, Liu L, Zhang M, et al. Correlation of CD34+ cells with tissue angiogenesis after traumatic brain injury in a rat model. *J Neurotrauma*. 2009; 26: 1337-44.

101.   Roncalli JG, Tongers J, Renault MA and Losordo DW. Endothelial progenitor cells in regenerative medicine and cancer: a decade of research. *Trends Biotechnol*. 2008; 26: 276-83.

102.   Du R, Lu KV, Petritsch C, et al. HIF1alpha induces the recruitment of bone marrow-derived vascular modulatory cells to regulate tumor angiogenesis and invasion. *Cancer Cell*. 2008; 13: 206-20.

103.   Liu L, Liu H, Jiao J, et al. Changes in circulating human endothelial progenitor cells after brain injury. *J Neurotrauma*. 2007; 24: 936-43.

104.   Reale A, Melaccio A, Lamanuzzi A, et al. Functional and Biological Role of Endothelial Precursor Cells in Tumour Progression: A New Potential Therapeutic Target in Haematological Malignancies. *Stem Cells Int*. 2016; 2016: 7954580.

105.   Ziegelhoeffer T, Fernandez B, Kostin S, et al. Bone marrow-derived cells do not incorporate into the adult growing vasculature. *Circ Res*. 2004; 94: 230-8.

106.   Urbich C, Aicher A, Heeschen C, et al. Soluble factors released by endothelial progenitor cells promote migration of endothelial cells and cardiac resident progenitor cells. *J Mol Cell Cardiol*. 2005; 39: 733-42.

107.   Miller JT, Bartley JH, Wimborne HJ, et al. The neuroblast and angioblast chemotaxic factor SDF-1 (CXCL12) expression is briefly up regulated by reactive

astrocytes in brain following neonatal hypoxic-ischemic injury. *BMC neuroscience*. 2005; 6: 63.

108.   Treutiger CJ, Mullins GE, Johansson AS, et al. High mobility group 1 B-box mediates activation of human endothelium. *J Intern Med*. 2003; 254: 375-85.

109.   Hayakawa K, Pham LD, Katusic ZS, Arai K and Lo EH. Astrocytic high-mobility group box 1 promotes endothelial progenitor cell-mediated neurovascular remodeling during stroke recovery. *Proc Natl Acad Sci U S A*. 2012; 109: 7505-10.

110.   Hayakawa K, Miyamoto N, Seo JH, et al. High-mobility group box 1 from reactive astrocytes enhances the accumulation of endothelial progenitor cells in damaged white matter. *J Neurochem*. 2013; 125: 273-80.

111.   Jones EV and Bouvier DS. Astrocyte-secreted matricellular proteins in CNS remodelling during development and disease. *Neural Plast*. 2014; 2014: 321209.

112.   Ribotta MG, Menet V and Privat A. Glial scar and axonal regeneration in the CNS: lessons from GFAP and vimentin transgenic mice. *Acta Neurochir Suppl*. 2004; 89: 87-92.

113.   Villapol S, Byrnes KR and Symes AJ. Temporal dynamics of cerebral blood flow, cortical damage, apoptosis, astrocyte-vasculature interaction and astrogliosis in the pericontusional region after traumatic brain injury. *Front Neurol*. 2014; 5: 82.

114.   Abbott NJ, Ronnback L and Hansson E. Astrocyte-endothelial interactions at the blood-brain barrier. *Nat Rev Neurosci*. 2006; 7: 41-53.

115.   Raza A, Franklin MJ and Dudek AZ. Pericytes and vessel maturation during tumor angiogenesis and metastasis. *Am J Hematol*. 2010; 85: 593-8.

116.   Zehendner CM, Sebastiani A, Hugonnet A, Bischoff F, Luhmann HJ and Thal SC. Traumatic brain injury results in rapid pericyte loss followed by reactive pericytosis in the cerebral cortex. *Sci Rep*. 2015; 5: 13497.

117.   Yemisci M, Gursoy-Ozdemir Y, Vural A, Can A, Topalkara K and Dalkara T. Pericyte contraction induced by oxidative-nitrative stress impairs capillary reflow despite successful opening of an occluded cerebral artery. *Nat Med*. 2009; 15: 1031-7.

118.   Hori S, Ohtsuki S, Hosoya K, Nakashima E and Terasaki T. A pericyte-derived angiopoietin-1 multimeric complex induces occludin gene expression in brain capillary endothelial cells through Tie-2 activation in vitro. *J Neurochem*. 2004; 89: 503-13.

119.   Bergers G and Song S. The role of pericytes in blood-vessel formation and maintenance. *Neuro Oncol*. 2005; 7: 452-64.

120.   Parent JM, Vexler ZS, Gong C, Derugin N and Ferriero DM. Rat forebrain neurogenesis and striatal neuron replacement after focal stroke. *Annals of neurology*. 2002; 52: 802-13.

121.   Kojima T, Hirota Y, Ema M, et al. Subventricular zone-derived neural progenitor cells migrate along a blood vessel scaffold toward the post-stroke striatum. *Stem Cells*. 2010; 28: 545-54.

122.   Skardelly M, Gaber K, Burdack S, et al. Long-term benefit of human fetal neuronal progenitor cell transplantation in a clinically adapted model after traumatic brain injury. *J Neurotrauma*. 2011; 28: 401-14.

123.   Schiera G, Proia P, Alberti C, Mineo M, Savettieri G and Di Liegro I. Neurons produce FGF2 and VEGF and secrete them at least in part by shedding extracellular vesicles. *J Cell Mol Med*. 2007; 11: 1384-94.

124.   Okabe K, Kobayashi S, Yamada T, et al. Neurons limit angiogenesis by titrating VEGF in retina. *Cell*. 2014; 159: 584-96.

125.   Hsieh CL, Kim CC, Ryba BE, et al. Traumatic brain injury induces macrophage subsets in the brain. *Eur J Immunol*. 2013; 43: 2010-22.

126.   Spiller KL, Anfang RR, Spiller KJ, et al. The role of macrophage phenotype in vascularization of tissue engineering scaffolds. *Biomaterials*. 2014; 35: 4477-88.

127.   Kim CC, Nakamura MC and Hsieh CL. Brain trauma elicits non-canonical macrophage activation states. *J Neuroinflammation*. 2016; 13: 117.

128.   Kumar A, Alvarez-Croda DM, Stoica BA, Faden AI and Loane DJ. Microglial/Macrophage Polarization Dynamics following Traumatic Brain Injury. *J Neurotrauma*. 2016; 33: 1732-50.

129.   Frautschy SA, Walicke PA and Baird A. Localization of basic fibroblast growth factor and its mRNA after CNS injury. *Brain Res*. 1991; 553: 291-9.

130.   Lobov IB, Rao S, Carroll TJ, et al. WNT7b mediates macrophage-induced programmed cell death in patterning of the vasculature. *Nature*. 2005; 437: 417-21.

131.   Liu C, Wu C, Yang Q, et al. Macrophages Mediate the Repair of Brain Vascular Rupture through Direct Physical Adhesion and Mechanical Traction. *Immunity*. 2016; 44: 1162-76.

132.   Fantin A, Vieira JM, Gestri G, et al. Tissue macrophages act as cellular chaperones for vascular anastomosis downstream of VEGF-mediated endothelial tip cell induction. *Blood*. 2010; 116: 829-40.

133.   He H, Mack JJ, Guc E, et al. Perivascular Macrophages Limit Permeability. *Arterioscler Thromb Vasc Biol*. 2016; 36: 2203-12.

134.   Zhang Z, Zhang ZY, Wu Y and Schluesener HJ. Lesional accumulation of CD163+ macrophages/microglia in rat traumatic brain injury. *Brain Res*. 2012; 1461: 102-10.

135.	Lin EY, Li JF, Gnatovskiy L, et al. Macrophages regulate the angiogenic switch in a mouse model of breast cancer. *Cancer Res*. 2006; 66: 11238-46.

136.	Addington CP, Roussas A, Dutta D and Stabenfeldt SE. Endogenous repair signaling after brain injury and complementary bioengineering approaches to enhance neural regeneration. *Biomark Insights*. 2015; 10: 43-60.

137.	Thau-Zuchman O, Shohami E, Alexandrovich AG and Leker RR. Subacute treatment with vascular endothelial growth factor after traumatic brain injury increases angiogenesis and gliogenesis. *Neuroscience*. 2012; 202: 334-41.

138.	Thau-Zuchman O, Shohami E, Alexandrovich AG and Leker RR. Combination of vascular endothelial and fibroblast growth factor 2 for induction of neurogenesis and angiogenesis after traumatic brain injury. *J Mol Neurosci*. 2012; 47: 166-72.

139.	Zhang ZG, Zhang L, Tsang W, et al. Correlation of VEGF and angiopoietin expression with disruption of blood-brain barrier and angiogenesis after focal cerebral ischemia. *J Cereb Blood Flow Metab*. 2002; 22: 379-92.

140.	Zhang A, Liang L, Niu H, Xu P and Hao Y. Protective effects of VEGF treatment on focal cerebral ischemia in rats. *Mol Med Rep*. 2012; 6: 1315-8.

141.	Dzietko M, Derugin N, Wendland MF, Vexler ZS and Ferriero DM. Delayed VEGF treatment enhances angiogenesis and recovery after neonatal focal rodent stroke. *Transl Stroke Res*. 2013; 4: 189-200.

142.	Shibuya M and Claesson-Welsh L. Signal transduction by VEGF receptors in regulation of angiogenesis and lymphangiogenesis. *Exp Cell Res*. 2006; 312: 549-60.

143.	Koch S and Claesson-Welsh L. Signal transduction by vascular endothelial growth factor receptors. *Cold Spring Harb Perspect Med*. 2012; 2: a006502.

144.	Gong D, Hao M, Liu L, et al. Prognostic relevance of circulating endothelial progenitor cells for severe traumatic brain injury. *Brain injury*. 2012; 26: 291-7.

145.	Li W, Wang H, Kuang CY, et al. An essential role for the Id1/PI3K/Akt/NFkB/survivin signalling pathway in promoting the proliferation of endothelial progenitor cells in vitro. *Mol Cell Biochem*. 2012; 363: 135-45.

146.	Goetz R and Mohammadi M. Exploring mechanisms of FGF signalling through the lens of structural biology. *Nat Rev Mol Cell Biol*. 2013; 14: 166-80.

147.	Kano MR, Morishita Y, Iwata C, et al. VEGF-A and FGF-2 synergistically promote neoangiogenesis through enhancement of endogenous PDGF-B-PDGFRbeta signaling. *J Cell Sci*. 2005; 118: 3759-68.

148.	Wang ZG, Cheng Y, Yu XC, et al. bFGF Protects Against Blood-Brain Barrier Damage Through Junction Protein Regulation via PI3K-Akt-Rac1 Pathway Following Traumatic Brain Injury. *Mol Neurobiol*. 2015.

149. Huang B, Krafft PR, Ma Q, et al. Fibroblast growth factors preserve blood-brain barrier integrity through RhoA inhibition after intracerebral hemorrhage in mice. *Neurobiol Dis*. 2012; 46: 204-14.

150. Li S, Wei M, Zhou Z, Wang B, Zhao X and Zhang J. SDF-1alpha induces angiogenesis after traumatic brain injury. *Brain Res*. 2012; 1444: 76-86.

151. Sun W, Liu J, Huan Y and Zhang C. Intracranial injection of recombinant stromal-derived factor-1 alpha (SDF-1alpha) attenuates traumatic brain injury in rats. *Inflamm Res*. 2014; 63: 287-97.

152. Cencioni C, Capogrossi MC and Napolitano M. The SDF-1/CXCR4 axis in stem cell preconditioning. *Cardiovasc Res*. 2012; 94: 400-7.

153. Wu Y and Yoder A. Chemokine coreceptor signaling in HIV-1 infection and pathogenesis. *PLoS Pathog*. 2009; 5: e1000520.

154. Rosenkranz K, Kumbruch S, Lebermann K, et al. The chemokine SDF-1/CXCL12 contributes to the 'homing' of umbilical cord blood cells to a hypoxic-ischemic lesion in the rat brain. *J Neurosci Res*. 2010; 88: 1223-33.

155. Egeblad M and Werb Z. New functions for the matrix metalloproteinases in cancer progression. *Nat Rev Cancer*. 2002; 2: 161-74.

156. van Hinsbergh VW and Koolwijk P. Endothelial sprouting and angiogenesis: matrix metalloproteinases in the lead. *Cardiovasc Res*. 2008; 78: 203-12.

157. Lee S, Jilani SM, Nikolova GV, Carpizo D and Iruela-Arispe ML. Processing of VEGF-A by matrix metalloproteinases regulates bioavailability and vascular patterning in tumors. *J Cell Biol*. 2005; 169: 681-91.

158. Frontczak-Baniewicz M, Walski M, Madejska G and Sulejczak D. MMP2 and MMP9 in immature endothelial cells following surgical injury of rat cerebral cortex--a preliminary study. *Folia Neuropathol*. 2009; 47: 338-46.

159. Huang PH, Chen YH, Wang CH, et al. Matrix metalloproteinase-9 is essential for ischemia-induced neovascularization by modulating bone marrow-derived endothelial progenitor cells. *Arterioscler Thromb Vasc Biol*. 2009; 29: 1179-84.

160. Heissig B, Hattori K, Dias S, et al. Recruitment of stem and progenitor cells from the bone marrow niche requires MMP-9 mediated release of kit-ligand. *Cell*. 2002; 109: 625-37.

161. Gurbel PA, Roe MT, Jakubowski JA, et al. Translational platelet research in patients with coronary artery disease: what are the major knowledge gaps? *Thromb Haemost*. 2012; 108: 12-20.

162.	Chen J, Cui X, Zacharek A and Chopp M. Increasing Ang1/Tie2 expression by simvastatin treatment induces vascular stabilization and neuroblast migration after stroke. *J Cell Mol Med*. 2009; 13: 1348-57.

163.	Nourhaghighi N, Teichert-Kuliszewska K, Davis J, Stewart DJ and Nag S. Altered expression of angiopoietins during blood-brain barrier breakdown and angiogenesis. *Lab Invest*. 2003; 83: 1211-22.

164.	Echavarria R and Hussain SN. Regulation of angiopoietin-1/Tie-2 receptor signaling in endothelial cells by dual-specificity phosphatases 1, 4, and 5. *J Am Heart Assoc*. 2013; 2: e000571.

165.	Genc S, Koroglu TF and Genc K. Erythropoietin and the nervous system. *Brain Res*. 2004; 1000: 19-31.

166.	Meng Y, Xiong Y, Mahmood A, Zhang Y, Qu C and Chopp M. Dose-dependent neurorestorative effects of delayed treatment of traumatic brain injury with recombinant human erythropoietin in rats. *Journal of neurosurgery*. 2011; 115: 550-60.

167.	Cherian L, Goodman JC and Robertson C. Neuroprotection with erythropoietin administration following controlled cortical impact injury in rats. *J Pharmacol Exp Ther*. 2007; 322: 789-94.

168.	Tsai PT, Ohab JJ, Kertesz N, et al. A critical role of erythropoietin receptor in neurogenesis and post-stroke recovery. *J Neurosci*. 2006; 26: 1269-74.

169.	Sautina L, Sautin Y, Beem E, et al. Induction of nitric oxide by erythropoietin is mediated by the {beta} common receptor and requires interaction with VEGF receptor 2. *Blood*. 2010; 115: 896-905.

170.	Wang L, Chopp M, Gregg SR, et al. Neural progenitor cells treated with EPO induce angiogenesis through the production of VEGF. *J Cereb Blood Flow Metab*. 2008; 28: 1361-8.

171.	Wang L, Wang X, Su H, et al. Recombinant human erythropoietin improves the neurofunctional recovery of rats following traumatic brain injury via an increase in circulating endothelial progenitor cells. *Transl Stroke Res*. 2015; 6: 50-9.

172.	Hirata A, Minamino T, Asanuma H, et al. Erythropoietin enhances neovascularization of ischemic myocardium and improves left ventricular dysfunction after myocardial infarction in dogs. *J Am Coll Cardiol*. 2006; 48: 176-84.

173.	Yip HK, Tsai TH, Lin HS, et al. Effect of erythropoietin on level of circulating endothelial progenitor cells and outcome in patients after acute ischemic stroke. *Crit Care*. 2011; 15: R40.

174.   Yokota H, Naoe Y, Nakabayashi M, et al. Cerebral endothelial injury in severe head injury: the significance of measurements of serum thrombomodulin and the von Willebrand factor. *J Neurotrauma*. 2002; 19: 1007-15.

175.   Rauch A, Wohner N, Christophe OD, Denis CV, Susen S and Lenting PJ. On the versatility of von Willebrand factor. *Mediterr J Hematol Infect Dis*. 2013; 5: e2013046.

176.   Lenting PJ, Casari C, Christophe OD and Denis CV. von Willebrand factor: the old, the new and the unknown. *J Thromb Haemost*. 2012; 10: 2428-37.

177.   Zhang J, Jiang R, Liu L, Watkins T, Zhang F and Dong JF. Traumatic brain injury-associated coagulopathy. *J Neurotrauma*. 2012; 29: 2597-605.

178.   Starke RD, Ferraro F, Paschalaki KE, et al. Endothelial von Willebrand factor regulates angiogenesis. *Blood*. 2011; 117: 1071-80.

179.   Randi AM, Laffan MA and Starke RD. Von Willebrand factor, angiodysplasia and angiogenesis. *Mediterr J Hematol Infect Dis*. 2013; 5: e2013060.

180.   Wagner DD and Frenette PS. The vessel wall and its interactions. *Blood*. 2008; 111: 5271-81.

181.   MacDonald BT, Tamai K and He X. Wnt/beta-catenin signaling: components, mechanisms, and diseases. *Dev Cell*. 2009; 17: 9-26.

182.   Nusse R and Clevers H. Wnt/beta-Catenin Signaling, Disease, and Emerging Therapeutic Modalities. *Cell*. 2017; 169: 985-99.

183.   Lambert C, Cisternas P and Inestrosa NC. Role of Wnt Signaling in Central Nervous System Injury. *Mol Neurobiol*. 2015.

184.   Shtutman M, Zhurinsky J, Simcha I, et al. The cyclin D1 gene is a target of the beta-catenin/LEF-1 pathway. *Proc Natl Acad Sci U S A*. 1999; 96: 5522-7.

185.   Nelson WJ and Nusse R. Convergence of Wnt, beta-catenin, and cadherin pathways. *Science*. 2004; 303: 1483-7.

186.   Orsulic S, Huber O, Aberle H, Arnold S and Kemler R. E-cadherin binding prevents beta-catenin nuclear localization and beta-catenin/LEF-1-mediated transactivation. *J Cell Sci*. 1999; 112 (Pt 8): 1237-45.

187.   Wang Q, Sun ZX, Allgayer H and Yang HS. Downregulation of E-cadherin is an essential event in activating beta-catenin/Tcf-dependent transcription and expression of its target genes in Pdcd4 knockdown cells. *Oncogene*. 2010; 29: 128-38.

188.   Rao AS, Kremenevskaja N, Resch J and Brabant G. Lithium stimulates proliferation in cultured thyrocytes by activating Wnt/beta-catenin signalling. *Eur J Endocrinol*. 2005; 153: 929-38.

189.   Clement-Lacroix P, Ai M, Morvan F, et al. Lrp5-independent activation of Wnt signaling by lithium chloride increases bone formation and bone mass in mice. *Proc Natl Acad Sci U S A*. 2005; 102: 17406-11.

190.   Zeilbeck LF, Muller B, Knobloch V, Tamm ER and Ohlmann A. Differential angiogenic properties of lithium chloride in vitro and in vivo. *PLoS One*. 2014; 9: e95546.

191.   Shapira M, Licht A, Milman A, Pick CG, Shohami E and Eldar-Finkelman H. Role of glycogen synthase kinase-3beta in early depressive behavior induced by mild traumatic brain injury. *Mol Cell Neurosci*. 2007; 34: 571-7.

192.   Zhu ZF, Wang QG, Han BJ and William CP. Neuroprotective effect and cognitive outcome of chronic lithium on traumatic brain injury in mice. *Brain Res Bull*. 2010; 83: 272-7.

193.   Yu F, Wang Z, Tchantchou F, Chiu CT, Zhang Y and Chuang DM. Lithium ameliorates neurodegeneration, suppresses neuroinflammation, and improves behavioral performance in a mouse model of traumatic brain injury. *J Neurotrauma*. 2012; 29: 362-74.

194.   Yu F, Wang Z, Tanaka M, et al. Posttrauma cotreatment with lithium and valproate: reduction of lesion volume, attenuation of blood-brain barrier disruption, and improvement in motor coordination in mice with traumatic brain injury. *Journal of neurosurgery*. 2013; 119: 766-73.

195.   Valvezan AJ and Klein PS. GSK-3 and Wnt Signaling in Neurogenesis and Bipolar Disorder. *Front Mol Neurosci*. 2012; 5: 1.

196.   Waaler J, Machon O, von Kries JP, et al. Novel synthetic antagonists of canonical Wnt signaling inhibit colorectal cancer cell growth. *Cancer Res*. 2011; 71: 197-205.

197.   Stratford EW, Daffinrud J, Munthe E, et al. The tankyrase-specific inhibitor JW74 affects cell cycle progression and induces apoptosis and differentiation in osteosarcoma cell lines. *Cancer Med*. 2014; 3: 36-46.

198.   Daneman R, Agalliu D, Zhou L, Kuhnert F, Kuo CJ and Barres BA. Wnt/beta-catenin signaling is required for CNS, but not non-CNS, angiogenesis. *Proc Natl Acad Sci U S A*. 2009; 106: 641-6.

199.   Stenman JM, Rajagopal J, Carroll TJ, Ishibashi M, McMahon J and McMahon AP. Canonical Wnt signaling regulates organ-specific assembly and differentiation of CNS vasculature. *Science*. 2008; 322: 1247-50.

200.   Liebner S, Corada M, Bangsow T, et al. Wnt/beta-catenin signaling controls development of the blood-brain barrier. *J Cell Biol*. 2008; 183: 409-17.

201.   Cattelino A, Liebner S, Gallini R, et al. The conditional inactivation of the beta-catenin gene in endothelial cells causes a defective vascular pattern and increased vascular fragility. *J Cell Biol*. 2003; 162: 1111-22.

202.   Corada M, Nyqvist D, Orsenigo F, et al. The Wnt/beta-catenin pathway modulates vascular remodeling and specification by upregulating Dll4/Notch signaling. *Dev Cell*. 2010; 18: 938-49.

203.   Corada M, Orsenigo F, Morini MF, et al. Sox17 is indispensable for acquisition and maintenance of arterial identity. *Nature communications*. 2013; 4: 1-14.

204.   Corada M, Morini MF and Dejana E. Signaling pathways in the specification of arteries and veins. *Arterioscler Thromb Vasc Biol*. 2014; 34: 2372-7.

205.   Dejana E. The role of wnt signaling in physiological and pathological angiogenesis. *Circ Res*. 2010; 107: 943-52.

206.   White BD, Nathe RJ, Maris DO, et al. Beta-catenin signaling increases in proliferating NG2+ progenitors and astrocytes during post-traumatic gliogenesis in the adult brain. *Stem Cells*. 2010; 28: 297-307.

207.   Zhang L, Yan R, Zhang Q, et al. Survivin, a key component of the Wnt/beta-catenin signaling pathway, contributes to traumatic brain injury-induced adult neurogenesis in the mouse dentate gyrus. *Int J Mol Med*. 2013; 32: 867-75.

208.   Wu X, Mao H, Liu J, et al. Dynamic change of SGK expression and its role in neuron apoptosis after traumatic brain injury. *Int J Clin Exp Pathol*. 2013; 6: 1282-93.

209.   SimWu H, Jiang H, Lu D, et al. Induction of angiogenesis and modulation of vascular endothelial growth factor receptor-2 by simvastatin after traumatic brain injury. *Neurosurgery*. 2011; 68: 1363-71; discussion 71.

210.   Krum JM, Mani N and Rosenstein JM. Roles of the endogenous VEGF receptors flt-1 and flk-1 in astroglial and vascular remodeling after brain injury. *Exp Neurol*. 2008; 212: 108-17.

211.   Seghezzi G, Patel S, Ren CJ, et al. Fibroblast growth factor-2 (FGF-2) induces vascular endothelial growth factor (VEGF) expression in the endothelial cells of forming capillaries: an autocrine mechanism contributing to angiogenesis. *J Cell Biol*. 1998; 141: 1659-73.

212.   Salvucci O, Yao L, Villalba S, Sajewicz A, Pittaluga S and Tosato G. Regulation of endothelial cell branching morphogenesis by endogenous chemokine stromal-derived factor-1. *Blood*. 2002; 99: 2703-11.

213.   Yamaguchi J, Kusano KF, Masuo O, et al. Stromal cell-derived factor-1 effects on ex vivo expanded endothelial progenitor cell recruitment for ischemic neovascularization. *Circulation*. 2003; 107: 1322-8.

214.	Xiong Y, Zhang Y, Mahmood A, Meng Y, Qu C and Chopp M. Erythropoietin mediates neurobehavioral recovery and neurovascular remodeling following traumatic brain injury in rats by increasing expression of vascular endothelial growth factor. *Transl Stroke Res*. 2011; 2: 619-32.

215.	Cipolla MJ. *The Cerebral Circulation*. San Rafael (CA)2009.

216.	Xing C, Arai K, Lo EH and Hommel M. Pathophysiologic cascades in ischemic stroke. *Int J Stroke*. 2012; 7: 378-85.

217.	Taoufik E and Probert L. Ischemic neuronal damage. *Curr Pharm Des*. 2008; 14: 3565-73.

218.	Muoio V, Persson PB and Sendeski MM. The neurovascular unit - concept review. *Acta Physiol (Oxf)*. 2014; 210: 790-8.

219.	Cauli B and Hamel E. Revisiting the role of neurons in neurovascular coupling. *Front Neuroenergetics*. 2010; 2: 9.

220.	Hughes S, Dashkin O and Defazio RA. Vessel painting technique for visualizing the cerebral vascular architecture of the mouse. *Methods in molecular biology*. 2014; 1135: 127-38.

221.	Li Y, Song Y, Zhao L, Gaidosh G, Laties AM and Wen R. Direct labeling and visualization of blood vessels with lipophilic carbocyanine dye DiI. *Nat Protoc*. 2008; 3: 1703-8.

222.	Moy AJ, Wiersma MP and Choi B. Optical histology: a method to visualize microvasculature in thick tissue sections of mouse brain. *PLoS One*. 2013; 8: e53753.

223.	Joshi VS, Reinhardt JM, Garvin MK and Abramoff MD. Automated method for identification and artery-venous classification of vessel trees in retinal vessel networks. *PLoS One*. 2014; 9: e88061.

224.	Bell RD, Winkler EA, Singh I, et al. Apolipoprotein E controls cerebrovascular integrity via cyclophilin A. *Nature*. 2012; 485: 512-6.

225.	Zudaire E, Gambardella L, Kurcz C and Vermeren S. A computational tool for quantitative analysis of vascular networks. *PLoS One*. 2011; 6: e27385.

226.	Di Ieva A, Grizzi F, Jelinek H, Pellionisz AJ and Losa GA. Fractals in the Neurosciences, Part I: General Principles and Basic Neurosciences. *Neuroscientist*. 2014; 20: 403-17.

227.	Di Ieva A, Esteban FJ, Grizzi F, Klonowski W and Martin-Landrove M. Fractals in the neurosciences, Part II: clinical applications and future perspectives. *Neuroscientist*. 2015; 21: 30-43.

228.   Karperien A, Ahammer H and Jelinek HF. Quantitating the subtleties of microglial morphology with fractal analysis. *Front Cell Neurosci*. 2013; 7: 3.

229.   Borodinsky LN and Fiszman ML. A single-cell model to study changes in neuronal fractal dimension. *Methods*. 2001; 24: 341-5.

230.   Caserta F, Eldred WD, Fernandez E, et al. Determination of fractal dimension of physiologically characterized neurons in two and three dimensions. *J Neurosci Methods*. 1995; 56: 133-44.

231.   Gadde SG, Anegondi N, Bhanushali D, et al. Quantification of Vessel Density in Retinal Optical Coherence Tomography Angiography Images Using Local Fractal Dimension. *Investigative ophthalmology & visual science*. 2016; 57: 246-52.

232.   Di Ieva A, Grizzi F, Sherif C, Matula C and Tschabitscher M. Angioarchitectural heterogeneity in human glioblastoma multiforme: a fractal-based histopathological assessment. *Microvasc Res*. 2011; 81: 222-30.

233.   Obenaus A, Ng M, Orantes AM, et al. Traumatic brain injury results in acute rarefication of the vascular network. *Sci Rep*. 2017; 7: 239.

234.   Honig MG and Hume RI. Dil and diO: versatile fluorescent dyes for neuronal labelling and pathway tracing. *Trends Neurosci*. 1989; 12: 333-5, 40-1.

235.   Konno A, Matsumoto N and Okazaki S. Improved vessel painting with carbocyanine dye-liposome solution for visualisation of vasculature. *Sci Rep*. 2017; 7: 10089.

236.   Okyere B, Giridhar K, Hazy A, et al. Endothelial-Specific EphA4 Negatively Regulates Native Pial Collateral Formation and Re-Perfusion following Hindlimb Ischemia. *PLoS One*. 2016; 11: e0159930.

237.   Schindelin J, Arganda-Carreras I, Frise E, et al. Fiji: an open-source platform for biological-image analysis. *Nat Methods*. 2012; 9: 676-82.

238.   Okyere B, Creasey M, Lebovitz Y and Theus MH. Temporal remodeling of pial collaterals and functional deficits in a murine model of ischemic stroke. *J Neurosci Methods*. 2017; 293: 86-96.

239.   Harb R, Whiteus C, Freitas C and Grutzendler J. In vivo imaging of cerebral microvascular plasticity from birth to death. *J Cereb Blood Flow Metab*. 2013; 33: 146-56.

240.   Kienast Y, von Baumgarten L, Fuhrmann M, et al. Real-time imaging reveals the single steps of brain metastasis formation. *Nat Med*. 2010; 16: 116-22.

241.   Fumagalli S, Ortolano F and De Simoni MG. A close look at brain dynamics: cells and vessels seen by in vivo two-photon microscopy. *Prog Neurobiol*. 2014; 121: 36-54.

242.   Shen Q, Huang S and Duong TQ. Ultra-high spatial resolution basal and evoked cerebral blood flow MRI of the rat brain. *Brain Res*. 2015; 1599: 126-36.

243.   Sato Y, Nakajima S, Shiraga N, et al. Three-dimensional multi-scale line filter for segmentation and visualization of curvilinear structures in medical images. *Med Image Anal*. 1998; 2: 143-68.

244.   Zeller K, Vogel J and Kuschinsky W. Postnatal distribution of Glut1 glucose transporter and relative capillary density in blood-brain barrier structures and circumventricular organs during development. *Brain Res Dev Brain Res*. 1996; 91: 200-8.

245.   Wang DB, Blocher NC, Spence ME, Rovainen CM and Woolsey TA. Development and remodeling of cerebral blood vessels and their flow in postnatal mice observed with in vivo videomicroscopy. *J Cereb Blood Flow Metab*. 1992; 12: 935-46.

246.   Krafft PR, Rolland WB, Duris K, et al. Modeling intracerebral hemorrhage in mice: injection of autologous blood or bacterial collagenase. *J Vis Exp*. 2012: e4289.

247.   Suzuki H, Ayer R, Sugawara T, et al. Protective effects of recombinant osteopontin on early brain injury after subarachnoid hemorrhage in rats. *Crit Care Med*. 2010; 38: 612-8.

248.   Mu J, Ostrowski RP, Krafft PR, Tang J and Zhang JH. Serum leptin levels decrease after permanent MCAo in the rat and remain unaffected by delayed hyperbaric oxygen therapy. *Med Gas Res*. 2013; 3: 8.

249.   Hama H, Hioki H, Namiki K, et al. ScaleS: an optical clearing palette for biological imaging. *Nat Neurosci*. 2015; 18: 1518-29.

250.   Richardson DS and Lichtman JW. Clarifying Tissue Clearing. *Cell*. 2015; 162: 246-57.

251.   Zhang Lin-Yuan, Lin Pan, Pan Jiaji, et al. CLARITY for High-resolution Imaging and Quantification of Vasculature in the Whole Mouse Brain. *Aging and Disease* 2018; 9.

252.   Hama H, Kurokawa H, Kawano H, et al. Scale: a chemical approach for fluorescence imaging and reconstruction of transparent mouse brain. *Nat Neurosci*. 2011; 14: 1481-8.

253.   Salehi A, Zhang JH and Obenaus A. Response of the cerebral vasculature following traumatic brain injury. *J Cereb Blood Flow Metab*. 2017; 37: 2320-39.

254.   Adams JH, Jennett B, Murray LS, Teasdale GM, Gennarelli TA and Graham DI. Neuropathological findings in disabled survivors of a head injury. *J Neurotrauma*. 2011; 28: 701-9.

255.   Zhang ZG, Zhang L, Jiang Q, et al. VEGF enhances angiogenesis and promotes blood-brain barrier leakage in the ischemic brain. *J Clin Invest*. 2000; 106: 829-38.

256.   Birdsey GM, Shah AV, Dufton N, et al. The endothelial transcription factor ERG promotes vascular stability and growth through Wnt/beta-catenin signaling. *Dev Cell*. 2015; 32: 82-96.

257.   Zhou Y, Wang Y, Tischfield M, et al. Canonical WNT signaling components in vascular development and barrier formation. *J Clin Invest*. 2014; 124: 3825-46.

258.   Wang X, Xiao Y, Mou Y, Zhao Y, Blankesteijn WM and Hall JL. A role for the beta-catenin/T-cell factor signaling cascade in vascular remodeling. *Circ Res*. 2002; 90: 340-7.

259.   Kim KI, Cho HJ, Hahn JY, et al. Beta-catenin overexpression augments angiogenesis and skeletal muscle regeneration through dual mechanism of vascular endothelial growth factor-mediated endothelial cell proliferation and progenitor cell mobilization. *Arterioscler Thromb Vasc Biol*. 2006; 26: 91-8.

260.   Zhang YM, Dai QF, Chen WH, et al. Effects of acupuncture on cortical expression of Wnt3a, beta-catenin and Sox2 in a rat model of traumatic brain injury. *Acupunct Med*. 2016; 34: 48-54.

261.   Cole JT, Yarnell A, Kean WS, et al. Craniotomy: true sham for traumatic brain injury, or a sham of a sham? *J Neurotrauma*. 2011; 28: 359-69.

262.   Obenaus A, Ng M, Orantes A, et al. Traumatic brain injury results in acute rarefication of the vascular network. *Scientific Reports*. 2017; In Press.

263.   Walchli T, Mateos JM, Weinman O, et al. Quantitative assessment of angiogenesis, perfused blood vessels and endothelial tip cells in the postnatal mouse brain. *Nat Protoc*. 2015; 10: 53-74.

264.   Grumolato L, Liu G, Mong P, et al. Canonical and noncanonical Wnts use a common mechanism to activate completely unrelated coreceptors. *Genes & development*. 2010; 24: 2517-30.

265.   Zanetta L, Marcus SG, Vasile J, et al. Expression of Von Willebrand factor, an endothelial cell marker, is up-regulated by angiogenesis factors: a potential method for objective assessment of tumor angiogenesis. *Int J Cancer*. 2000; 85: 281-8.

266.   Sakata N, Chan NK, Chrisler J, Obenaus A and Hathout E. Bone marrow cell cotransplantation with islets improves their vascularization and function. *Transplantation*. 2010; 89: 686-93.

267.   Lange C, Turrero Garcia M, Decimo I, et al. Relief of hypoxia by angiogenesis promotes neural stem cell differentiation by targeting glycolysis. *The EMBO journal*. 2016; 35: 924-41.

268.   Veenith TV, Carter EL, Geeraerts T, et al. Pathophysiologic Mechanisms of Cerebral Ischemia and Diffusion Hypoxia in Traumatic Brain Injury. *JAMA Neurol*. 2016; 73: 542-50.

269.   Xu K and Lamanna JC. Chronic hypoxia and the cerebral circulation. *Journal of applied physiology*. 2006; 100: 725-30.

270.   Ward NL, Moore E, Noon K, et al. Cerebral angiogenic factors, angiogenesis, and physiological response to chronic hypoxia differ among four commonly used mouse strains. *Journal of applied physiology*. 2007; 102: 1927-35.

271.   Robertson RT, Levine ST, Haynes SM, et al. Use of labeled tomato lectin for imaging vasculature structures. *Histochem Cell Biol*. 2015; 143: 225-34.

272.   Schwarzmaier SM, Kim SW, Trabold R and Plesnila N. Temporal profile of thrombogenesis in the cerebral microcirculation after traumatic brain injury in mice. *J Neurotrauma*. 2010; 27: 121-30.

273.   Lu D, Mahmood A, Goussev A, Qu C, Zhang ZG and Chopp M. Delayed thrombosis after traumatic brain injury in rats. *J Neurotrauma*. 2004; 21: 1756-66.

274.   Goentoro L and Kirschner MW. Evidence that fold-change, and not absolute level, of beta-catenin dictates Wnt signaling. *Molecular cell*. 2009; 36: 872-84.

275.   Topol L, Jiang X, Choi H, Garrett-Beal L, Carolan PJ and Yang Y. Wnt-5a inhibits the canonical Wnt pathway by promoting GSK-3-independent beta-catenin degradation. *J Cell Biol*. 2003; 162: 899-908.

276.   Bernard P, Fleming A, Lacombe A, Harley VR and Vilain E. Wnt4 inhibits beta-catenin/TCF signalling by redirecting beta-catenin to the cell membrane. *Biology of the cell*. 2008; 100: 167-77.

277.   Lengfeld JE, Lutz SE, Smith JR, et al. Endothelial Wnt/beta-catenin signaling reduces immune cell infiltration in multiple sclerosis. *Proc Natl Acad Sci U S A*. 2017; 114: E1168-E77.

278.   Lim RG, Quan C, Reyes-Ortiz AM, et al. Huntington's Disease iPSC-Derived Brain Microvascular Endothelial Cells Reveal WNT-Mediated Angiogenic and Blood-Brain Barrier Deficits. *Cell reports*. 2017; 19: 1365-77.

279.   Lennmyr F, Ata KA, Funa K, Olsson Y and Terent A. Expression of vascular endothelial growth factor (VEGF) and its receptors (Flt-1 and Flk-1) following permanent and transient occlusion of the middle cerebral artery in the rat. *Journal of neuropathology and experimental neurology*. 1998; 57: 874-82.

280.   Nag S, Takahashi JL and Kilty DW. Role of vascular endothelial growth factor in blood-brain barrier breakdown and angiogenesis in brain trauma. *Journal of neuropathology and experimental neurology*. 1997; 56: 912-21.

281.   Papavassiliou E, Gogate N, Proescholdt M, et al. Vascular endothelial growth factor (vascular permeability factor) expression in injured rat brain. *J Neurosci Res*. 1997; 49: 451-60.

282.   Easwaran V, Lee SH, Inge L, et al. beta-Catenin regulates vascular endothelial growth factor expression in colon cancer. *Cancer Res*. 2003; 63: 3145-53.

283.   Xing C, Hayakawa K, Lok J, Arai K and Lo EH. Injury and repair in the neurovascular unit. *Neurol Res*. 2012; 34: 325-30.

284.   Bouma GJ and Muizelaar JP. Cerebral blood flow, cerebral blood volume, and cerebrovascular reactivity after severe head injury. *J Neurotrauma*. 1992; 9 Suppl 1: S333-48.

285.   Lee SH, Jeong D, Han YS and Baek MJ. Pivotal role of vascular endothelial growth factor pathway in tumor angiogenesis. *Ann Surg Treat Res*. 2015; 89: 1-8.

286.   Hayashi T, Noshita N, Sugawara T and Chan PH. Temporal profile of angiogenesis and expression of related genes in the brain after ischemia. *J Cereb Blood Flow Metab*. 2003; 23: 166-80.

287.   Dore-Duffy P, Wang X, Mehedi A, Kreipke CW and Rafols JA. Differential expression of capillary VEGF isoforms following traumatic brain injury. *Neurol Res*. 2007; 29: 395-403.

288.   Nag S, Eskandarian MR, Davis J and Eubanks JH. Differential expression of vascular endothelial growth factor-A (VEGF-A) and VEGF-B after brain injury. *Journal of neuropathology and experimental neurology*. 2002; 61: 778-88.

289.   Wright DK, Trezise J, Kamnaksh A, et al. Behavioral, blood, and magnetic resonance imaging biomarkers of experimental mild traumatic brain injury. *Sci Rep*. 2016; 6: 28713.

290.   Scott A, Powner MB, Gandhi P, et al. Astrocyte-derived vascular endothelial growth factor stabilizes vessels in the developing retinal vasculature. *PLoS One*. 2010; 5: e11863.

291.   Qu B, Liu BR, Du YJ, et al. Wnt/beta-catenin signaling pathway may regulate the expression of angiogenic growth factors in hepatocellular carcinoma. *Oncol Lett*. 2014; 7: 1175-8.

292.   Reis M, Czupalla CJ, Ziegler N, et al. Endothelial Wnt/beta-catenin signaling inhibits glioma angiogenesis and normalizes tumor blood vessels by inducing PDGF-B expression. *J Exp Med*. 2012; 209: 1611-27.

293.   Ghosh N, Yuan X, Turenius CI, et al. Automated core-penumbra quantification in neonatal ischemic brain injury. *J Cereb Blood Flow Metab*. 2012; 32: 2161-70.

294.   Tong KA, Ashwal S, Obenaus A, Nickerson JP, Kido D and Haacke EM. Susceptibility-weighted MR imaging: a review of clinical applications in children. *AJNR Am J Neuroradiol*. 2008; 29: 9-17.

295.   Lin JB, Sene A, Wiley LA, et al. WNT7A/B promote choroidal neovascularization. *Experimental eye research*. 2018; 174: 107-12.

296.   Yano H, Hara A, Shinoda J, et al. Immunohistochemical analysis of beta-catenin in N-ethyl-N-nitrosourea-induced rat gliomas: implications in regulation of angiogenesis. *Neurol Res*. 2000; 22: 527-32.

297.   Yano H, Hara A, Takenaka K, et al. Differential expression of beta-catenin in human glioblastoma multiforme and normal brain tissue. *Neurol Res*. 2000; 22: 650-6.

298.   Guo S, Arai K, Stins MF, Chuang DM and Lo EH. Lithium upregulates vascular endothelial growth factor in brain endothelial cells and astrocytes. *Stroke*. 2009; 40: 652-5.

299.   Silva R, Martins L, Longatto-Filho A, Almeida OF and Sousa N. Lithium prevents stress-induced reduction of vascular endothelium growth factor levels. *Neurosci Lett*. 2007; 429: 33-8.

300.   Kim YR, van Meer MP, Tejima E, et al. Functional MRI of delayed chronic lithium treatment in rat focal cerebral ischemia. *Stroke*. 2008; 39: 439-47.

301.   Yu SW, Friedman B, Cheng Q and Lyden PD. Stroke-evoked angiogenesis results in a transient population of microvessels. *J Cereb Blood Flow Metab*. 2007; 27: 755-63.

302.   Simard JM, Kent TA, Chen M, Tarasov KV and Gerzanich V. Brain oedema in focal ischaemia: molecular pathophysiology and theoretical implications. *Lancet Neurol*. 2007; 6: 258-68.

303.   Simard JM, Kilbourne M, Tsymbalyuk O, et al. Key role of sulfonylurea receptor 1 in progressive secondary hemorrhage after brain contusion. *J Neurotrauma*. 2009; 26: 2257-67.

304.   Kurland D, Hong C, Aarabi B, Gerzanich V and Simard JM. Hemorrhagic progression of a contusion after traumatic brain injury: a review. *J Neurotrauma*. 2012; 29: 19-31.

305.   Di Giovanni S, Movsesyan V, Ahmed F, et al. Cell cycle inhibition provides neuroprotection and reduces glial proliferation and scar formation after traumatic brain injury. *Proc Natl Acad Sci U S A*. 2005; 102: 8333-8.

306.   Motoike T, Loughna S, Perens E, et al. Universal GFP reporter for the study of vascular development. *Genesis*. 2000; 28: 75-81.

307.   Ma B-L, Yang Y, Dai Y, Li Q, Lin G and Ma Y-M. Polyethylene glycol 400 (PEG400) affects the systemic exposure of oral drugs based on multiple mechanisms: taking berberine as an example. *RSC Advances*. 2017; 7: 2435-42.

308.   Thau-Zuchman O, Shohami E, Alexandrovich AG and Leker RR. Vascular endothelial growth factor increases neurogenesis after traumatic brain injury. *J Cereb Blood Flow Metab*. 2010; 30: 1008-16.

309.   Schoch HJ, Fischer S and Marti HH. Hypoxia-induced vascular endothelial growth factor expression causes vascular leakage in the brain. *Brain*. 2002; 125: 2549-57.

310.   Walker EJ, Shen F, Young WL and Su H. Cerebrovascular casting of the adult mouse for 3D imaging and morphological analysis. *J Vis Exp*. 2011: e2958.

311.   Hasan MR, Herz J, Hermann DM and Doeppner TR. Intravascular perfusion of carbon black ink allows reliable visualization of cerebral vessels. *J Vis Exp*. 2013.

312.   Ghanavati S, Lerch JP and Sled JG. Automatic anatomical labeling of the complete cerebral vasculature in mouse models. *Neuroimage*. 2014; 95: 117-28.

313.   Smith LE, Wesolowski E, McLellan A, et al. Oxygen-induced retinopathy in the mouse. *Investigative ophthalmology & visual science*. 1994; 35: 101-11.

314.   Lametschwandtner A, Lametschwandtner U and Weiger T. Scanning electron microscopy of vascular corrosion casts--technique and applications. *Scan Electron Microsc*. 1984: 663-95.

315.   Ohtani O and Ohtani Y. A corrosion casting/scanning electron microscope method that simultaneously demonstrates clear outlines of endothelial cells and three-dimensional vascular organization. *Arch Histol Cytol*. 2000; 63: 425-9.

316.   Hintermüller C, Coats JS, Obenaus A, Nelson G, Krucker T and Stampanoni M. 3D quantification of brain microvessels exposed to heavy particle radiation. *Journal of Physics: Conference Series*. 2009; 186: 012087.

317.   Hashimoto H, Kusakabe M and Ishikawa H. A novel method for three-dimensional observation of the vascular networks in the whole mouse brain. *Microscopy research and technique*. 2008; 71: 51-9.

318.   Maeda K, Hata R and Hossmann KA. Differences in the cerebrovascular anatomy of C57black/6 and SV129 mice. *Neuroreport*. 1998; 9: 1317-9.

319.   Meng H, Peng Y, Hasan R, Yu G and Wang MM. Nuclear contrast angiography: a simple method for morphological characterization of cerebral arteries. *Brain Res*. 2009; 1261: 75-81.

320.   Rymer CC and Sims-Lucas S. In utero intra-cardiac tomato-lectin injections on mouse embryos to gauge renal blood flow. *J Vis Exp*. 2015.

321.   Lokmic Z and Mitchell GM. Visualisation and stereological assessment of blood and lymphatic vessels. *Histol Histopathol*. 2011; 26: 781-96.

322.   Jilani SM, Murphy TJ, Thai SN, Eichmann A, Alva JA and Iruela-Arispe ML. Selective binding of lectins to embryonic chicken vasculature. *J Histochem Cytochem*. 2003; 51: 597-604.

323.   Faustino J, Chip S, Derugin N, et al. CX3CR1-CCR2-dependent monocyte-microglial signaling modulates neurovascular leakage and acute injury in a mouse model of childhood stroke. *J Cereb Blood Flow Metab*. 2019: 271678X18817663.

324.   Wendel KM, Lee JB, Affeldt BM, et al. Corpus Callosum Vasculature Predicts White Matter Microstructure Abnormalities after Pediatric Mild Traumatic Brain Injury. *J Neurotrauma*. 2018.

325.   Leeds PR, Yu F, Wang Z, et al. A new avenue for lithium: intervention in traumatic brain injury. *ACS Chem Neurosci*. 2014; 5: 422-33.

326.   Said SS, Pickering JG and Mequanint K. Advances in growth factor delivery for therapeutic angiogenesis. *J Vasc Res*. 2013; 50: 35-51.

327.   Kazmi SM, Richards LM, Schrandt CJ, Davis MA and Dunn AK. Expanding applications, accuracy, and interpretation of laser speckle contrast imaging of cerebral blood flow. *Journal of cerebral blood flow and metabolism : official journal of the International Society of Cerebral Blood Flow and Metabolism*. 2015; 35: 1076-84.

328.   White SM, Hingorani R, Arora RP, Hughes CC, George SC and Choi B. Longitudinal in vivo imaging to assess blood flow and oxygenation in implantable engineered tissues. *Tissue engineering Part C, Methods*. 2012; 18: 697-709.

329.   White SM, George SC and Choi B. Automated computation of functional vascular density using laser speckle imaging in a rodent window chamber model. *Microvascular research*. 2011; 82: 92-5.

330.   He J, Lu H, Young L, et al. Real-time quantitative monitoring of cerebral blood flow by laser speckle contrast imaging after cardiac arrest with targeted temperature management. *Journal of cerebral blood flow and metabolism : official journal of the International Society of Cerebral Blood Flow and Metabolism*. 2017: 271678X17748787.